CONSTITUTIVE MODELING OF STRAIN-DEPENDENT BOND BREAKING AND HEALING KINETICS OF POLYAMPHOLYTE (PA) GELS

A Thesis

Presented to the Faculty of the Graduate School

of Cornell University

In Partial Fulfillment of the Requirements for the Degree of

Master of Science

by

SAIRAM PAMULAPARTHI VENKATA

May 2021

ABSTRACT

A hydrogel is a three-dimensional network of cross-linked hydrophilic polymer chains swollen in water. The large water content allows hydrogels to be biocompatible. Conventional hydrogels are mechanically soft and weak, which severely limits their applications, especially in structural biomaterials. Studies on double network (DN) hydrogels consisting of two interpenetrating networks of brittle and ductile polymers, revealed a general strategy to toughen network materials. The first network is densely cross-linked, easily breakable, and is brittle in nature, while the second network is loosely cross-linked, highly extensible, and is ductile in nature. During deformation, the first network breaks preferentially to dissipate energy, while the second network keeps the sample intact. As a result, DN hydrogels have high mechanical strength and toughness (~ 1000 J/m^2, which is comparable to the cartilage). By adopting a similar strategy of incorporating sacrificial network into polymer network to dissipate mechanical energy, Polyampholyte (PA) gels are developed.

In this thesis, a three-dimensional finite strain nonlinear viscoelastic model is developed to study the mechanical behavior of PA gels (both purely physically cross-linked PA gel and chemical PA gel with both physical and chemical cross-links). The time dependent behavior of the PA gel is due to the ionic interactions of oppositely charged monomers randomly distributed along the chain backbone. Our constitutive model connects the strain dependent bond breaking and reforming kinetics in the microscopic regime to the deformation of the gel at the continuum level. We compare the predictions of our model with uniaxial tension, tensile-relaxation, cyclic, and small strain torsional relaxation tests. The material parameters in our model are obtained using least squares error optimization. Our theory agrees well with the experimental behavior of the gel.

BIOGRAPHICAL SKETCH

Sairam Pamulaparthi Venkata was born in Telangana, India. All through school and college, he actively participated in sports and community development programmes. In 2010, he went to SR Edu Center to pursue his higher secondary education, where he developed an interest in mathematics and physics. Motivated by these interests, he took an admission into the undergraduate program in the department of mechanical engineering at the Indian Institute of Technology, Hyderabad (IITH) in 2012. After receiving his bachelor's degree in 2016, he worked as a project assistant at the Indian Institute of Science, Bangalore and as a Junior Research Fellow at IITH. In 2018, he went to Cornell University to pursue his graduate study in the field of theoretical and applied mechanics. As a part of the Master of Science degree, his research focussed on constitutive modeling of mechanical behavior of self-healing hydrogels.

To my parents, grandparents, sister and Purva

ACKNOWLEDGMENTS

My learning at Cornell for two and half years has truly been an enriching experience that I will cherish for the rest of my life.

I am very grateful to my thesis advisor, Prof. Herbert Hui, for being supportive and mentoring me through out my research. Prof. Herbert Hui is dedicated to his research in the field of mechanics and has always been an inspiration to his mentees. Along with the true commitment to his research, he is passionate about playing tennis and exploring new recipes, ensuring a good work life balance. He was also gracious enough to host our group during the thanksgiving dinner at his home. Working with my advisor has been a wonderful experience which enhanced my research skills and made me aware of my strengths and weaknesses.

I want to thank my co-advisor Prof. Alan Zehnder and my co-worker Jingyi Guo for their insightful inputs and valuable contributions. I also want to thank Kunpeng Cui for providing us with the experimental data and for being a part of meaningful discussions.

Interactions with my advisor, co-advisor and my co-workers have helped me get a better understanding of physics of hydrogels. I also like to thank my lab mates, my friends, and my family for being strong pillars of support throughout my academic journey.

TABLE OF CONTENTS

Supporting Information – Constitutive modeling of strain-dependent bond breaking and healing kinetics of chemical Polyampholyte (PA) gel

CHAPTER 1
Constitutive modeling of bond breaking and healing kinetics of physical Polyampholyte (PA) gel

Sairam Pamulaparthi Venkata[a,1#], Kunpeng Cui[b,1#], Jingyi Guo[a], Alan T. Zehnder[a], Jian Ping Gong[b,c,d], & Chung-Yuen Hui[a,c*]

[a] Field of Theoretical and Applied Mechanics, Department of Mechanical and Aerospace Engineering, Cornell University, Ithaca, New York, 14853, United States

[b] Institute for Chemical Reaction Design and Discovery (WPI-ICReDD), Hokkaido University, Sapporo 001-0021, Japan

[c] Soft Matter GI-CoRE, Hokkaido University, Sapporo 001-0021, Japan

[d] Faculty of Advanced Life Science, Hokkaido University, Sapporo 001-0021, Japan

[*] **Corresponding Author**, E-mail: ch45@cornell.edu (C.-Y.H.)

#These two authors contributed equally to this paper.

Abstract:

A three-dimensional finite strain nonlinear viscoelastic model is developed to study the mechanical behavior of a physically cross-linked Polyampholyte (PA) gel. The time dependent behavior of this gel is due to the ionic interactions of oppositely charged monomers randomly distributed along the chain backbone. In this work, we divide the physical cross-links broadly into weak and strong bonds, depending on their survival and reformation characteristics. Our constitutive model connects the strain dependent bond breaking and reforming kinetics in the microscopic regime to the deformation of the gel at the continuum level. We compare the predictions of our model with uniaxial tension, tensile-relaxation, cyclic, and small strain torsional relaxation tests. The material parameters in our model are obtained using least squares optimization. Our theory agrees well with the experimental behavior of the gel.

---

[1] These authors contributed equally to this work. Numerical simulations are done by Sairam Pamulaparthi Venkata. Experimental data is provided by Kunpeng Cui.

Keywords: self-healing, hydrogel, large deformation, nonlinear viscoelasticity

1. Introduction:

A hydrogel is a three-dimensional network of cross-linked hydrophilic polymer chains swollen in water. The large water content allows hydrogels to be biocompatible. For example, hydrogels are used as scaffolding materials in tissue engineering [1–3] and as self-regulatory vehicles in drug delivery systems[4,5]. Polyelectrolyte hydrogels have been explored as a replacement to artificial muscles, cornea, and cartilage[6,7]. For hydrogels to be substitutes for load-bearing structural biomaterials, properties such as mechanical strength, stiffness, resistance to wear, shock-absorption, high toughness, and self-healing properties are desired. Traditional hydrogels are too brittle and are not ideal candidates for bio-structural materials. The synthesis of double network (DN) hydrogels has shown promising results for development of highly extensible gels with high fracture toughness property.

Double network hydrogels consist of two interpenetrating networks of brittle and ductile polymers. The first network is densely cross-linked, easily breakable, and is brittle in nature, while the second network is loosely cross-linked, highly extensible, and is ductile in nature[8–11]. When the DN hydrogel is subjected to mechanical loading, the first network carries most of the load and undergoes internal fracture, acting as a sacrificial network. The second network, being highly extensible, prevents the formation and propagation of macroscopic cracks and a sudden failure of the gel under mechanical loading. Due to the continuous damage of the first network under loading, energy is effectively dissipated, and the toughness of the material is improved[12–15]. In DN hydrogels with only covalent type of bonds, the rupture of the first network is permanent which lowers fatigue resistance. To address this limitation, the chemical bonds in the sacrificial network can be replaced with physical bonds which can break and re-attach[16–18]. These reversible physical bonds help the gel to recover partially or fully, depending on the resting period[19,20]. As a result, the gel can maintain its fatigue resistance, high extensibility, and toughness for cyclic tests. Due to the breaking and healing kinetics of reversible bonds, the mechanical

properties of these gels are time dependent, and the gel behaves like a viscoelastic material[21].

Many researchers have been successful in synthesizing tough self-healing hydrogels, but the quantitative understanding of bond breaking and healing kinetics of these viscoelastic gels is still in progress[22–31]. In our previous works, we developed constitutive models to study time-dependent mechanical behavior of a dual cross-linked polyvinyl alcohol (PVA) gel, where PVA chains form physical cross-links with borax ions and chemical cross-links with glutaraldehyde ions[32–34]. The PVA gel has simpler bond kinetics as the chemical bonds do not break under mechanical loading and the kinetics of physical bonds are not dependent on the applied strain. Therefore, understanding the microscopic interactions of bond kinetics of PVA gel through macroscopic mechanical models help us in dealing with more complex gels, where the kinetics of temporary bonds are time, rate, and strain dependent.

In most polymeric materials, the dissociation and association of physical bonds is dependent on the strain/stress experienced by the bonds[35–38]. The rate of dissociation is expected to be high when the force acting on these bonds or the stretch is high. In this paper, we study the strain-dependent bond breaking and healing kinetics of a physically cross-linked polyampholyte (PA) gel synthesized by Gong's group[39]. We develop a finite strain constitutive model to quantitatively understand the bond kinetics of the PA gel.

The purely physical PA gel is synthesized by random co-polymerization of oppositely charged ionic monomers. In each polymer chain, the positive and negative charged monomers are randomly distributed along the chain backbone. PA gel has a phase-separated structure composed of soft and stiff phases, with a structure length of ~ 100 nm[40–43]. The soft and stiff phases differ in polymer densities, where the soft phase has a low polymer density, and the stiff phase has a high polymer density. As the ionic interactions depend on polymer density[39], the ionic bonds can be divided into two types: strong bonds and weak bonds. These bonds serve as sacrificial structure and enhance the fatigue[44] and fracture resistance, self-healing behavior[45], and shock

absorbance of PA gel. We adopt a similar principle to DN gels, using rupture of sacrificial bonds to dissipate energy and enhance the toughness of the overall material. The PA gels have 50-70 wt.% of water content at an equilibrium state, much less than that of conventional hydrogels (> 80 wt. %). These gels are strongly viscoelastic (due to dynamics of physical bonds), have high toughness (fracture energy of 4000 $J.m^{-2}$), and can recover completely. These gels show yielding behaviour at a critical strain[39], which suggests that the kinetics of physical bonds are sensitive to strain. The wide range of mechanical properties, high toughness, and the healing behavior motivates us to study the behavior of PA gel, as the gel exhibits promising properties that can be utilized in real world applications. For example, these PA gels show adjustable adhesion to charged surfaces in water[46], and dramatically improve the toughness of glass-fiber-reinforced soft composites when used as a matrix [47].

This paper is organized as follows. In Section 2, we describe our constitutive model for purely physically cross-linked PA gel and state the assumptions considered in our model. The strain-dependent bond breaking function and the survivability function are introduced. The strain energy density function of undamaged network and total strain energy density of the gel are mentioned. Finally, a nominal stress-strain relationship which depends on the history of loading is presented for different types of mechanical tests. In Section 3, an experimental procedure for the synthesis and mechanical tests of our PA gel is laid out. In Section 4, we estimate few material parameters from experiments. In Section 5, a least squares optimization method is proposed to capture all the material parameters involved in our constitutive model. During this optimization process, multiple data sets of material parameters are obtained. We select one data set of material parameters based on physical intuition and the estimates computed in Section 4. In Section 6, we present the results and discuss the accuracy of our model for different types of loading histories using the data set of material parameters chosen in Section 5. We observe that our model captures the mechanical behavior of physically cross-linked PA gel reasonably well. Conclusions are in Section 7.

2. *Theoretical Model*

We state the basic assumptions of our theory here, many of which are similar to those in our previous PVA gel work[33,34] and in Guo[48]. For the sake of clarity, these assumptions are restated here.

2.1 Assumptions

1. The polymer network consists of chains connected by physical bonds.
2. In reality, physical bonds have a distribution of interaction strengths, and bond breaking/reforming kinetics. For simplicity, we categorize these interactions into two groups of bonds: weak and strong bonds.
3. Both weak and strong bonds can break and reattach according to breaking and healing kinetics. The breaking kinetics are specified by two survivability functions ϕ_{B_i} ($i=1$ refer to weak bonds, $i=2$ refer to strong bonds), where ϕ_{B_i} *is the fraction of bonds that survived from the time of their birth,* τ *to the current time,* t.
4. We assume that the stress sustained by a chain is instantaneously relaxed when it breaks, and immediately after a chain is reattached, it is in a relaxed state and carries no strain energy. The deformation of a chain reconnected at time τ can be described by the deformation gradient tensor $\mathbf{F}^{\tau\to t}$. The superscript $\tau\to t$ indicates that the chain experiences the deformation history from its birth (reattachment) at time τ to the current time t. The special case of $\tau=0$ applies to the chains that are connected before mechanical loading. We assume that before loading, the gel has been rested sufficiently long that the physical bonds achieve dynamic equilibrium. Dynamic equilibrium results in a constant molar fraction of connected and broken temporary chains and a constant reforming rate which is equal to the breaking rate.
5. The healing kinetics for weak and strong bonds are specified by the reattachment rates χ_i ($i=1,2$) which *represents the fraction of weak/strong bonds reattached per unit time per unit reference volume*. Physically, the healing rate must increase with the number of broken bonds. Here we use the

simplest assumption that healing rate is directly proportional to the number of broken bonds divided by a characteristic healing time. This is a reasonable assumption since healing is achieved by the bonding of borax ions to the number of available sites, so the reaction rate should be proportional to the number of broken bonds. The reforming rate $\chi_i(t)$ is assumed to be proportional to the number of broken or unconnected bonds $N_{b_i}(t)$ per unit reference volume. Specifically, let $\hat{\chi}_i(t) = \chi_i(t) N_0$ be the number of weak/strong bonds reattached per unit time per unit reference volume, where N_0 is the total number of physical bonds per unit reference volume, then

$$\hat{\chi}_i(t) = N_{b_i}(t) / t_{H_i}, \quad \text{or } \chi_i(t) = \frac{1}{t_{H_i}} \frac{N_{b_i}(t)}{N_0}, \tag{1}$$

where t_{H_i} is the characteristic healing time of i^{th} type of physical bonds. Here, we simplify notation by writing χ_i as a function of time t only, whereas it also depends on the entire loading history.

6. We assume strong and weak bonds break and heal independently. Specifically, breaking and healing kinetics are completely specified by ϕ_{B_i}, χ_i.
7. In the continuum scale, the gel is incompressible and isotropic. Since chains connecting by physical bonds are identical, the same strain energy function applies to network connected by weak and strong bonds.

The following notations are introduced to describe our PA gel model:

- The total number of weak (strong) bonds per unit reference volume is denoted by $N_i = \omega_i N_0$ where ω_i is the molar fraction, weak bonds and strong bonds are referred to $i = 1$ and $i = 2$ respectively. Note $\omega_1 + \omega_2 = 1$ and that both ω_1, ω_2 are constants, independent of time. However, it is important to note that not all weak or strong bonds are connected after the synthesis of the gel, even under no applied load or deformation.

- The total number of weak or strong bonds that are connected per unit reference volume at time t is given by $N_{c_i}(t)$. Similarly, the total number weak or strong bonds that are broken per unit reference volume at t is denoted by $N_{b_i}(t)$. Therefore, we have $N_i(t) = N_{c_i}(t) + N_{b_i}(t)$.

2.2 Survivability function

The concept of a survivability function, $\phi_B(\tau, t)$ was introduced in our previous works to study the breaking kinetics of a PVA hydrogel [33,34]. A surprising aspect of the PVA gel is that $\phi_B(\tau, t)$ is *independent* of the force acting on the physical bonds. This result leads us to propose that the breaking rate for the PVA gel is given by

$$-\frac{\partial \phi_B}{\partial t} = \frac{1}{t_B}\phi_B{}^{\alpha_B}, \qquad (2)$$

where t_B is a characteristic breaking time for physical bonds and $2 > \alpha_B > 1$ is a material constant that specifies the rate of decay of ϕ_B. For the PA gel system, Eq. (2) is inadequate since the bond breaking is sensitive to the stretch experienced by the bond. To reflect this effect, we modify Eq. (2) by allowing the rate of bond breaking to be dependent on the stretch experienced by a bond from its birth at time τ to the current time $t > \tau$. In the affine model, this stretch is characterized by the first invariant of the right Cauchy-Green tensor, given by $H(\tau, t) = \text{trace}\left[\left(\mathbf{F}^{\tau \to t}\right)^T \mathbf{F}^{\tau \to t}\right]$. Thus, for the PA gel, we modify Eq. (2) to

$$-\frac{\partial \phi_B}{\partial t} = \frac{1}{t_B}\phi_B{}^{\alpha_B} f\left[H(\tau, t)\right], \qquad (3)$$

where f is the accelerating breaking function. Physically, we expect f to increase monotonically with H. Also, for small deformations we have $f(H^{\tau \to t} \approx 3) \approx 1$. Consistent with the tension test results in Fig. 2 we allow f to increase rapidly after some critical deformation, I_c. When the sample is loaded beyond this critical deformation, the gel shows yield behaviour due to the acceleration of breaking kinetics. Experiments (see Fig. 2) show that although the "yield" stress increases

rapidly with the applied loading rate, the "yield" strain characterized by I_c is insensitive to the loading rate. Eq. (3) can be integrated to obtain

$$\phi_B(\tau,t,H^{\tau\to t})=\left[1+\frac{\alpha_B-1}{t_B}\int_{\tau}^{t} f\left(H^{\tau\to s}\right)ds\right]^{\frac{1}{1-\alpha_B}}. \quad (4)$$

It is important to note that the survivability function depends on the time τ when the bond is formed, current time t, and the deformation history $H(\tau,s)\equiv H^{\tau\to s}$ for $s\in(\tau,t]$. In the following, we simplify notations by writing $\phi_B(\tau,t,H^{\tau\to t})\equiv\phi_B(\tau,t)$. A more detailed discussion on the physics of Eq. (2) and Eq. (3) is given in supporting information (SI, see Section S1).

The accelerating breaking function $f_i(I_1)$ used in this work is

$$f_i(I_1)=\exp\left\{\left(1+\frac{I_1-3}{I_c-3}\right)^{m_i}-1\right\},\quad I_c=\lambda_c^2+\frac{2}{\lambda_c}, \quad (5)$$

where I_c is the first invariant of the right Cauchy-Green tensor calculated at the critical stretch λ_c, after which the bond breaking kinetics accelerate, and m_i is a material parameter. When chains are stretched beyond their critical strain limit, $f_i(I_1)$ increases significantly and this accelerated bond breaking phenomenon results in macroscopic softening of the gel. The critical strain related parameter I_c is assumed to be same for the weak and strong bonds. An estimate of I_c can be obtained from tensile test data, where the slope of nominal stress versus nominal strain decreases rapidly (see Fig. 2). When the deformation is small compared to the critical strain, i.e., $|I_1-3|\ll|I_c-3|$, $f_i(I_1)\approx 1$, we recover our previous PVA constitutive model where breaking kinetics is independent of strain/stress.

Since the breaking rate of physical bonds is dependent on the deformation applied, we can no longer use the steady-state assumption of dynamic equilibrium once loading starts. In other words, once loading starts, the breaking and healing rates are history dependent and not necessarily equal. The healing rate is considered next.

2.3 Healing rates for physical bonds

For each type of bonds, the number of bonds per unit reference volume reattached between τ and $\tau + d\tau$ which survive until $t > \tau$ is

$$\phi_{B_i}(\tau, t)\hat{\chi}_i(\tau)d\tau. \tag{6a}$$

The total number of reattached bonds of type i from when the gel is synthesized ($\tau = -\infty$) to the current time, $N_{c_i}(t)$ is

$$N_{c_i}(t) = \int_{-\infty}^{t} \phi_{B_i}(\tau, t)\hat{\chi}_i(\tau)d\tau. \tag{6b}$$

By Eq. (1), the total number of unconnected bonds is $N_{b_i}(t) = \hat{\chi}_i(t)t_{H_i}$. Since $N_i = N_{b_i}(t) + N_{c_i}(t)$, we have

$$\omega_i N_0 = \hat{\chi}_i(t)t_{H_i} + \int_{-\infty}^{t} \phi_{B_i}(\tau, t)\hat{\chi}_i(\tau)d\tau \Leftrightarrow \omega_i = \chi_i(t)t_{H_i} + \int_{-\infty}^{t} \phi_{B_i}(\tau, t)\chi_i(\tau)d\tau. \tag{7}$$

Eq. (7) states that the healing rate χ_i depends on the loading history and can be obtained by solving an integral equation.

Eq. (7) can be simplified since we assume loading starts at $t = 0$. Before loading starts, the bonds are in a state of dynamic equilibrium so $\chi_i(t) = \chi_i^{ss}$ for $t < 0$. The steady state healing rate χ_i^{ss} can be found by setting $t = 0$ in Eq. (7). In SI (Section S2), we show that

$$\chi_i^{ss} = \frac{\omega_i}{t_{H_i} + \dfrac{t_{B_i}}{2 - \alpha_{B_i}}}. \tag{8}$$

We use Eq. (7) along with $\chi_i(t) = \chi_i^{ss}, \forall t \le 0$ and $\int_{-\infty}^{0} \phi_{B_i}(\tau, t)\chi_i(\tau)d\tau = \chi_i^{ss}\dfrac{t_{B_i}}{2 - \alpha_{B_i}}\left[\phi_{B_i}(0, t)\right]^{2-\alpha_{B_i}}$ to derive

$$\omega_i - \chi_i^{ss}\frac{t_{B_i}}{2 - \alpha_{B_i}}\left[\phi_{B_i}(0, t)\right]^{2-\alpha_{B_i}} = \chi_i(t)t_{H_i} + \int_{0}^{t} \phi_{B_i}(\tau, t)\chi_i(\tau)d\tau. \tag{9}$$

Eq. (9) allows us to find the reattachment rates given the loading history.

2.4 *Strain Energy:*

The total strain energy of the PA gel is the sum of strain energies carried by the network connected to both the weak and strong bonds. In the following Section 2.5, we assume that the strain energy density W_0 of the undamaged network depends only on the invariant $I_1 = \text{trace}\left(\mathbf{F}^T\mathbf{F}\right)$. The total strain energy density of the gel W is

$$\begin{aligned} W &= \sum_{i=1}^{2}\int_{-\infty}^{t}\phi_{B_i}(\tau,t)\chi_i(\tau)W_0\left[H(\tau,t)\right]d\tau, \\ &= \left\{\sum_{i=1}^{2}\chi_i^{ss}\frac{t_{B_i}}{2-\alpha_{B_i}}\left[\phi_{B_i}(0,t)\right]^{2-\alpha_{B_i}}\right\}W_0\left(I_1(t)\right)+\sum_{i=1}^{2}\int_{0}^{t}\phi_{B_i}(\tau,t)\chi_i(\tau)W_0\left[H(\tau,t)\right]d\tau. \end{aligned} \tag{10}$$

The first term on the RHS of Eq. (10) corresponds to the strain energy of physical bonds that survive to current time t from the start of the loading ($t=0$). The second term on the RHS of Eq. (10) represents the increase in strain energy due to the reattachment of broken bonds during the loading phase. Note, we have used assumption 4 which states that when a chain is reattached, it carries no energy or attaches in a relaxed state. The assumption is reflected in the argument of W_0 in Eq. (10). Specifically, $\phi_{B_i}(\tau,t)\chi_i(\tau)d\tau$ is the fraction of bonds that are reattached between the time τ and $\tau+d\tau$ and survive until the current time *t*. Since these bonds carry energy from their birth at τ, the argument of W_0 is $H(\tau,t)=\text{trace}\left[\left(\mathbf{F}^{\tau\to t}\right)^T\left(\mathbf{F}^{\tau\to t}\right)\right]$.

2.5 *Strain energy density function:*

PA gels are highly stretchable as shown in Fig. 2. In this work, we use a three term Yeoh's strain energy function to capture the network's strain hardening behavior

$$W_0(I_1)=\sum_{i=1}^{3}c_i(I_1-3)^i, \tag{11}$$

where $\mu\equiv 2c_1$ is small strain shear modulus of the undamaged PA gel. The hardening behavior is controlled by the parameters c_2 and c_3 which have dimensions of stress.

The first term in the Eq. (11) is the classical neo-Hookean strain energy density, so there is no significant difference between a Yeoh and a neo-Hookean solid at small stretches.

2.6 Nominal stress:

Following the Coleman-Noll procedure[49] (see SI, Section S3), the first Piola-Kirchhoff stress is given by

$$\begin{aligned}\mathbf{P}(t) = &-p\left(\mathbf{F}^{0\to t}\right)^{-T} + \left\{\sum_{i=1}^{2}\chi_i^{ss}\frac{t_{B_i}}{2-\alpha_{B_i}}\left[\phi_{B_i}(0,t)\right]^{2-\alpha_{B_i}}\right\}2\frac{dW_0}{dI_1}\bigg|_{I_1(t)}\mathbf{F}^{0\to t}\\ &+\sum_{i=1}^{2}\int_0^t \phi_{B_i}(\tau,t)\chi_i(\tau)2\frac{dW_0}{dI_1}\bigg|_{I_1=H(\tau,t)}\mathbf{F}^{\tau\to t}\left(\mathbf{F}^{0\to\tau}\right)^{-T}d\tau,\end{aligned} \tag{12}$$

where p is the Lagrange multiplier which enforces the incompressibility condition.

Of particular interest are the relations between nominal stress and stretch ratio in uniaxial tension and relaxation tests. In uniaxial tension, the nominal stress $\mathbf{P}$ is related to the stretch ratio $\lambda(t)$ in the loading direction (see Section S3.1 for derivation) by

$$\begin{aligned}P(t) = &\left[\sum_{i=1}^{2}\chi_i^{ss}\frac{t_{B_i}}{2-\alpha_{B_i}}\left[\phi_{B_i}(0,t)\right]^{2-\alpha_{B_i}}\right]2\frac{dW_0}{dI_1}\bigg|_{I_1(t)}\left(\lambda(t)-\lambda(t)^{-2}\right)\\ &+\sum_{i=1}^{2}\int_0^t \chi_i(\tau)\phi_{B_i}(\tau,t,H(\tau,t))2\frac{dW_0}{dI_1}\bigg|_{H(\tau,t)}\left[\frac{\lambda(t)}{\lambda^2(\tau)}-\frac{\lambda(\tau)}{\lambda^2(t)}\right]d\tau,\end{aligned} \tag{13}$$

where $I_1 = \lambda^2(t) + \dfrac{2}{\lambda(t)}$. In an *ideal* tensile-relaxation test, *the stretch ratio is increased suddenly (at t = 0) to* $\lambda_0 > 1$ *and held constant for all t > 0.*

The nominal stress P decreases with time. Using Eq. (13), P in the direction of stretch is given by

$$P(t) = 2\left(\lambda_0 - \lambda_0^{-2}\right)\frac{dW_0}{dI_1}\bigg|_{I_1(\lambda_0)}\left\{\sum_{i=1}^{2}\rho_i\left[1+\frac{\alpha_{B_i}-1}{t_{B_i}}f_i\left(I_1(\lambda_0)\right)t\right]^{\frac{2-\alpha_{B_i}}{1-\alpha_{B_i}}}\right\}, \tag{14a}$$

where

$$I_1(\lambda_0) = \lambda_0^2 + \frac{2}{\lambda_0}, \qquad \rho_i = \frac{\chi_i^{ss} t_{B_i}}{2-\alpha_{B_i}}. \tag{14b,c}$$

Here ρ_i is the molar fraction of attached weak/strong bonds when the gel is in dynamic equilibrium. In an actual relaxation test, the stretch ratio is increased at a rapid but finite rate to reach λ_0. As a result, Eq. (14a) needs to be modified (see SI, Section S3.2).

In the SI (Section S4), we show that the relaxation modulus *G* in the small strain regime for a torsional relaxation test is given by

$$G = \mu \left\{ \sum_{i=1}^{2} \chi_i^{ss} \frac{t_{B_i}}{2-\alpha_{B_i}} \left[1 + \frac{\alpha_{B_i} - 1}{t_{B_i}} t \right]^{\frac{2-\alpha_{B_i}}{1-\alpha_{B_i}}} \right\}. \tag{15}$$

3. *Experimental Procedure:*

Materials: Anionic monomer p-styrenesulfonate (NaSS), cationic monomer 3-(methacryloylamino)- propyl-trimethylammonium chloride (MPTC), and photoinitiator α- ketoglutaric acid (α-keto) were purchased from Wako Pure Chemical Industries, Ltd., Japan. All chemicals were used without further purification, and deionized water was used in all experiments.

Gel Synthesis: The preparation process of tough PA gel was described in detail in our previous work[39]. In brief, the gel was synthesized by one-step random copolymerization of cationic and anionic monomers at a high concentration with balanced charges. First, an aqueous solution containing NaSS, MPTC, and α-keto was prepared at 50 °C. The total monomer concentration, C_m, was 2.1 M, and the molar ratio of NaSS/MPTC was 0.525:0.475. The concentration of α-keto was 0.25 mol %, relative to C_m. Then the solution was injected into a reaction cell consisting of two glasses separated by a 2 mm-thick spacer. UV polymerization was performed in an argon atmosphere for 11 h with a 365 nm UV light. The resulting gel was put into a large amount of water longer than one week to remove the counterions and unreacted

small chemicals. The equilibrated gel has a water content around 50 wt% and has high toughness.

Uniaxial Tensile Test: Gel samples for uniaxial tensile test were cut into a dumbbell-like shape according to JIS K 6261-7 standard. The gauge length, width, and thickness of samples were 12, 2, and 1.75 mm, respectively. Samples were loaded in tension by a Shimadzu autograph machine with a 100 N load cell. The measurement was conducted in a water vapor environment to prevent gel dehydration. Six strain rates were used: 0.0014, 0.0042, 0.014, 0.042, 0.14, and 0.42 s^{-1}. A maximum stretch ratio of 4.0 was used to avoid the structure damage to the phase structure[40]. Here, the nominal stress P is defined as the tensile force divided by the cross-section area of the undeformed sample. The stretch ratio λ is defined as the displacement divided by the gauge length of the undeformed sample. The strain rate is defined as the stretching speed divided by the gauge length of the undeformed sample.

Tensile Cyclic Test: The tensile cyclic test was performed with the same sample geometry and experimental device as that in the uniaxial tensile test. The samples were clamped and stretched to a predetermined λ of 3.0 at a constant strain rate. Then the clamp returned to the original position with a same or different constant strain rate without stopping at the peak stretch ratio. Six cyclic tests were performed with different combinations of loading/unloading rates: 0.14/0.14, 0.14/0.014, 0.14/0.0014, 0.0014/0.14, 0.0014/0.014, 0.0014/0.0014 s^{-1}.

Large Strain Tensile Relaxation Test: The large strain relaxation test was performed with the same sample geometry and experimental device as that in the uniaxial tensile test. Samples were stretched to a prescribed stretch ratio at a constant strain rate of 0.14 s^{-1} and then were held, and stress change was recorded. Four stretch ratios were used: 1.51, 2.01, 3.01, and 4.01.

Small Strain Torsional Relaxation Test: Gel samples for small strain relaxation test were cut into a disk shape with a diameter of 15.0 mm and a thickness of 1.75 mm. Samples were sheared to a strain (λ-1) of 0.5% within 0.03 s and then held fixed by an ARES rheometer in a parallel plate geometry. Samples were adhered to two plates by superglue to prevent them from slipping and surrounded by water to prevent

dehydration during the measurement. Prior to measurement, the built-in autostrain function of the ARES rheometer was used to minimize compression on the sample. Finally, it should be noted that the hydrogels we used in this work are in water-equilibrated state. So, there is no excess water flow between gel and water or water vapor during the measurement.

4. *Estimate of Material Parameters:*

Our PA gel constitutive model has 13 unknown independent material parameters in total. These unknown parameters are listed below in Table 1.

Table 1: Summary of material parameters for PA gel constitutive model.

Steady state parameters						
α_{B_1}	t_{B_1}	t_{H_1}	α_{B_2}	t_{B_2}	t_{H_2}	ω_1 or ω_2
Strain dependent accelerated breaking function parameters, f						
m_1		m_2		λ_c		
Undamaged network strain energy density function, Yeoh's model, W_0						
$c_1 \equiv \mu/2$		c_2/c_1		c_3/c_1		

Some of the material parameters in Table 1 can be estimated using uniaxial tension and tensile-relaxation experimental data. These estimates serve as initial conditions or bounds for the least square optimization process discussed in Section 5. The least squares method provides us multiple local optimums; these estimates guide us in selecting an optimal parameter set which is close to the physical properties of the gel. Once the material parameters in Table 1 are found, molar fractions of the connected physical bonds in dynamic equilibrium (ρ_1 or ρ_2), steady state healing rates of the physical bonds (χ_1^{ss} or χ_2^{ss}), and small strain instantaneous shear modulus of PA gel ($\mu\rho_1 + \mu\rho_2$) can be determined using Eqs. (8) and (14c). In the following Section 4.1, we show how a relaxation test can be used to estimate $\mu\rho_1 + \mu\rho_2$. An estimate of the critical stretch ratio λ_c or I_c can be determined from tensile data. The procedure to determine these estimates is described below.

4.1 Estimate for small strain shear modulus

The nominal stress in uniaxial tension test is given by Eq. (13). For small times and small strains, the fraction of physical bonds connected in the material are almost the same as their steady state fractions (ρ_1 or ρ_2), and the very few newly formed bonds hardly carry any load. Mathematically, this means that integral term in the Eq. (13) is small in comparison with the first term. Since strains are small at short times, we neglect strain hardening and strain dependent breaking, resulting in

$$P(t) \approx \left(\sum_{i=1}^{2} \rho_i\right) \mu \left(\lambda(t) - \left[\lambda(t)\right]^{-2}\right), \quad \text{as } 2\left.\frac{dW_0}{dI_1}\right|_{I_1(t)} \approx \mu \text{ (at low strains)},$$
$$\approx \left(\sum_{i=1}^{2} \rho_i\right) 3\mu\varepsilon, \tag{16}$$

for short times and sufficiently fast loading rate. Eq. (16) implies that the instantaneous Young's modulus E_0, measured using the initial slope of the nominal stress –strain curve, is related to $\mu\sum_{i=1}^{2}\rho_i$ by

$$E_0 = 3\mu\sum_{i=1}^{2}\rho_i \,. \tag{17}$$

Hence, we can use the loading portion of relaxation test to determine $\mu\sum_{i=1}^{2}\rho_i$. This is illustrated in Fig. 1.

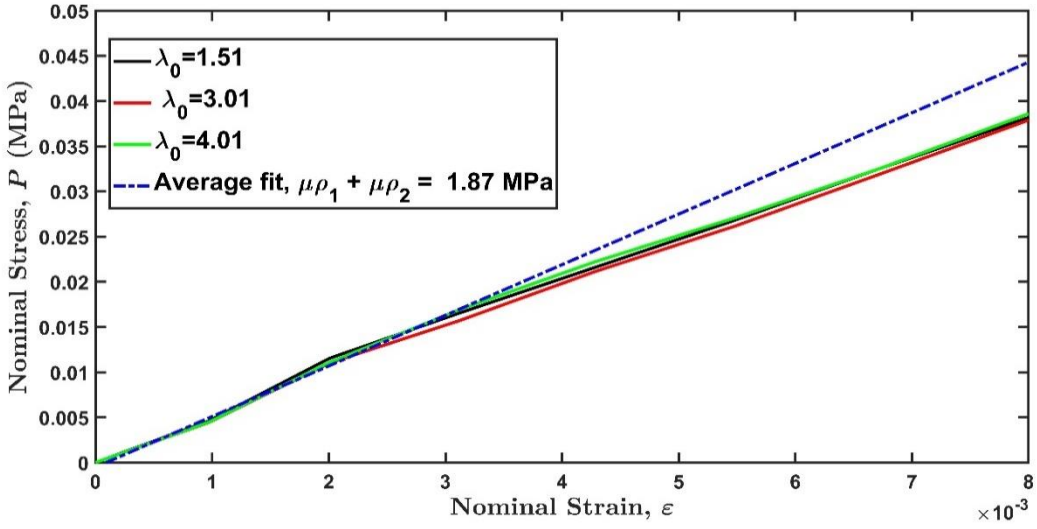

Fig. 1. Fitting the initial slope of nominal stress – nominal strain plots from three tensile-relaxation tests carried out at three stretch ratios λ_0 (solid lines). The experimental plots shown here are from the loading part of three tensile relaxation tests of the same data set. Note that all three relaxation tests fall on the same line at small strains (less than 0.3%). The small strain instantaneous shear modulus is $\mu\rho_1 + \mu\rho_2 \approx 1.87$ MPa (1/3 of the slope of the dotted blue line).

4.2 Estimate for critical stretch ratio λ_c

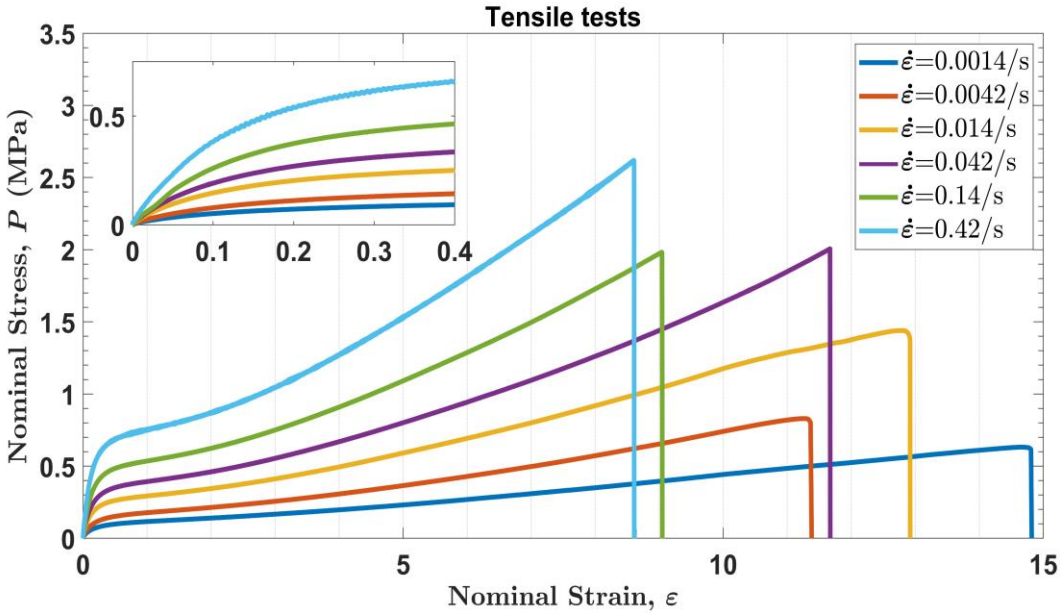

Fig. 2. Uniaxial tension test data for purely physical PA-gel for different strain rates $\left(\dot{\varepsilon} \equiv \dot{\lambda}\right)$.

Fig. 2 shows that the slope of nominal stress versus nominal strain decreases rapidly after a critical strain around 15% is reached. The inset shows that although stress increases rapidly with the strain rate, the critical strain where "yielding" occurs is insensitive to strain rate. This behavior is reflected in Eq. (5) where we propose that breaking kinetics is controlled by strain experienced by the network. The procedure of determining the estimate of critical stretch ratio λ_c is mentioned in SI (Section S6). We found that λ_c lies between 1.1 to 1.3. Within this range, the fitting result of nominal stress is not particularly sensitive to λ_c.

The inset in Fig. 2 seems to suggest that the instantaneous modulus E_0 is dependent on the loading rate. In theory, all the curves in Fig. 2 at *very short time* should have the same slope. In practice, the loading rate needs to be sufficiently fast for the strains to be measurable. The strains in the insert in Fig. 2 are too large to see this effect. In Fig. 1, all the tensile-relaxation tests for different stretch ratios are loaded at *a fast rate* of 0.14/s, and we notice that at *small strains* (in the order of 10^{-3}) all the curves fall on the same line suggesting the accuracy of data.

5. *Least squares error optimization method*

We use least squares error optimization to determine the 13 unknown material parameters in Table 1. First, we select data from three data sets (simple tension, relaxation, and cyclic tests). Fig. 3 shows some representative data. In these plots, loading and unloading rates are denoted by LR and UR respectively. Experimental data are solid black lines. The basic idea is to choose parameters so that model prediction of nominal stress minimizes the least squares error at selected points, indicated by blue dotted circles in Fig. 3. More data points are chosen in regions where the slope of the stress-strain curve changes rapidly. In cyclic and simple tension tests, *xdata* is a vector consisting of selected nominal stretch values and *ydata* is the corresponding experimental nominal stress values. In tensile-relaxation tests, *xdata* is a vector storing selected time points and *ydata* is the corresponding experimental

nominal stress values. Let $\boldsymbol{\eta}$ denote a vector of 13 material parameters, our goal is to determine $\boldsymbol{\eta}$ which minimizes the objective function:

$$\sum_i \left(\mathcal{F}(\boldsymbol{\eta}, xdata_i) - ydata_i\right)^2, \quad lb \le \boldsymbol{\eta} \le ub. \qquad (18)$$

The lower and upper bonds on $\boldsymbol{\eta}$ are denoted by *lb* and *ub* respectively. The notation $\mathcal{F}$ refers to the solution of the nominal stress equation in either loading-unloading or simple tension or tensile-relaxation test. $\mathcal{F}(\boldsymbol{\eta}, xdata_i)$ in Eq. (18) is determined using a *lsqcurvefit* inbuilt function with *trust-region-reflective* algorithm in *MATLAB 2018a* version. In the optimization process, it is possible to find multiple data sets that have similar least squares error (less than 10 percent average error between simulated result and experimental stress data).

We find a set of optimal parameters by replacing the history dependent reattachment rates $\left(\chi_1(t) \text{ or } \chi_2(t)\right)$ with the steady state values $\left(\chi_1^{ss} \text{ or } \chi_2^{ss}\right)$. This reduces the computing time of $\mathcal{F}(\boldsymbol{\eta}, xdata_i)$, as we avoid solving the integral equation (Eq. (9)). Using this set of optimal parameters, we recalculate $\mathcal{F}(\boldsymbol{\eta}, xdata_i)$ using the full theory (solving the Eq. (9)) to check whether the results are within the error bound (less than 10 percent average error between simulated result and experimental stress data). Details of these calculations are given in the SI (Section S5). In all cases, we found that these assumptions give material parameters that are consistent with experimental data.

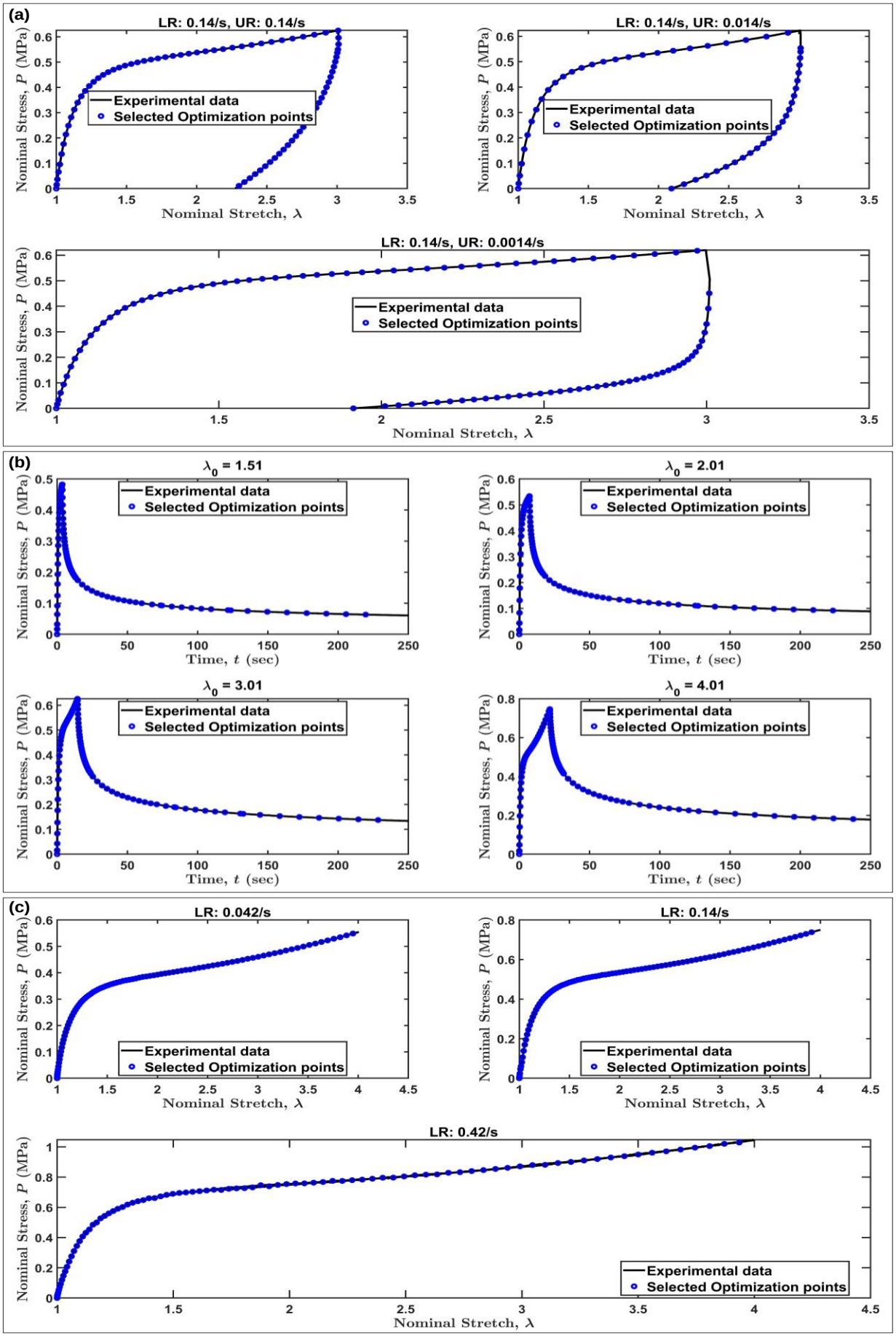
(a)
LR: 0.14/s, UR: 0.14/s
LR: 0.14/s, UR: 0.014/s
LR: 0.14/s, UR: 0.0014/s
Experimental data
Selected Optimization points
Nominal Stress, P (MPa)
Nominal Stretch, λ
(b)
λ0 = 1.51
λ0 = 2.01
λ0 = 3.01
λ0 = 4.01
Time, t (sec)
(c)
LR: 0.042/s
LR: 0.14/s
LR: 0.42/s

Fig. 3. Selected plots from three data sets: (a) cyclic tests, (b) tensile-relaxation tests, and (c) simple tension tests. We optimize 13 material parameters in Table 1 to get the minimum least squares error in nominal stress from all these plots (see SI, Section S5 for the entire data set use in optimization). Here LR and UR denotes loading and unloading rates respectively.

Table 2 summarizes the parameters we determined using the optimization process. We notice from Table 2 that the characteristic breaking time of strong bonds is almost ten times the breaking time of weak bonds. Furthermore, the characteristic healing time of the strong bonds is almost twice the characteristic healing time of weak bonds. We also note from Table 3 that the healing rate of strong bonds is less than half of healing rate of weak bonds. This is reasonable as the strong bonds break and reattach at a slower pace. As a consequence, using Eq. (14c) we get $\rho_2 > \rho_1$ (see Table 3). Table 2 also shows $m_1 < m_2$, which implies that the breaking of weak bonds is less dependent on strain when compared to the strong bonds.

Table 2: The independent material parameters determined using least squares optimisation process.

Steady state parameters						
$\alpha_{B_1} =$ 1.7712	$t_{B_1} =$ 0.0031s	$t_{H_1} =$ 0.1276s	$\alpha_{B_2} =$ 1.7441	$t_{B_2} =$ 0.0324s	$t_{H_2} =$ 0.2038s	$\omega_1 = 1-\omega_2$ = 0.5016
Strain dependent accelerated breaking function parameters, f						
$m_1 =$ 0.4606		$m_2 =$ 0.5845		$\lambda_c =$ 1.1226		
Undamaged network strain energy density function, Yeoh's model, W_0						
$c_1 \equiv \mu/2 =$ 4.6929 MPa		$c_2/c_1 = 0.4485$		$c_3/c_1 = 0.2100$		

Using the material parameter values in Table 2, the rest of the parameters are computed and shown below.

Table 3: The dependent material parameters determined using values from Table 2.

Steady state healing rates (from Eq. (8))	
$\chi_1^{ss} = 3.5583\ s^{-1}$	$\chi_2^{ss} = 1.5088\,s^{-1}$
Molar fraction of connected physical bonds in dynamic equilibrium (from Eq. (14c))	
$\rho_1 = 0.0476$	$\rho_2 = 0.1908$
Small strain shear modulus	

$$\mu\rho_1 + \mu\rho_2 \equiv \frac{E_0}{3} = 2.2376\,\text{MPa}$$

As a check on the validity of the parameters, we note that the values of small strain instantaneous shear modulus ($\mu(\rho_1+\rho_2)$) and critical stretch ratio (λ_c) from Table 2 and Table 3 are consistent with the estimates obtained from experimental data in Section 4.

6. *Results and Discussion*

We compare modeling results with experimental data from cyclic tension, tensile relaxation and simple tension tests. Modeling results are determined using parameters in Table 2 and solving Eq. (13) and Eq. (9) for the nominal stress and the healing rates respectively.

6.1 Cyclic tests

Fig. 4 compares experimental data with model. Experiments consists of uniaxial tension cyclic test with different loading (LR) and unloading rates (UR). Fig. 4 shows that our model predicts the experimental data well for all cases. For very small loading rates of 0.0014/s, our model slightly overestimates the nominal stress in the loading phase.

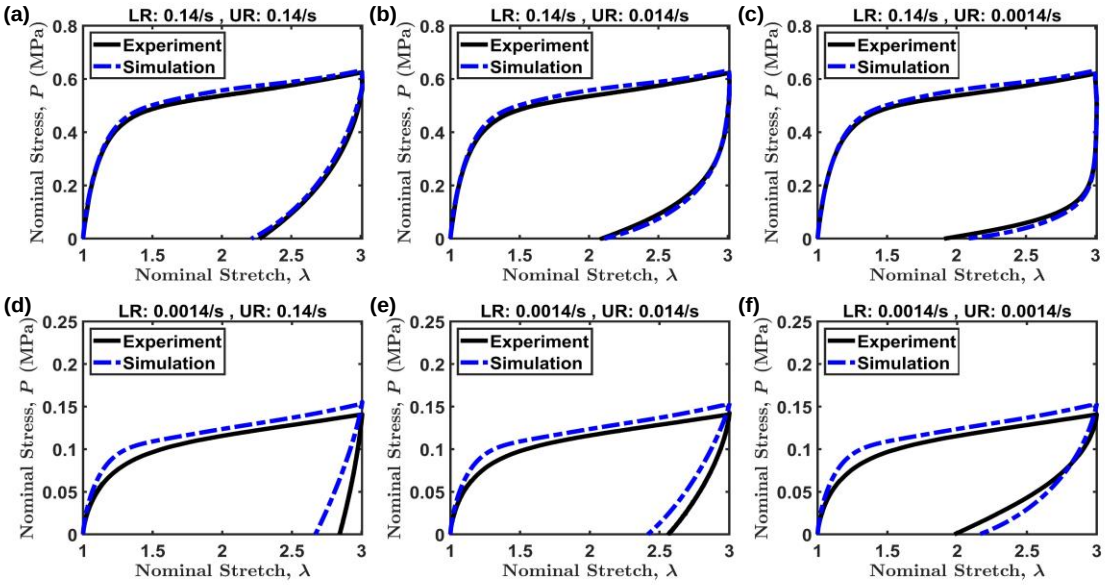

Fig. 4. Nominal stress P (MPa) vs nominal stretch λ for loading and unloading tests with different strain rates. (a), (b), and (c): The upper plots have a loading rate (LR) of 0.14/s and unloading rates (UR) of 0.14/s, 0.014/s, and 0.0014/s from left to right respectively. (d), (e), and (f): Similarly, the lower plots have a loading rate of 0.0014/s and unloading rates of 0.14/s, 0.014/s, and 0.0014/s from left to right respectively. Experiments are shown as solid black lines and dashed blue lines are model predictions using parameters in Table 2.

6.2 Tensile-Relaxation tests

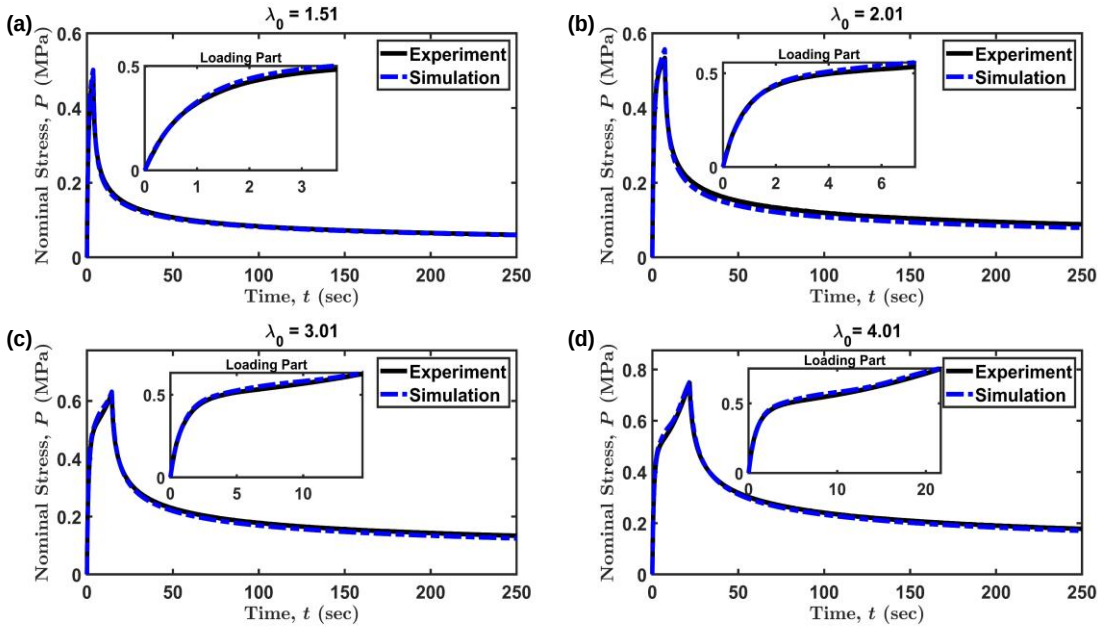

Fig. 5. Nominal stress P (MPa) vs time t (sec) for tensile-relaxation tests with different nominal stretch ratios. Experiments are solid black lines and dashed blue lines are model predictions using parameters in Table 2. Insets show the loading part of the test. Relaxation tests are carried out using 4 stretch ratios (a) $\lambda_0 = 1.51$, (b) $\lambda_0 = 2.01$, (c) $\lambda_0 = 3.01$, and (d) $\lambda_0 = 4.01$.

Fig. 5 plots show that our model (blue dashed lines) is in excellent agreement with experimental data in both the loading and the relaxation phases $(\lambda_0 \approx 1.5-4)$.

6.3 Simple Tension

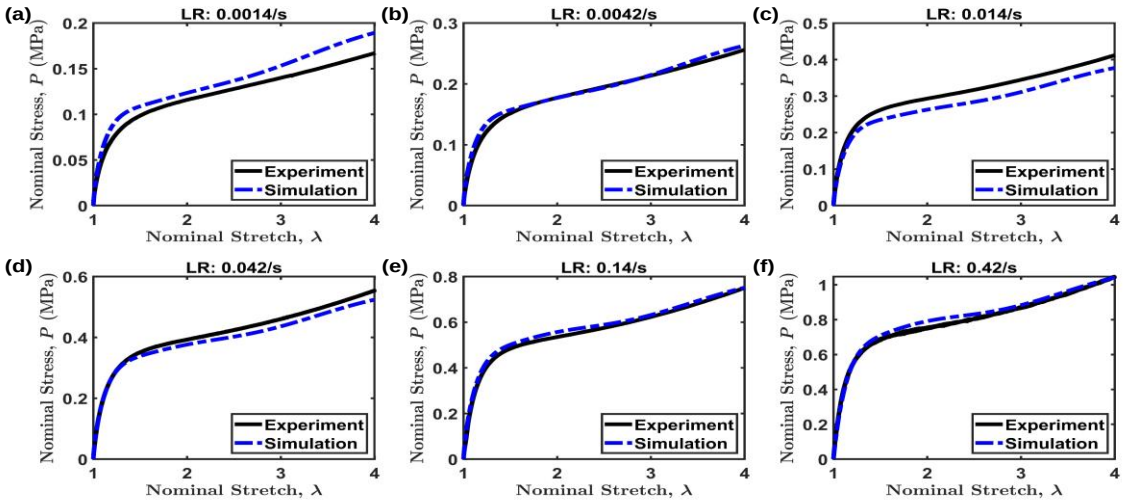

Fig. 6. Nominal stress P (MPa) vs nominal stretch λ for simple tension tests with 5 loading rates (LR) (a) 0.0014/s, (b) 0.0042/s, (c) 0.014/s, (d) 0.042/s, (e) 0.14/s, and (f) 0.42/s. The Solid black lines are experiments and dashed blue lines are model predictions using parameters in Table 2.

Fig. 6 presents simple tension tests with 6 different loading rates covering 2 decades. Our model predicts the experimental data very well for the loading rates of 0.0042/s, 0.14/s, and 0.42/s cases. For the loading rates 0.0014/s and 0.014/s, the model did not do as well. Nevertheless, for LR = 0.0014/s, the relative error between theory and experiment is less than 10%. For LR = 0.042/s, we slightly underestimate the stress, the relative error between theory and experiments is less than 6%.

6.4 Time dependent healing rate ($\chi_1(t)$ or $\chi_2(t)$)

The time evolution of the healing rate during the mechanical loading for select loading-unloading and tensile-relaxation tests is shown in Fig. 7. Red and blue lines denote the healing rates for weak and strong bonds respectively. These results are obtained by solving the integral equation (Eq. (9)) using the material parameters in Table 2. For both tests the healing rate increases until the end of loading and then starts to decrease.

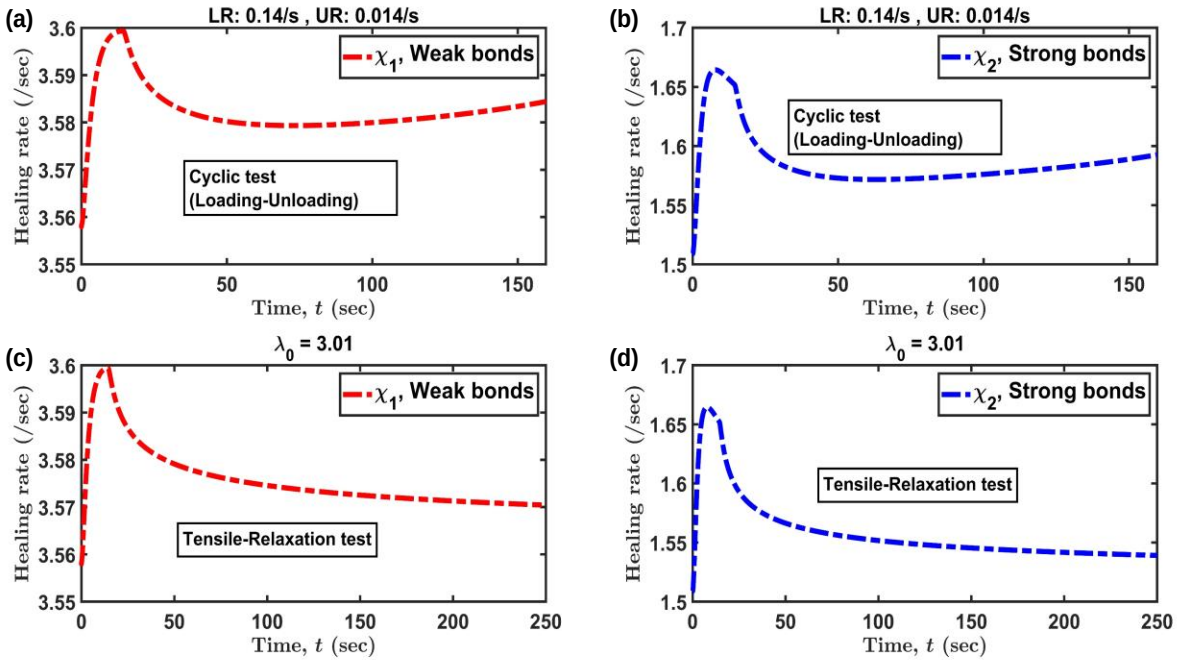

Fig. 7. Healing rate ($\chi_1(t)$ or $\chi_2(t)$) (/s) for weak (red dotted lines) and strong bonds (blue dotted lines) vs time (s) for two types of mechanical testing. (a) and (b): The two upper plots are loading-unloading tests with a loading rate (LR) of 0.14/s and unloading rate (UR) of 0.014/s. (c) and (d): The two lower plots are tensile-relaxation tests with a nominal stretch ratio of $\lambda_0 \approx 3$.

Fig. 7 plots show that the time dependent healing rates for both weak ($\chi_1(t)$) and strong bonds ($\chi_2(t)$) for cyclic and tensile-relaxation loading histories. Here we present only two loading histories, but the general behavior is similar for other loading histories: the healing rate of weak or strong bonds increases until maximum load and there is a drop in the healing rate after that. During unloading, less chains are stretched which decreases the breaking rate of bonds and less increase in the fraction of the broken bonds during this phase. Therefore, the healing rates for both strong and weak bonds change only slightly during the unloading phase. During relaxation, bonds are broken and healed, but the newly healed bonds do not carry load, so the stress carried by physical bonds gradually decreases (see also Fig. 8(b)). These results suggest a simple way to improve the efficiency of the optimization procedure. Since solving the integral equation is time consuming, one may assume that the healing rate is given

by the steady state healing rate in the optimization process. We found this procedure hardly changes the fitting.

6.5 Load bearing characteristics of strong and weak bonds

The stress contributions from strong and weak bonds are shown in Fig. 8 for different loading histories. The general trend can be captured by selecting one case from each of the three loading histories (simple tension, relaxation and cyclic). Table 2 and Table 3 indicate that $m_1 < m_2$, implying that the breaking of weak bonds depend less on strain when compared to strong bonds. Also, since $\chi_1^{ss} > \chi_2^{ss}$, weak bonds heal more than twice as fast as strong bonds. These suggest that the stress contribution from weak bonds is higher than strong bonds at higher stretch ratios and lower at low stretch ratios, as shown in the simple tension data (Fig. 8(b)). This is because at high stretch ratios, the number of broken strong bonds increases much faster than the number of broken weak bonds (see SI, Section S7). On the other hand, the weak bonds heal much faster than the strong bonds, so they bear more of the applied load. A similar trend can be observed for different types of loadings (tensile, tensile-relaxation and cyclic test).

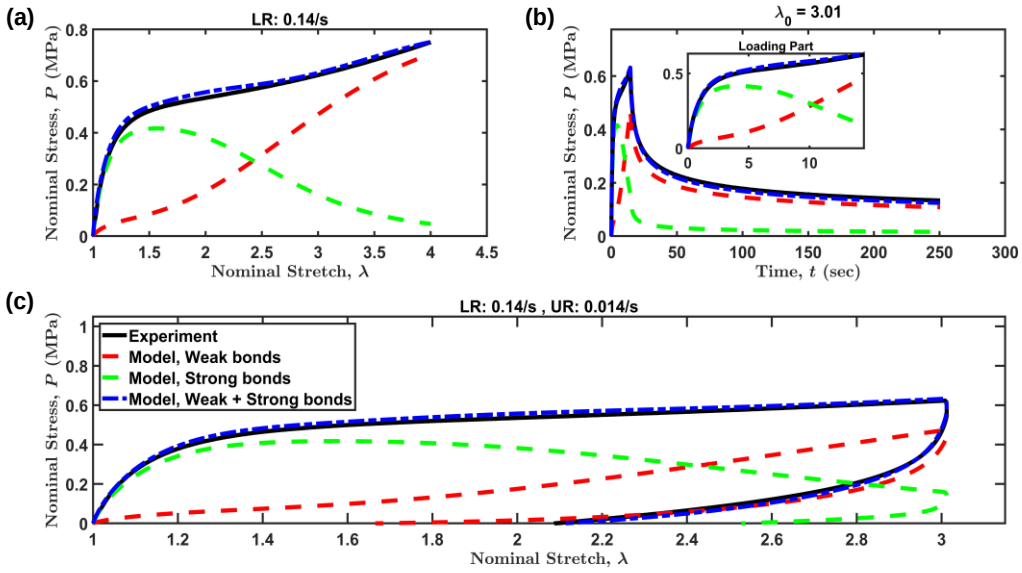

Fig. 8. Stress contributions from physical bonds computed using our model for different loading histories: (a) simple tension, (b) tensile-relaxation, and (c) cyclic test. The tensile test is carried out using a loading rate (LR) of 0.14/s. The stretch ratio in the tensile-relaxation test is $\lambda_0 \approx 3$. The cyclic test has a loading rate (LR) of 0.14/s and an unloading rate (UR) of 0.014/s. Experimental data is indicated by solid black lines, the stress contribution from weak bonds are red dotted lines, the stress contribution from strong bonds are green dotted lines, and total stress contribution from physical bonds (weak + strong) are blue dash-dotted lines.

6.6 Small strain torsional relaxation test

The constitutive model is expected to work for multi-axial state of stress and strain. Although the main focus of this work is on uniaxial tension behavior, it is interesting to see whether the same parameters in Table 2 can capture the shear stress measured in a small strain torsional rheology test, which is commonly used to study viscoelastic behavior. Fig. 9 shows two small strain relaxation tests in torsion (solid lines). In this test, the sample is twisted rapidly to a shear strain of $\varepsilon_0 = 0.005$. The relaxation modulus $G(t)$ of two experiments are shown as solid lines in Fig. 9. These experimental results are compared to the small strain relaxation modulus given by Eq. (15) which is plotted as a blue dashed line.

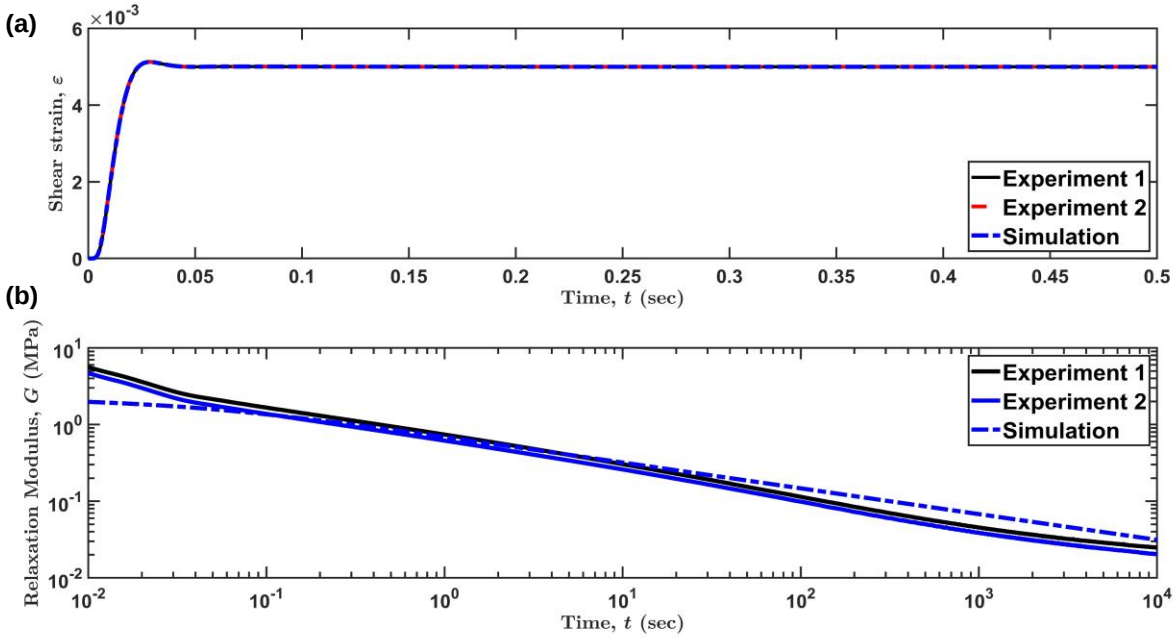

Fig. 9. The sample is sheared to a strain of 0.005 in a torsional relaxation test. (a) Shear strain vs time for short times. This figure shows that the desired strain is

achieved at 30-40 milli seconds. (b) Relaxation modulus, G (MPa) vs time, t (sec) is shown. The solid lines are experiments (same test repeated) and the dashed blue line is model prediction Eq. (15) based on Table 2.

Our model underestimates the modulus for $t < 0.1\text{s}$. This is because we used Eq. (15) which models an ideal relaxation test where the desired strain ($\varepsilon_0 = 0.5\%$ in Fig. 9) is achieved instantaneously. However, in the experiment, this strain is achieved at around 30-40 milli-seconds. The discrepancy of Eq. (15) and experimental data during short times can be attributed to this finite rate effect.

7. Conclusions

We developed a rate and strain dependent bond breaking/reforming constitutive model to quantify the mechanical behavior of a physically crosslinked PA gel. The predictions from our model are validated by comparing with uniaxial tension, tensile-relaxation, cyclic (loading-unloading), and small strain rheology tests. The comparisons between the theoretical predictions and experimental data are generally good. We found some discrepancies between theory and experiment in simple tension tests where the loading is slow. As noted by an anonymous reviewer, this discrepancy can be caused by the fact that the critical stretch ratio is not exactly a constant or independent of strain rate. Another possibility could be our choice of accelerated breaking function which tends to shift the "yield point" slightly depending on the loading rate and this contradicts the assumption the critical stretch is a constant. These are possibilities that we will consider in the future.

The main difficulty is that there are 13 material parameters in our model and there is no simple experimental procedure to determine all of them. There are also limitations in our model. For example, we assume the stress sustained by a temporary chain is instantaneously relaxed when one of the connecting bond breaks, and that immediately after a temporary chain is reattached, it is in a relaxed state and carries no strain energy (Assumption 4). This scenario may not be true at high loading rates where newly broken bonds may still carry load and newly reattached chains may still carry some strain energy. In addition, most of our experiments are performed in uniaxial tension so our model may not work well in multi-axial loading. An extensive

validation of our theory will be conducted in future works by subjecting the gel to more complex multi-axial loading histories.

Acknowledgements

This material is based upon work supported by the National Science Foundation under Grant No. CMMI-1903308. J.P.G. acknowledges support from the Japan Society for the Promotion of Science KAKENHI (grant no. JP17H06144). K.P.C. acknowledges support from the Japan Society for the Promotion of Science KAKENHI (grant no. JP19K23617). J.P.G. and K. P. C. acknowledge support from the Institute for Chemical Reaction Design and Discovery by World Premier International Research Initiative, MEXT, Japan. The authors would like to thank two anonymous reviewers for suggestions.

REFERENCES

[1] L.J. Suggs, E.Y. Kao, L.L. Palombo, R.S. Krishnan, M.S. Widmer, A.G. Mikos, Preparation and characterization of poly(propylene fumarate-co-ethylene glycol) hydrogels, Journal of Biomaterials Science, Polymer Edition. 9 (1998) 653–666. https://doi.org/10.1163/156856298X00073.

[2] C.K. Kuo, P.X. Ma, Ionically crosslinked alginate hydrogels as scaffolds for tissue engineering: Part 1. Structure, gelation rate and mechanical properties, Biomaterials. 22 (2001) 511–521. https://doi.org/10.1016/S0142-9612(00)00201-5.

[3] K.Y. Lee, D.J. Mooney, Hydrogels for Tissue Engineering, Chemical Reviews. 101 (2001) 1869–1880. https://doi.org/10.1021/cr000108x.

[4] Haesun. Park, Kinam. Park, Waleed.S. Shalaby, Biodegradable hydrogels for drug delivery, 1993.

[5] Y. Qiu, K. Park, Environment-sensitive hydrogels for drug delivery, Advanced Drug Delivery Reviews. 64 (2012) 49–60. https://doi.org/10.1016/j.addr.2012.09.024.

[6] H.J. Kwon, K. Yasuda, J.P. Gong, Y. Ohmiya, Polyelectrolyte hydrogels for replacement and regeneration of biological tissues, Macromolecular Research. 22 (2014) 227–235. https://doi.org/10.1007/s13233-014-2045-6.

[7] H.J. Kwon, Tissue Engineering of Muscles and Cartilages Using Polyelectrolyte Hydrogels, Advances in Materials Science and Engineering. 2014 (2014) 1–7. https://doi.org/10.1155/2014/154071.

[8] J.P. Gong, Y. Katsuyama, T. Kurokawa, Y. Osada, Double-network hydrogels with extremely high mechanical strength, Advanced Materials. 15 (2003) 1155–1158. https://doi.org/10.1002/adma.200304907.

[9] A. Nakayama, A. Kakugo, J.P. Gong, Y. Osada, M. Takai, T. Erata, S. Kawano, High Mechanical Strength Double-Network Hydrogel with Bacterial Cellulose, Advanced Functional Materials. 14 (2004) 1124–1128. https://doi.org/10.1002/adfm.200305197.

[10] Y.-H. Na, Y. Tanaka, Y. Kawauchi, H. Furukawa, T. Sumiyoshi, J.P. Gong, Y. Osada, Necking Phenomenon of Double-Network Gels, Macromolecules. 39 (2006) 4641–4645. https://doi.org/10.1021/ma060568d.

[11] R.E. Webber, C. Creton, H.R. Brown, J.P. Gong, Large strain hysteresis and mullins effect of tough double-network hydrogels, Macromolecules. 40 (2007) 2919–2927. https://doi.org/10.1021/ma062924y.

[12] H.R. Brown, A model of the fracture of double network gels, Macromolecules. 40 (2007) 3815–3818. https://doi.org/10.1021/ma062642y.

[13] J.P. Gong, Why are double network hydrogels so tough?, Soft Matter. 6 (2010) 2583–2590. https://doi.org/10.1039/b924290b.

[14] X. Wang, W. Hong, Pseudo-elasticity of a double network gel, Soft Matter. 7 (2011) 8576. https://doi.org/10.1039/c1sm05787a.

[15] T. Nakajima, T. Kurokawa, S. Ahmed, W. Wu, J.P. Gong, Characterization of internal fracture process of double network hydrogels under uniaxial elongation, Soft Matter. 9 (2013) 1955–1966. https://doi.org/10.1039/C2SM27232F.

[16] K.J. Henderson, T.C. Zhou, K.J. Otim, K.R. Shull, Ionically Cross-Linked Triblock Copolymer Hydrogels with High Strength, Macromolecules. 43 (2010) 6193–6201. https://doi.org/10.1021/ma100963m.

[17] W.-C. Lin, W. Fan, A. Marcellan, D. Hourdet, C. Creton, Large Strain and Fracture Properties of Poly(dimethylacrylamide)/Silica Hybrid Hydrogels, Macromolecules. 43 (2010) 2554–2563. https://doi.org/10.1021/ma901937r.

[18] M.A. Haque, T. Kurokawa, G. Kamita, J.P. Gong, Lamellar bilayers as reversible sacrificial bonds to toughen hydrogel: Hysteresis, self-recovery, fatigue resistance, and

crack blunting, Macromolecules. 44 (2011) 8916–8924. https://doi.org/10.1021/ma201653t.
[19] J.-Y. Sun, X. Zhao, W.R.K. Illeperuma, O. Chaudhuri, K.H. Oh, D.J. Mooney, J.J. Vlassak, Z. Suo, Highly stretchable and tough hydrogels., Nature. 489 (2012) 133–6. https://doi.org/10.1038/nature11409.
[20] K. Mayumi, A. Marcellan, G. Ducouret, C. Creton, T. Narita, Stress–Strain Relationship of Highly Stretchable Dual Cross-Link Gels: Separability of Strain and Time Effect, ACS Macro Letters. 2 (2013) 1065–1068. https://doi.org/10.1021/mz4005106.
[21] T. Narita, K. Mayumi, G. Ducouret, P. Hébraud, Viscoelastic Properties of Poly(vinyl alcohol) Hydrogels Having Permanent and Transient Cross-Links Studied by Microrheology, Classical Rheometry, and Dynamic Light Scattering, Macromolecules. 46 (2013) 4174–4183. https://doi.org/10.1021/ma400600f.
[22] N.M. Ames, V. Srivastava, S.A. Chester, L. Anand, A thermo-mechanically coupled theory for large deformations of amorphous polymers. Part II: Applications, International Journal of Plasticity. 25 (2009) 1495–1539. https://doi.org/10.1016/j.ijplas.2008.11.005.
[23] L. Anand, N.M. Ames, V. Srivastava, S.A. Chester, A thermo-mechanically coupled theory for large deformations of amorphous polymers. Part I: Formulation, International Journal of Plasticity. 25 (2009) 1474–1494. https://doi.org/10.1016/j.ijplas.2008.11.004.
[24] X. Zhao, A theory for large deformation and damage of interpenetrating polymer networks, Journal of the Mechanics and Physics of Solids. 60 (2012) 319–332. https://doi.org/10.1016/j.jmps.2011.10.005.
[25] H. Cho, R.G. Rinaldi, M.C. Boyce, Constitutive modeling of the rate-dependent resilient and dissipative large deformation behavior of a segmented copolymer polyurea, Soft Matter. 9 (2013) 6319–6330. https://doi.org/10.1039/c3sm27125k.
[26] X. Zhao, Multi-scale multi-mechanism design of tough hydrogels: building dissipation into stretchy networks, Soft Matter. 10 (2014) 672–687. https://doi.org/10.1039/C3SM52272E.
[27] Y. Liu, H. Zhang, Y. Zheng, A Micromechanically Based Constitutive Model for the Inelastic and Swelling Behaviors in Double Network Hydrogels, Journal of Applied Mechanics. 83 (2016). https://doi.org/10.1115/1.4031897.
[28] T. Lu, J. Wang, R. Yang, T.J. Wang, A Constitutive Model for Soft Materials Incorporating Viscoelasticity and Mullins Effect, Journal of Applied Mechanics. 84 (2017). https://doi.org/10.1115/1.4035180.
[29] Y. Mao, S. Lin, X. Zhao, L. Anand, A large deformation viscoelastic model for double-network hydrogels, Journal of the Mechanics and Physics of Solids. 100 (2017) 103–130. https://doi.org/10.1016/j.jmps.2016.12.011.
[30] V.N. Khiêm, T.-T. Mai, K. Urayama, J.P. Gong, M. Itskov, A Multiaxial Theory of Double Network Hydrogels, Macromolecules. 52 (2019) 5937–5947. https://doi.org/10.1021/acs.macromol.9b01044.
[31] R. Huang, S. Zheng, Z. Liu, T.Y. Ng, Recent Advances of the Constitutive Models of Smart Materials — Hydrogels and Shape Memory Polymers, International Journal of Applied Mechanics. 12 (2020) 2050014. https://doi.org/10.1142/S1758825120500143.
[32] R. Long, K. Mayumi, C. Creton, T. Narita, C.Y. Hui, Time dependent behavior of a dual cross-link self-healing gel: Theory and experiments, Macromolecules. 47 (2014) 7243–7250. https://doi.org/10.1021/ma501290h.
[33] R. Long, K. Mayumi, C. Creton, T. Narita, C.-Y. Hui, Rheology of a dual crosslink self-healing gel: Theory and measurement using parallel-plate torsional rheometry, Journal of Rheology. 59 (2015) 643–665. https://doi.org/10.1122/1.4915275.

[34] J. Guo, R. Long, K. Mayumi, C.Y. Hui, Mechanics of a Dual Cross-Link Gel with Dynamic Bonds: Steady State Kinetics and Large Deformation Effects, Macromolecules. 49 (2016) 3497–3507. https://doi.org/10.1021/acs.macromol.6b00421.
[35] A. Ghatak, K. Vorvolakos, H. She, D.L. Malotky, M.K. Chaudhury, Interfacial Rate Processes in Adhesion and Friction, The Journal of Physical Chemistry B. 104 (2000) 4018–4030. https://doi.org/10.1021/jp9942973.
[36] M.K. Beyer, H. Clausen-Schaumann, Mechanochemistry: The Mechanical Activation of Covalent Bonds, Chemical Reviews. 105 (2005) 2921–2948. https://doi.org/10.1021/cr030697h.
[37] S.R. Lavoie, R. Long, T. Tang, A rate-dependent damage model for elastomers at large strain, Extreme Mechanics Letters. 8 (2016) 114–124. https://doi.org/10.1016/j.eml.2016.05.016.
[38] K. Yu, A. Xin, Q. Wang, Mechanics of self-healing polymer networks crosslinked by dynamic bonds, Journal of the Mechanics and Physics of Solids. 121 (2018) 409–431. https://doi.org/10.1016/j.jmps.2018.08.007.
[39] T.L. Sun, T. Kurokawa, S. Kuroda, A. Bin Ihsan, T. Akasaki, K. Sato, M.A. Haque, T. Nakajima, J.P. Gong, Physical hydrogels composed of polyampholytes demonstrate high toughness and viscoelasticity, Nature Materials. 12 (2013) 932–937. https://doi.org/10.1038/nmat3713.
[40] K. Cui, T.L. Sun, X. Liang, K. Nakajima, Y.N. Ye, L. Chen, T. Kurokawa, J.P. Gong, Multiscale Energy Dissipation Mechanism in Tough and Self-Healing Hydrogels, Physical Review Letters. 121 (2018) 185501. https://doi.org/10.1103/PhysRevLett.121.185501.
[41] K. Cui, Y.N. Ye, T.L. Sun, L. Chen, X. Li, T. Kurokawa, T. Nakajima, T. Nonoyama, J.P. Gong, Effect of Structure Heterogeneity on Mechanical Performance of Physical Polyampholytes Hydrogels, Macromolecules. 52 (2019) 7369–7378. https://doi.org/10.1021/acs.macromol.9b01676.
[42] K. Cui, Y.N. Ye, T.L. Sun, C. Yu, X. Li, T. Kurokawa, J.P. Gong, Phase Separation Behavior in Tough and Self-Healing Polyampholyte Hydrogels, Macromolecules. 53 (2020) 5116–5126. https://doi.org/10.1021/acs.macromol.0c00577.
[43] K. Cui, Y.N. Ye, C. Yu, X. Li, T. Kurokawa, J.P. Gong, Stress Relaxation and Underlying Structure Evolution in Tough and Self-Healing Hydrogels, ACS Macro Lett. (2020) 1582–1589. https://doi.org/10.1021/acsmacrolett.0c00600.
[44] X. Li, K. Cui, T.L. Sun, L. Meng, C. Yu, L. Li, C. Creton, T. Kurokawa, J.P. Gong, Mesoscale bicontinuous networks in self-healing hydrogels delay fatigue fracture, Proc Natl Acad Sci USA. 117 (2020) 7606–7612. https://doi.org/10.1073/pnas.2000189117.
[45] A.B. Ihsan, T.L. Sun, T. Kurokawa, S.N. Karobi, T. Nakajima, T. Nonoyama, C.K. Roy, F. Luo, J.P. Gong, Self-Healing Behaviors of Tough Polyampholyte Hydrogels, Macromolecules. 49 (2016) 4245–4252. https://doi.org/10.1021/acs.macromol.6b00437.
[46] C.K. Roy, H.L. Guo, T.L. Sun, A.B. Ihsan, T. Kurokawa, M. Takahata, T. Nonoyama, T. Nakajima, J.P. Gong, Self-Adjustable Adhesion of Polyampholyte Hydrogels, Adv. Mater. 27 (2015) 7344–7348. https://doi.org/10.1002/adma.201504059.
[47] D.R. King, T.L. Sun, Y. Huang, T. Kurokawa, T. Nonoyama, A.J. Crosby, J.P. Gong, Extremely tough composites from fabric reinforced polyampholyte hydrogels, Mater. Horiz. 2 (2015) 584–591. https://doi.org/10.1039/C5MH00127G.
[48] Guo, Jingyi, Constitutive Modeling and Fracture Mechanics of a Self-Healing Hydrogel with Chemical and Physical Cross-Links, (2019). https://doi.org/10.7298/V58W-4H93.
[49] G.A. Holzapfel, Nonlinear solid mechanics: a continuum approach for engineering, Wiley, Chichester ; New York, 2000.

SUPPORTING INFORMATION

Constitutive modeling of bond breaking and healing kinetics of physical Polyampholyte (PA) gel

Sairam Pamulaparthi Venkata[a,2#], Kunpeng Cui[b,2#], Jingyi Guo[a], Alan T. Zehnder[a], Jian Ping Gong[b,c,d], & Chung-Yuen Hui[a,c*]

[a] Field of Theoretical and Applied Mechanics, Department of Mechanical and Aerospace Engineering, Cornell University, Ithaca, New York, 14853, United States

[b] Institute for Chemical Reaction Design and Discovery (WPI-ICReDD), Hokkaido University, Sapporo 001-0021, Japan

[c] Soft Matter GI-CoRE, Hokkaido University, Sapporo 001-0021, Japan

[d] Faculty of Advanced Life Science, Hokkaido University, Sapporo 001-0021, Japan

[*] **Corresponding Author**, E-mail: ch45@cornell.edu (C.-Y.H.)

#These two authors contributed equally to this paper.

1. Discussion on survivability function

Eq. (3) (main file) strictly speaking, is an empirical result. However, there is physical reasoning behind it. The physical reasoning is that rate of *decrease* of connected bonds N should increase with the number of connected bonds, that is,

$$-dN/dt \propto b(N), \qquad \text{(S1)}$$

where b is a monotonically increasing function of N. The function b can be inferred from a load relaxation test, since in our theory the healed bonds during a perfect relaxation test do not carry load. In a relaxation test, the amount of load relaxation is directly proportional to the number of broken bonds, this allows us to determine $N(t)$ and we found $b(N) \propto N^{\alpha_B}$. In our previous *PVA* gel system[1,2], experiments showed

[2] These authors contributed equally to this work. Numerical simulations are done by Sairam Pamulaparthi Venkata. Experimental data is provided by Kunpeng Cui.

that the bond breaking kinetics is *insensitive* to the applied stretch, this means that the rate of change of the survivability function can be written as

$$-\frac{d\phi_B}{dt}=\frac{1}{t_B}\phi_B^{\alpha_B}. \qquad \text{(S2)}$$

However, for the PA gel system, we found that the bond breaking kinetics is sensitive to the stretch. Therefore, we modify Eq. (S2) to reflect the effect of stretching on bond breaking. Using the affine approximation, we assume that the force acting on a chain is a function of first invariant of right Cauchy-Green tensor $I_1=\mathbf{F}^T\mathbf{F}$, where $\mathbf{F}$ is the deformation tensor. As a result, the function b in Eq. (S1) also depends on I_1. We assume that b is separable, so for a chain formed at a time τ and survived until a time $t>\tau$, the rate of change of survivability function is

$$-\frac{d\phi_B}{dt}=\frac{1}{t_B}\phi^{\alpha_B}f\left[H(\tau,t)\right],\qquad H(\tau,t)=\text{trace}\left[\left(F^{\tau\to t}\right)^T F^{\tau\to t}\right]. \qquad \text{(S3)}$$

There is some similarity between our idea and Erying's theory [3] (e.g. separability) which proposed that the bond dissociation rate has the form

$$-dN/dt\propto N\,exp\left(\frac{L_a\bar{F}}{k_BT}\right), \qquad \text{(S4)}$$

where L_a is the activation length for bond dissociation and $\bar{F}$ is the tensile force acting on a single polymer chain.

2. *Steady state healing rate*

The steady state healing rate of physical bonds χ_i^{ss} can be calculated using Eq. (7) (main file) along with $\chi_i(t)=\chi_i^{ss},\ \forall\ t\le 0$, $\int_{-\infty}^{0}\phi_{B_i}(\tau,t)\chi_i(\tau)d\tau=\chi_i^{ss}\frac{t_{B_i}}{2-\alpha_{B_i}}\left[\phi_{B_i}(0,t)\right]^{2-\alpha_{B_i}}$ and by setting $t=0$ as

$$\chi_i^{ss}t_{H_i}+0=\omega_i-\chi_i^{ss}\frac{t_{B_i}}{2-\alpha_{B_i}}\left[\underbrace{\phi_{B_i}(0,0)}_{1}\right]^{2-\alpha_{B_i}}\Rightarrow\chi_i^{ss}=\frac{\omega_i}{t_{H_i}+\frac{t_{B_i}}{2-\alpha_{B_i}}}. \qquad \text{(S5)}$$

3. *Derivation of nominal stress from strain energy: Coleman-Noll Procedure*

Since the procedure was used in our previous works[1,2,4], we briefly summarize our approach here. The general expression for time dependent strain energy density $W(t)$ is

$$W(t)=\int_{-\infty}^{t}\chi_i(\tau)\phi_{B_i}(\tau,t,H(\tau,t))W_0\left[H(\tau,t)\right]d\tau, \tag{S6}$$

where, subscript i is used to indicate that there can be multiple physical networks of different breaking and healing kinetics, and Einstein summation is adopted here. The time rate of change of strain energy density is given by

$$\begin{aligned}\dot{W}(t)&\equiv\frac{dW(t)}{dt},\\&=\chi_i(t)\phi_{B_i}(t,t,H(t,t))W_0\left[H(t,t)\right]+\int_{-\infty}^{t}\chi_i(\tau)\frac{\partial}{\partial t}\left(\phi_{B_i}(\tau,t,H(\tau,t))W_0\left[H(\tau,t)\right]\right)d\tau,\\&=\int_{-\infty}^{t}\chi_i(\tau)\phi_{B_i}(\tau,t,H(\tau,t))\frac{dW_0(I_1)}{dI_1}\bigg|_{I_1=H(\tau,t)}\frac{\partial H(\tau,t)}{\partial t}d\tau\\&+\int_{-\infty}^{t}\chi_i(\tau)\frac{\partial}{\partial t}\left(\phi_{B_i}(\tau,t,H(\tau,t))\right)W_0\left[H(\tau,t)\right]d\tau.\end{aligned} \tag{S7}$$

Here, $W_0\left[H(t,t)\right]=0$, as $H(t,t)=3$. The time derivative terms in Eq. (S7) are

$$\begin{aligned}\frac{\partial H(\tau,t)}{\partial t}&=\frac{\partial}{\partial t}\left(\text{trace}\left[\left(\mathbf{F}^{\tau\to t}\right)^T\mathbf{F}^{\tau\to t}\right]\right)=\frac{\partial}{\partial t}\left(\text{trace}\left[\left(\mathbf{F}^{0\to\tau}\right)^{-T}\left(\mathbf{F}^{0\to t}\right)^T\mathbf{F}^{0\to t}\left(\mathbf{F}^{0\to\tau}\right)^{-1}\right]\right),\\&=\frac{\partial}{\partial t}\left(\left[\left(\mathbf{F}^{0\to\tau}\right)^{-T}\left(\mathbf{F}^{0\to t}\right)^T\mathbf{F}^{0\to t}\left(\mathbf{F}^{0\to\tau}\right)^{-1}\right]_{ii}\right)=\frac{\partial}{\partial t}\left(\left(F_{ji}{}^{0\to\tau}\right)^{-1}\left(F_{kj}{}^{0\to t}\right)F_{kl}{}^{0\to t}\left(F_{li}{}^{0\to\tau}\right)^{-1}\right),\\&=2\left(F_{ji}{}^{0\to\tau}\right)^{-1}F_{kl}{}^{0\to t}\left(F_{li}{}^{0\to\tau}\right)^{-1}\cdot\dot{F}_{kj}{}^{0\to t}=2F_{ik}{}^{\tau\to t}\left(F_{jk}{}^{0\to\tau}\right)^{-1}\cdot\dot{F}_{ij}{}^{0\to t},\end{aligned}$$

(S8a)

and

$$\frac{\partial\left(\phi_{B_i}\left(\tau,t,H(\tau,t)\right)\right)}{\partial t}=\frac{\partial}{\partial t}\left[1+\frac{\alpha_{B_i}-1}{t_{B_i}}\int_{\tau}^{t}\left(1+\frac{H(\tau,s)-3}{I_c-3}\right)^{m_i}ds\right]^{\frac{1}{1-\alpha_{B_i}}}\quad\text{(no summation)},$$

$$=\frac{1}{1-\alpha_{B_i}}\left[1+\frac{\alpha_{B_i}-1}{t_{B_i}}\int_{\tau}^{t}\exp\left\{\left(1+\frac{H(\tau,s)-3}{I_c-3}\right)^{m_i}-1\right\}ds\right]^{\frac{\alpha_{B_i}}{1-\alpha_{B_i}}}\qquad\text{(S8b)}$$

$$\left\{\frac{\alpha_{B_i}-1}{t_{B_i}}\exp\left\{\left(1+\frac{H(\tau,t)-3}{I_c-3}\right)^{m_i}-1\right\}\right\}.$$

Note the RHS of Eq. (S8b) does not contain $\dot{F}_{ij}^{\,0\to t}$. Briefly, we equate the terms associated with $\dot{\mathbf{F}}$ in Eq. (S7) with $\left[P_{ij}+p\left(F_{ji}^{\,0\to t}\right)^{-1}\right]\dot{F}_{ij}^{\,0\to t}$ in the energy balance equation to get

$$\int_{-\infty}^{t}\chi_i(\tau)\phi_{B_i}(\tau,t,H(\tau,t))\frac{dW_0(I_1)}{dI_1}\bigg|_{I_1=H(\tau,t)}\frac{\partial H(\tau,t)}{\partial t}d\tau=\left[P_{ij}+p\left(F_{ji}^{\,0\to t}\right)^{-1}\right]\dot{F}_{ij}^{\,0\to t},\quad\text{(S9)}$$

where $\mathbf{P}$ is the first Piola-Kirchhoff stress tensor, and p is the Lagrange multiplier required to enforce incompressibility. Combining Eqs. (S7)-(S9) we have,

$$\left[P_{ij}+p\left(F_{ji}^{\,0\to t}\right)^{-1}\right]\dot{F}_{ij}^{\,0\to t}=\int_{-\infty}^{t}\chi_n(\tau)\phi_{B_n}(\tau,t,H(\tau,t))\frac{dW_0(I_1)}{dI_1}\bigg|_{I_1=H(\tau,t)}2F_{ik}^{\,\tau\to t}\left(F_{jk}^{\,0\to\tau}\right)^{-1}\cdot\dot{F}_{ij}^{\,0\to t}d\tau.$$

(S10)

Eq. (S10) implies that

$$P_{ij}=-p\left(F_{ji}^{\,0\to t}\right)^{-1}+\int_{-\infty}^{t}\chi_n(\tau)\phi_{B_n}(\tau,t,H(\tau,t))2\frac{dW_0(I_1)}{dI_1}\bigg|_{I_1=H(\tau,t)}F_{ik}^{\,\tau\to t}\left(F_{jk}^{\,0\to\tau}\right)^{-1}d\tau$$

(S11)

Breaking the integral in Eq. (S11) into two parts, we have

$$P_{ij}=-p\left(F_{ji}^{\,0\to t}\right)^{-1}+\int_{-\infty}^{0}\chi_n^{ss}\phi_{B_n}(\tau,t,H(\tau,t))2\frac{dW_0(I_1)}{dI_1}\bigg|_{I_1(t)}F_{ij}^{\,0\to t}d\tau+$$
$$\int_{0}^{t}\chi_n(\tau)\phi_{B_n}(\tau,t,H(\tau,t))2\frac{dW_0(I_1)}{dI_1}\bigg|_{I_1=H(\tau,t)}F_{ik}^{\,\tau\to t}\left(F_{jk}^{\,0\to\tau}\right)^{-1}d\tau.\qquad\text{(S12)}$$

or re-written in tensor form for two types of physical bonds (weak and strong bonds) as

$$\mathbf{P}(t)=-p\left(\mathbf{F}^{0\to t}\right)^{-T}+\left\{\sum_{i=1}^{2}\chi_i^{ss}\frac{t_{B_i}}{2-\alpha_{B_i}}\left[\phi_{B_i}\left(0,t,I_1(t)\right)\right]^{2-\alpha_{B_i}}\right\}2\left.\frac{dW_0}{dI_1}\right|_{I_1(t)}\mathbf{F}^{0\to t}$$
$$+\sum_{i=1}^{2}\int_0^t\phi_{B_i}(\tau,t,H(\tau,t))\chi_i(\tau)2\left.\frac{dW_0}{dI_1}\right|_{I_1=H(\tau,t)}\mathbf{F}^{\tau\to t}\left(\mathbf{F}^{0\to\tau}\right)^{-T}d\tau. \tag{S13}$$

3.1. Nominal stress in Uniaxial Tension test

Let the nominal stretch experienced by the physical bonds in uniaxial tension be λ. Using the incompressibility condition $\left(\det\mathbf{F}=1\right)$, the deformation gradient is given by

$$\boldsymbol{F}^{0\to t}=\begin{bmatrix}\lambda(t) & 0 & 0\\ 0 & 1/\sqrt{\lambda(t)} & 0\\ 0 & 0 & 1/\sqrt{\lambda(t)}\end{bmatrix}. \tag{S14}$$

Using the Eq. (S14), the deformation gradient from the time τ to the current time t is

$$\boldsymbol{F}^{\tau\to t}=\boldsymbol{F}^{0\to t}\left(\boldsymbol{F}^{0\to\tau}\right)^{-1}=\begin{bmatrix}\lambda(t) & 0 & 0\\ 0 & 1/\sqrt{\lambda(t)} & 0\\ 0 & 0 & 1/\sqrt{\lambda(t)}\end{bmatrix}\begin{bmatrix}1/\lambda(\tau) & 0 & 0\\ 0 & \sqrt{\lambda(\tau)} & 0\\ 0 & 0 & \sqrt{\lambda(\tau)}\end{bmatrix}$$
$$=\begin{bmatrix}\lambda(t)/\lambda(\tau) & 0 & 0\\ 0 & \sqrt{\lambda(\tau)}/\sqrt{\lambda(t)} & 0\\ 0 & 0 & \sqrt{\lambda(\tau)}/\sqrt{\lambda(t)}\end{bmatrix} \tag{S15}$$

Using the Eqs. (S13)-(S15), the nominal stress under uniaxial tension loading is given by

$$P_{11}(t)\equiv P(t)=\left[\sum_{i=1}^{2}\chi_i^{ss}\int_{-\infty}^{0}\phi_{B_i}(\tau,t,H(\tau,t))d\tau\right]2\left.\frac{dW_0}{dI_1}\right|_{I_1(t)}\left(\lambda(t)-\lambda(t)^{-2}\right)$$
$$+\sum_{i=1}^{2}\int_0^t\chi_i(\tau)\phi_{B_i}(\tau,t,H(\tau,t))2\left.\frac{dW_0}{dI_1}\right|_{H(\tau,t)}\left[\frac{\lambda(t)}{\lambda^2(\tau)}-\frac{\lambda(\tau)}{\lambda^2(t)}\right]d\tau,$$
$$=\left[\sum_{i=1}^{2}\chi_i^{ss}\frac{t_{B_i}}{2-\alpha_{B_i}}\left[\phi_{B_i}(0,t)\right]^{2-\alpha_{B_i}}\right]2\left.\frac{dW_0}{dI_1}\right|_{I_1(t)}\left(\lambda(t)-\lambda(t)^{-2}\right) \tag{S16}$$
$$+\sum_{i=1}^{2}\int_0^t\chi_i(\tau)\phi_{B_i}(\tau,t,H(\tau,t))2\left.\frac{dW_0}{dI_1}\right|_{H(\tau,t)}\left[\frac{\lambda(t)}{\lambda^2(\tau)}-\frac{\lambda(\tau)}{\lambda^2(t)}\right]d\tau.$$

3.2. Nominal stress in Tensile-Relaxation test

In practice, it is impossible to conduct an ideal relaxation test. It takes a finite loading time t_1 before the desired nominal stretch ratio λ_0 is reached, and the data during the loading part is captured. The initial loading part is similar to a uniaxial tension test, till the desired stretch ratio is reached and held constant, when the actual relaxation test starts.

The nominal stress is related to the stretch ratio $\lambda(t)$ in the loading direction as

$$P_{11}(t) \equiv P(t) = \begin{cases} \left[\sum_{i=1}^{2} \chi_i^{ss} \frac{t_{B_i}}{2-\alpha_{B_i}} \left[\phi_{B_i}(0,t)\right]^{2-\alpha_{B_i}}\right] 2\frac{dW_0}{dI_1}\Big|_{I_1(t)} \left(\lambda(t) - \lambda(t)^{-2}\right) \\ +\sum_{i=1}^{2} \int_0^t \chi_i(\tau)\phi_{B_i}(\tau,t,H(\tau,t)) 2\frac{dW_0}{dI_1}\Big|_{H(\tau,t)} \left[\frac{\lambda(t)}{\lambda^2(\tau)} - \frac{\lambda(\tau)}{\lambda^2(t)}\right] d\tau, & \text{if } t \le t_1 \\ \left[\sum_{i=1}^{2} \chi_i^{ss} \frac{t_{B_i}}{2-\alpha_{B_i}} \left[\phi_{B_i}(0,t)\right]^{2-\alpha_{B_i}}\right] 2\frac{dW_0}{dI_1}\Big|_{I_1(t)} \left(\lambda_0 - \lambda_0^{-2}\right) \\ +\sum_{i=1}^{2} \int_0^{t_1} \chi_i(\tau)\phi_{B_i}(\tau,t,H(\tau,t)) 2\frac{dW_0}{dI_1}\Big|_{H(\tau,t)} \left[\frac{\lambda_0}{\lambda^2(\tau)} - \frac{\lambda(\tau)}{\lambda_0^2}\right] d\tau. & \text{if } t > t_1 \end{cases}$$

(S17)

4. Derivation of torsional relaxation modulus: Small strain rheology test

In the small strain regime, strain hardening can be neglected (the strain energy density reduces to neo-Hookean model). The effect of deformation on bond breaking can also be neglected (that is, $f_i(I_1) = 1$). Thus, the formulation reduces to our previous steady state PVA gel model[2] except that there are no chemical cross-links and we have two types of physical bonds. Thus, the dominant stress component is

$$\sigma_{\theta z} = \sigma_{z\theta} \qquad \text{(S18a)}$$

The rest of the stress components are either zero or quadratic in the twist angle. According to Long [4] and using small strain assumption $2\left.\frac{dW_0}{dI_1}\right|_{I_1(t)} \approx \mu$, the total stress due to the both weak and strong bonds is

$$\sigma_{z\theta} = \mu\sum_{i=1}^{2}\left\{\chi_i^{ss}\frac{t_{B_i}}{2-\alpha_{B_i}}\left[\phi_{B_i}(0,t)\right]^{2-\alpha_{B_i}}\psi(t)r + \chi_i^{ss}r\int_0^t \phi_{B_i}(\tau,t)\left(\psi(t)-\psi(\tau)\right)d\tau\right\} \tag{S18b}$$

The integral in the Eq. (S18b) vanishes for a perfect torsional relaxation test, where a circular plate sample of radius *l* and thickness *h*, is suddenly sheared to a small twist angle $\psi(t)h = \theta_0 h$ for $t \geq 0$. The shear stress for this case relaxes according to

$$\sigma_{z\theta}(t) = \mu\theta_0 r\sum_{i=1}^{2}\chi_i^{ss}\frac{t_{B_i}}{2-\alpha_{B_i}}\left[1+\frac{\alpha_{B_i}-1}{t_{B_i}}t\right]^{\frac{2-\alpha_{B_i}}{1-\alpha_{B_i}}} \tag{S19}$$

Using Eq. (S19), the applied moment is computed using

$$\begin{aligned} M &= \int_0^l \left(2\pi r dr\right)\sigma_{z\theta}\cdot r, \\ &= \mu\theta_0\frac{\pi l^4}{2}\left\{\sum_{i=1}^{2}\chi_i^{ss}\frac{t_{B_i}}{2-\alpha_{B_i}}\left[1+\frac{\alpha_{B_i}-1}{t_{B_i}}t\right]^{\frac{2-\alpha_{B_i}}{1-\alpha_{B_i}}}\right\}. \end{aligned} \tag{S20}$$

The torsional moment of inertia is $\frac{\pi l^4}{2}$. Relaxation modulus $G = \frac{M}{\theta_0\frac{\pi l^4}{2}}$ is the direct output from the rheometer. Therefore, in small strain regime for a perfect torsional relaxation test, the relaxation modulus is

$$G = \mu\sum_{i=1}^{2}\chi_i^{ss}\frac{t_{B_i}}{2-\alpha_{B_i}}\left[1+\frac{\alpha_{B_i}-1}{t_{B_i}}t\right]^{\frac{2-\alpha_{B_i}}{1-\alpha_{B_i}}}. \tag{S21}$$

5. Data sets used for optimization process:

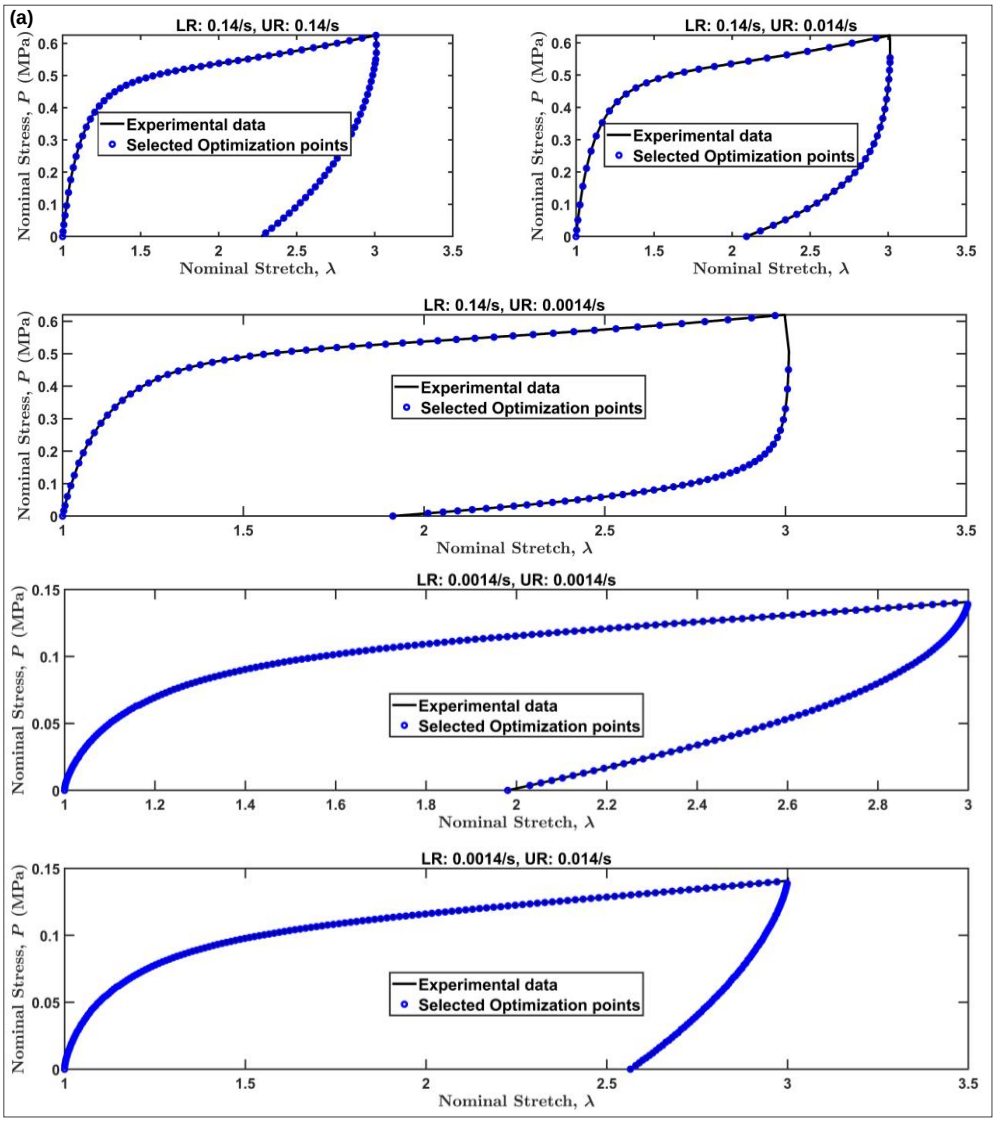
(a)
LR: 0.14/s, UR: 0.14/s
LR: 0.14/s, UR: 0.014/s
LR: 0.14/s, UR: 0.0014/s
LR: 0.0014/s, UR: 0.0014/s
LR: 0.0014/s, UR: 0.014/s
Experimental data
Selected Optimization points
Nominal Stress, P (MPa)
Nominal Stretch, λ

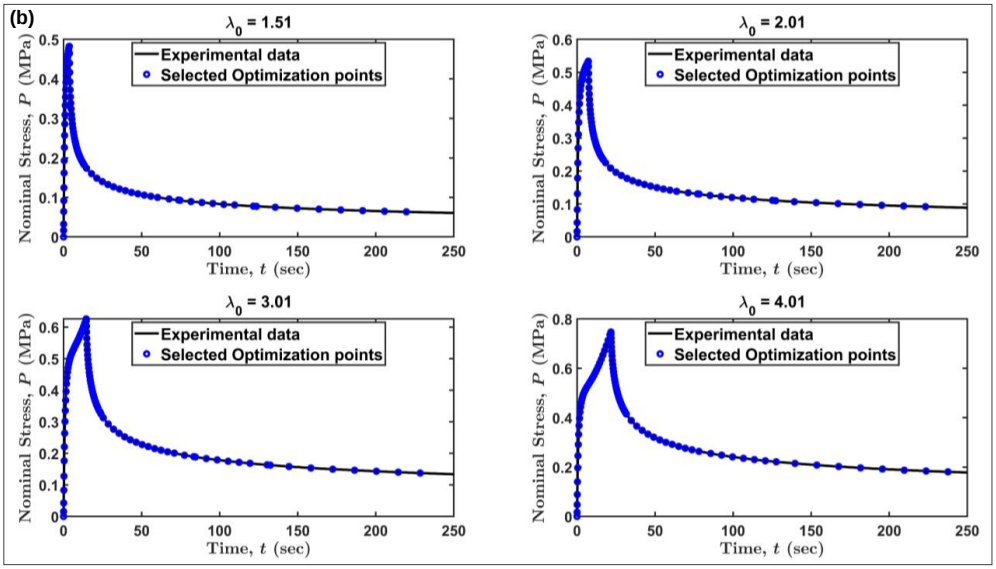
(b)
λ0 = 1.51
λ0 = 2.01
λ0 = 3.01
λ0 = 4.01
Experimental data
Selected Optimization points
Nominal Stress, P (MPa)
Time, t (sec)

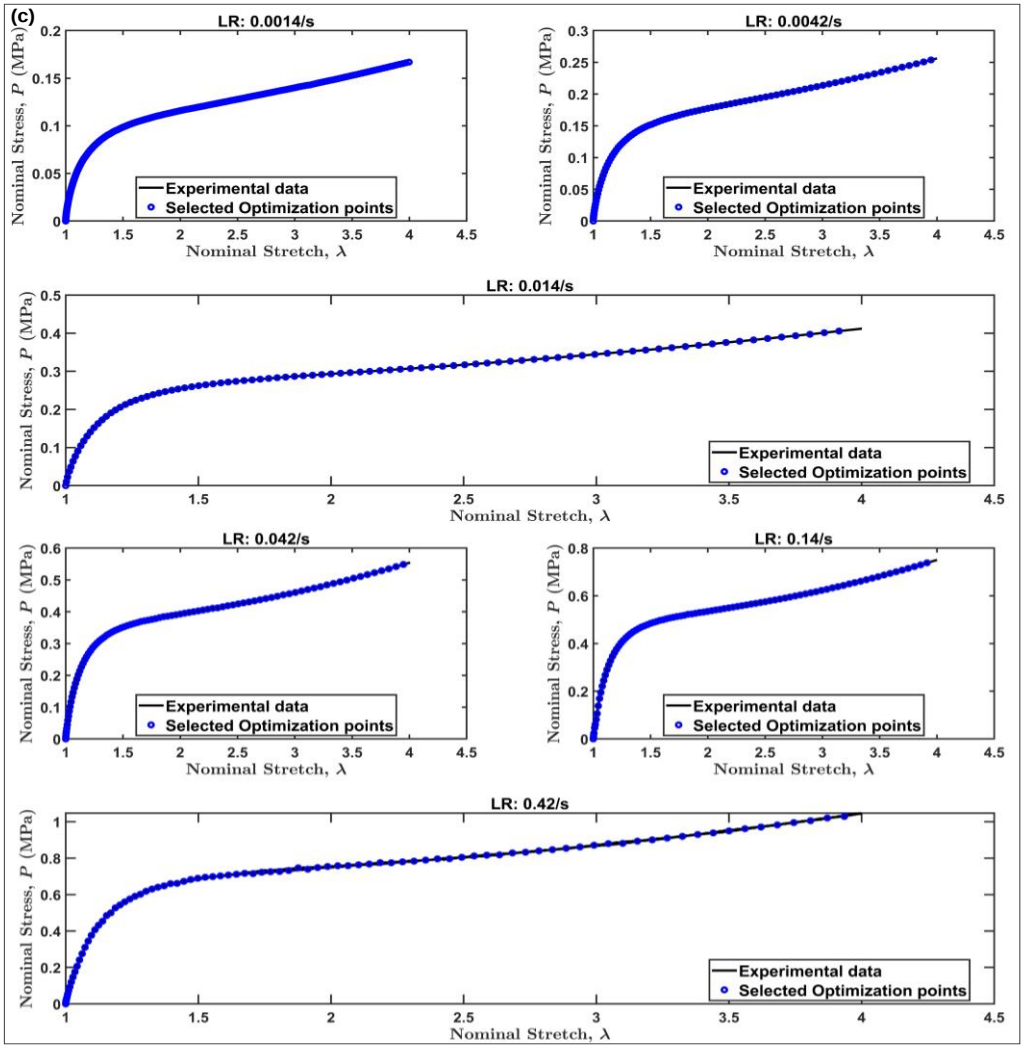

Fig. S1. All plots from three representative data sets (a) loading-unloading tests, (b) tensile-relaxation tests, and (c) tensile loading tests which are used for least squares optimization process are presented here. We optimize 13 material parameters in Table 1 (main file) to get the minimum least squares error in nominal stress from all the curves simultaneously between the simulated and the experimental data at the selected optimization points (shown as blue dotted circles). Here, LR represents loading rate and UR represents unloading rate.

6. Estimate for critical stretch ratio λ_c

The estimate for critical stretch ratio λ_c is found by the intersection of two tangent lines (just for illustration) as shown in the Fig. S2. The tangent lines can be drawn around the visible region of maximum curvature change of nominal stress. Depending on the location of these tangent lines around the maximum curvature change, the

critical stretch ratio could lie between $1.1 < \lambda_c < 1.3$. This process is carried out for tensile data with two different stretch/strain rates. For different stretch rates, there is a small difference in the value of critical stretch ratio. Nevertheless, in our theory, we assume that the critical stretch ratio is independent of the applied strain rate.

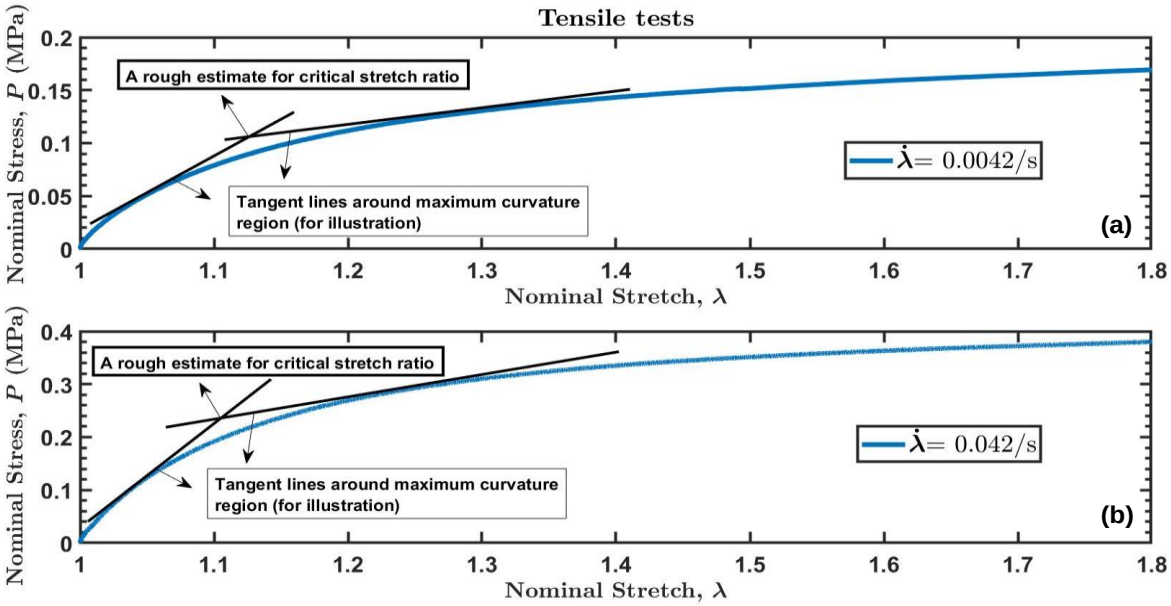

Fig. S2. Estimating the critical stretch ratio value (λ_c) from the slope of $P-\lambda$ plot using the tensile data of two different strain rates (a) $\dot{\lambda} = 0.0042/s$ and (b) $\dot{\lambda} = 0.042/s$.

7. Strain dependent breaking function

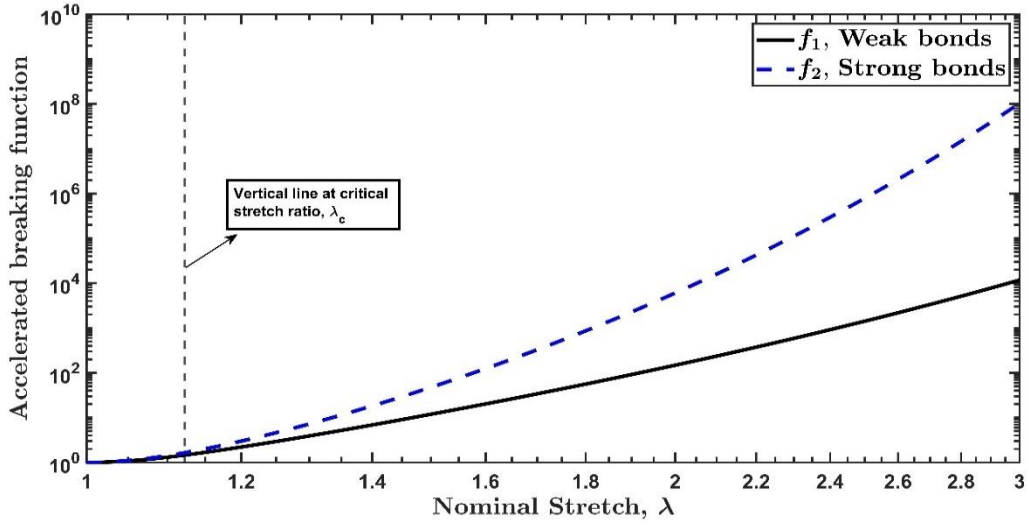

Fig. S3. We plot strain dependent accelerated breaking function (f_1 or f_2) with nominal stretch ratio, λ. The solid black line refers to weak bonds' breaking function, and the dotted blue line refers to strong bonds' breaking function. The dotted vertical solid black line is drawn at the critical stretch ratio, λ_c.

High value of accelerated breaking function refers to breaking of physical bonds' being significantly dependent on the applied strain. From the Fig. S3 we observe that breaking of strong bonds is strongly dependent on applied strain than weak bonds at high stretch ratios. We also notice that after the critical stretch ratio, fraction of strong bonds that break is much higher when compared to weak bonds. Healing rates and healing times from Table 2-3 (main file) suggest us that strong bonds heal relatively slowly than weak bonds. As a result, at high stretch ratios weak bonds may carry more load when compared to strong bonds and this can be seen in Fig. 8 (main file).

REFERENCES

[1] R. Long, K. Mayumi, C. Creton, T. Narita, C.-Y. Hui, Time Dependent Behavior of a Dual Cross-Link Self-Healing Gel: Theory and Experiments, Macromolecules. 47 (2014) 7243–7250. https://doi.org/10.1021/ma501290h.

[2] J. Guo, R. Long, K. Mayumi, C.-Y. Hui, Mechanics of a Dual Cross-Link Gel with Dynamic Bonds: Steady State Kinetics and Large Deformation Effects, Macromolecules. 49 (2016) 3497–3507. https://doi.org/10.1021/acs.macromol.6b00421.

[3] A. Tobolsky, H. Eyring, Mechanical Properties of Polymeric Materials, J. Chem. Phys. 11 (1943) 125–134. https://doi.org/10.1063/1.1723812.

[4] C.-Y. Hui, R. Long, A constitutive model for the large deformation of a self-healing gel, Soft Matter. 8 (2012) 8209. https://doi.org/10.1039/c2sm25367d.

[5] R. Long, K. Mayumi, C. Creton, T. Narita, C.-Y. Hui, Rheology of a dual crosslink self-healing gel: Theory and measurement using parallel-plate torsional rheometry, J. Rheol. 59 (2015) 643–665. https://doi.org/10.1122/1.4915275.

CHAPTER 2

Constitutive modeling of strain-dependent bond breaking and healing kinetics of chemical Polyampholyte (PA) gel

Sairam Pamulaparthi Venkata[a,3#], Kunpeng Cui[b,3#], Jingyi Guo[a], Alan T. Zehnder[a], Jian Ping Gong[b,c,d], & Chung-Yuen Hui[a,c*]

[a] Field of Theoretical and Applied Mechanics, Department of Mechanical and Aerospace Engineering, Cornell University, Ithaca, New York, 14853, United States

[b] Institute for Chemical Reaction Design and Discovery (WPI-ICReDD), Hokkaido University, Sapporo 001-0021, Japan

[c] Soft Matter GI-CoRE, Hokkaido University, Sapporo 001-0021, Japan

[d] Faculty of Advanced Life Science, Hokkaido University, Sapporo 001-0021, Japan

[*] **Corresponding Author**, E-mail: ch45@cornell.edu (C.-Y.H.)

#These two authors contributed equally to this paper.

Abstract:

A finite strain nonlinear viscoelastic constitutive model is used to study the uniaxial tension behaviour of a chemical Polyampholyte (PA) gel. This PA gel is cross-linked by chemical and physical bonds. Our constitutive model attempts to capture the time and strain dependent breaking and healing kinetics of physical bonds. We compare model prediction with uniaxial tension, cyclic and relaxation tests. Material parameters in our model are obtained by least squares optimization. These parameters gave fits that are in good agreement with the experiments.

Keywords: self-healing, hydrogel, large deformation, nonlinear viscoelasticity.

1. Introduction:

[3] These authors contributed equally to this work. Numerical simulations are done by Sairam Pamulaparthi Venkata. Experimental data is provided by Kunpeng Cui.

Hydrogels are soft and wet materials often occurring in nature as biotissues[1]. Hydrogels are composed of a polymer network swollen by water. These features make hydrogels well suited for many bio-engineering applications, such as cell scaffolds in tissue engineering[2–4], as artificial cartilage[5,6], and as vehicles for drug delivery[7–9]. Conventional hydrogels are mechanically soft and weak[10], which severely limits their applications, especially in structural biomaterials[10]. The pioneering work of double network hydrogels (DN gels) by Gong et al.[11] improves the mechanical strength and toughness of hydrogels[12,13]. DN gels are composed of a stiff/brittle first network and a soft/stretchable second network. During deformation, the first network breaks preferentially to dissipate energy, while the second network keeps the sample intact. DN gels have a high toughness of ~ 1000 J/m^2, which is comparable to the cartilage[14].

Studies on DN gels revealed a general strategy to toughen network materials. That is, incorporating sacrificial structure into polymer network to dissipate mechanical energy[10]. Along this line, many strong and tough hydrogels have been developed in recent years[15–21]. Among them, the hydrogels with physical bonds as sacrificial structures are especially interesting. Diverse physical bonds have been used to toughen hydrogels, including metal-ion interaction[15], hydrogen bonding[22–24], ionic interaction[25,26], host-guest interaction[27,28], π-π stacking[29], and so on[30,31]. Physical bonds are dynamic and reversible; thus, they not only improve toughness, but also endow the gels time- or rate-dependent mechanical behaviour, together with self-recovery and self-healing abilities[25]. As the dissociation and association of physical bonds fundamentally govern the mechanical properties[32], it is important to understand the bond kinetics of these gels.

In a recent work, we developed a generalized constitutive model to quantitatively understand the bond kinetics of a purely physically cross-linked hydrogels composed of polyampholytes (PA gels)[33]. PA gels are synthesized by random copolymerization of cationic and anionic monomers at a high concentration around the charge balanced point[25,34]. As a result, PA chains carry almost the same number of opposite charges on average, and the charges are randomly distributed on the chain

backbones. PA gels have a combination of mechanical performance, such as high toughness, high stiffness, high fatigue resistance, high viscoelasticity, self-recovery, and self-healing[25,35–37]. Pure physical PA gels, i.e. PA gels without a chemical cross-linker, have a phase-separated structure, with a polymer rich phase and a polymer poor phase[38–40]. Due to this phase separation, we used two types of bond kinetics to capture the time-dependent mechanical behaviour of these pure physical hydrogels[33]. For PA gels with a chemical cross-linker (greater than 1 mol% relative to the total monomer concentration), which are referred as chemical PA gels here, the gels become homogeneous and we observe no phase separation[40]. The chemical gel model in this work is modified from our previous physical gel model[33], where the effects of chemical crosslinker are considered in this current model. Even though the fraction of chemical bonds is almost as low as 0.01, the chemical PA gels *behave very differently* from physical PA gels due to the presence of chemical bonds. These major differences are: (I) the fracture strain of chemical PA gel (~150% strain) is much lower than the physical PA gel (> 800% strain). (II) The fracture strain of chemical PA gel is insensitive to the applied strain rate, which is not true for the physical gel. (III) No phase separation in the chemical PA gel due to the presence of 1% of chemical bonds. These dramatic differences motivate us to see whether our constitutive model can still describe the mechanical behaviour. For this purpose, we use one type of bond kinetics for all the physical cross-links and put into the role of chemical crosslinker, as this PA gel is chemically cross-linked and has a homogeneous structure. We found that the modified theory works well in describing the time-dependent mechanical behaviour of chemical PA gel.

Our present work is structured in the following manner. In Section 2, we state the theoretical model and the nominal stress-strain relationship for different types of loading histories. In Section 3, we briefly describe an experimental procedure for the synthesis and mechanical testing of the chemical PA gel. In Section 4, we identify and discuss the material parameters required in our finite strain constitutive model. In Section 5, we validate the accuracy of our theory by comparing the simulation results

with the experiments. We observe that our model predicts the experiments well. Conclusions are presented in the Section 6.

2. *Theory*

In our previous works, we formulated a 3D finite strain viscoelastic model for Polyvinyl alcohol (PVA) hydrogels consisting of physical and chemical cross-links[32,41,42]. The breaking kinetics of physical cross-links in a PVA gel is found to be independent of the applied strain. Although this is a good assumption for the PVA gel, we found that bond breaking kinetics in a physically cross-linked PA gel is strain dependent which is necessary to explain the mechanical behaviour for different loading histories[33]. As noted above, we used two types of bond kinetics to capture the time-dependent mechanical behaviour of pure physical hydrogels. In this current work, our chemical PA gel consists of both physical and chemical cross-links. These chemical crosslinks form a permanent network. Deformation of this permanent network is elastic and time independent. The idea is to modify our previous model[33] by replacing one type of physical crosslinks with permanent chemical crosslinks. By considering the stress contributions from chemical cross-links along with the physical cross-links, we obtain the nominal stress $P(t)$ in a uniaxial tension test where the stretch history $\lambda(t)$ is prescribed. Since the derivation of the constitutive model is practically identical to our previous work[33], we summarize the details in the Supporting information (SI). The nominal stress P is defined as the tensile force divided by the cross-section area of the undeformed sample. The stretch or stretch ratio λ is defined as the displacement divided by the gauge length of the undeformed sample. The strain rate is defined as the stretching speed divided by the gauge length of the undeformed sample. Here we provide physical explanations to the material parameters in the stress equation (Eq. (1a)) to aid better understanding.

The nominal stress P is given by (see, SI, Section S4 for detailed derivation)

$$P(t)=2\omega_{\text{chem}}\left.\frac{dW_0}{dI_1}\right|_{I_1(t)}\left(\lambda(t)-\lambda(t)^{-2}\right)+2\rho\left.\frac{dW_0}{dI_1}\right|_{I_1(t)}\left[\phi_B(\tau=0,t,H^{0\to t})\right]^{2-\alpha_B}\left(\lambda(t)-\lambda(t)^{-2}\right)$$
$$+\int_0^t\left[\chi(\tau)\phi_B\left(\tau,t,H^{\tau\to t}\right)2\left.\frac{dW_0}{dI_1}\right|_{I_1=H^{\tau\to t}}\left[\frac{\lambda(t)}{\lambda^2(\tau)}-\frac{\lambda(\tau)}{\lambda^2(t)}\right]\right]d\tau, \quad \text{(1a)}$$

where

$$\phi_B(\tau,t,H^{\tau\to t})=\left[1+\frac{\alpha_B-1}{t_B}\int_\tau^t f\left(H^{\tau\to s}\right)ds\right]^{\frac{1}{1-\alpha_B}}. \quad \text{(1b)}$$

Eq. (1a) has three terms, here we explain the physics behind each term:

1. The first term in Eq. (1a) is the stress carried by the chemical crosslinks, where ω_{chem} is the fraction of chemical crosslinks. In the constitutive model, chemical crosslinks are assumed to be permanent and do not break under mechanical loading. The strain energy density function for chemical and physical crosslinks is assumed to be the same and denoted by W_0. Since the gel is incompressible, we assume W_0 depends only on the first invariant of the right Cauchy-Green tensor $I_1(t)=\text{trace}\left[\left(\mathbf{F}^{0\to t}\right)^T\left(\mathbf{F}^{0\to t}\right)\right]$, where $\mathbf{F}$ is the deformation gradient tensor. The superscript $0\to t$ in the deformation gradient tensor $\mathbf{F}^{0\to t}$ indicates that it is measured from the reference configuration at $t=0$ when the gel is undeformed. In uniaxial loading, $I_1(t)=\lambda^2(t)+\frac{2}{\lambda(t)}$, where λ is the stretch ratio in the tensile test. The first term indicates that the network formed by chemical crosslinks is elastic, since the stress depends only on the current stretch. This term is absent from our previous work[33] due to the absence of chemical crosslinks.

2. Unlike chemical cross-links, crosslinks formed from physical bonds can break and heal. We assume before loading ($t<0$), the physical crosslinks have reached a state of dynamic equilibrium in which the healing rate is equal to the breaking rate; this steady state healing rate is denoted by χ^{ss}. The function $\phi_B(\tau,t,H^{\tau\to t})$ in Eq. (1a) is the survivability function, *it is the fraction of physical cross-links that survive from the time of their formation* τ *to the current time* t (in the 2nd term of Eq. (1a), $\tau=0$ and $H^{\tau\to t}\equiv H^{0\to t}=I_1(t)$). The notation $H^{\tau\to t}\equiv H(\tau,t)\equiv \text{trace}\left[\left(\mathbf{F}^{\tau\to t}\right)^T\mathbf{F}^{\tau\to t}\right]$. The reason for this notation is as follows: we assume that when a physical cross-link breaks, it loses all its strain energy, and when it is reattached at time τ, it carries no strain energy at that time. This means that these crosslinks can only feel the deformation at the time of their birth. Thus, the deformation of chains connected by these cross-links is described using the deformed configuration at time τ as the reference configuration. With this understanding, let us consider the third term in Eq. (1a) before discussing the second term: the third term represents the stress carried by physical cross-links that break and reattach during the loading history. To understand this, we first note that because bond breaking depends on deformation, the healing rate and the breaking rate are no longer the same once loading starts. We denote the healing rate at the current time by $\chi(t)$. In our model, the healing rate is equal to the fraction of broken physical bonds divided by the characteristic healing time t_H (for a physical motivation, see SI, Section S1). Thus, the term $\chi(\tau)\phi_B\left(\tau,t,H^{\tau\to t}\right)d\tau$ in the integral represents the fraction of bonds that reattach at time τ and survive to the current time t, and the stress they carry is $2\dfrac{dW_0}{dI_1}\bigg|_{I_1=H^{\tau\to t}}\left[\dfrac{\lambda(t)}{\lambda^2(\tau)}-\dfrac{\lambda(\tau)}{\lambda^2(t)}\right]$. Thus, the integral is the stress carried by reattached bonds from the time of loading to the current time.

The function $\chi(t)$ depends on the loading history and is obtained by solving the following integral equation (Eq. (2))[33]

$$\underbrace{\omega_{\text{phys}}}_{\substack{\text{Total fraction}\\ \text{of physical bonds}}} = 1-\omega_{\text{chem}} = \underbrace{\chi(t)t_H}_{\substack{\text{Fraction of broken}\\ \text{physical bonds}}} + \underbrace{\int_{-\infty}^{t} \phi_B(\tau,t,H^{\tau\to t})\chi(\tau)d\tau}_{\substack{\text{Fraction of connected}\\ \text{physical bonds}}}. \qquad (2)$$

3 Finally, let us consider the 2nd term in Eq. (1a). The fraction of connected physical cross-links (number of connected physical cross-links over the total number of physical and chemical cross-links) before the start of loading is denoted by ρ. Therefore, the second term in Eq. (1a) is the stress carried by the physical cross-links that remain connected from the start of loading ($\tau = 0$) to the current time t. Using the second term in the R.H.S of Eq. (2), ρ is found to be (also see SI, Section S2)

$$\rho = \frac{\chi^{ss} t_B}{2-\alpha_B}, \qquad \chi^{ss} = \frac{1-\omega_{\text{chem}}}{t_H + \dfrac{t_B}{2-\alpha_B}} \qquad (3a, 3b)$$

Finally, we assume the form of the survivability function is given by Eq. (1b). In Eq. (1b), t_B is the characteristic breaking time of physical crosslinks, $\alpha_B \in (1, 2)$ is a material parameter that controls the rate of decay of the survivability function and f is a function which measures the dependence of breaking rate on the stretch experienced by a physical cross-link from its formation at time τ to the current time $t > \tau$. The physical motivation behind Eq. (1b) can be found in the SI (Section S1).

In the following, we shall use Eqs. (1a) and (1b) to compute the nominal stresses during cyclic and relaxation tests. In these tests, the stretch ratio is given as a function of time. For example, in a perfect relaxation test, *the stretch ratio is increased suddenly (at $t = 0^+$) to a value $\lambda_0 > 1$ and then held constant thereafter. For this case,*

the third term in Eq. (1a) vanishes identically, indicating the heal bonds do not carry any load in a perfect relaxation test. The nominal stress $P(t)$ relaxes according to:

$$P(t)=2\left(\lambda_0-\lambda_0^{-2}\right)\frac{dW_0}{dI_1}\bigg|_{I_1(\lambda_0)}\left\{\omega_{\text{chem}}+\rho\left[1+\frac{\alpha_B-1}{t_B}f\left(I_1(\lambda_0)\right)t\right]^{\frac{2-\alpha_B}{1-\alpha_B}}\right\}. \tag{4}$$

In a real test, it is not possible to impose infinite strain rate, so Eq. (4) needs to be modified to account for finite loading rate, this modification is given in SI (Section S4.2).

We end this section by stating an explicit form of the breaking function and the strain energy density function. The accelerating breaking function f is given by

$$f(I_1)=\left(1+\frac{I_1-3}{I_c-3}\right)^m, \quad I_c=\lambda_c^2+\frac{2}{\lambda_c}, \tag{5}$$

where λ_c is a characteristic stretch at which the breaking rate of physical crosslinks increases rapidly and m is a material parameter controlling the breaking rate. For small strains, $\frac{I_1-3}{I_c-3}<<1$, $H^{\tau\to t}\approx 3$ and $f\approx 1$. Thus, in the small strain regime, the bond breaking kinetics is independent of strain, however, for larger strains, that is, when $I_1-3>I_c-3$, the breaking function f increases rapidly. Further discussion of the physics behind the breaking function and critical strain is given in Sections S1 and S5.2 (see, SI) respectively. Different forms of strain energy function have been used in our previous works to account for strain hardening effects[32,41,42]. In the most recent work, $W_0(I_1)$ is given by Yeoh's model[33], i.e.,

$$W_0(I_1)=\sum_{i=1}^{3}c_i(I_1-3)^i. \tag{6}$$

In Yeoh's model, $c_1=\mu/2$ where μ is the small strain shear modulus of the undamaged network. The material parameters c_2 and c_3 control the strain hardening behaviour.

3. *Experiments*

Gel sample preparation: The procedure to prepare the chemical PA hydrogels was described in detail in our previous work[38]. Briefly, anionic monomer p-styrenesulfonate (NaSS), cationic monomer 3-(methacryloylamino)-propyl-trimethylammonium chloride (MPTC), photoinitiator α- ketoglutaric acid (α-keto), and chemical cross-linker N,N-methylene-bis-acrylamide (MBAA) were mixed to form an aqueous solution and followed by UV polymerization. The obtained gels were immersed into large amount of water longer than one week to remove unreacted chemicals and counterions. The total monomer concentration, C_m, was 2.1 M, and the molar ratio of NaSS/MPTC was 0.525:0.475. The concentration of MBAA and α-keto were 3 and 0.25 mol %, respectively, relative to C_m.

Mechanical testing: The procedures for mechanical testing are basically the same as that in our previous study[33]. In brief, we performed four sets of mechanical testing: uniaxial tensile test, small strain tensile cyclic test, large strain tensile cyclic test, and tensile relaxation test. Gel samples for mechanical testing were cut into a dumbbell-like shape with JIS K 6261-7 standard. The gauge length, width and thickness of samples were 12, 2 and 1.74 mm, respectively. Samples were loaded in tension by a Shimadzu autograph machine with a 100 N load cell. The measurement was conducted in water vapor environment to prevent gel dehydration.

4. Material Parameters and their determination

The chemical PA gel constitutive model has 9 unknown independent material parameters in total. They are listed as follows: α_B, t_B, t_H, ω_{phys} or ω_{chem}, m, λ_c, $c_1 \equiv \mu/2$, c_2 and c_3. Once these 9 parameters are known, ρ and χ^{ss} can be determined using Eqs. (3a) and (3b).

Some of these material parameters can be estimated from uniaxial tension and tensile-relaxation experimental data. For example, an estimate of the small strain instantaneous shear modulus ($\equiv \mu(\omega_{\text{chem}} + \rho) \approx 3.30$ MPa) can be found from the initial loading part of tensile-relaxation test (see SI, Section S5.1). Similarly, an estimate of critical stretch ratio value, $\lambda_c \approx 1.20$ can be determined from the uniaxial tension data (see SI, Section S5.2). These estimates help us in selecting an optimal parameter set

amongst multiple local optimums obtained from least squares optimization process discussed in the SI (Section S6).

We use select data from simple tension, tensile-relaxation, and cyclic tests and a least squares error optimization scheme to determine the 9 parameters. Since the same least squares optimization procedure was used to determine parameters in our recent work[33], we give details of this procedure in the SI (Section S6). All the experimental data (see SI, Fig S3) except for one case (cyclic test with LR and UR - 0.0014/s and 0.14/s) were used in the optimization scheme to capture the material parameters mentioned in Table 1.

The material parameters obtained from the optimization process are summarized in Table 1. Table 1 shows that the characteristic breaking time of physical bonds is about ten times the healing time. Also, we note that the fraction of physical bonds connected before the start of loading (ρ) is just slightly lower than the total fraction of physical bonds (ω_{phys}). This tells us that most of the physical cross-links are connected in the beginning of the test.

Table 1: The material parameters required for constitutive model are listed below.

Strain dependent parameters			
$\alpha_B = 1.8001$	$t_B = 0.1136\,\text{sec}$	$t_H = 0.01\,\text{sec}$	$\omega_{\text{phys}} = 0.99$
Strain dependent accelerated breaking function parameters, f			
$m = 4.8221$		$\lambda_c = 1.2745$	
Undamaged network strain energy density function, Yeoh's model, W_0			
$c_1 \equiv \mu/2 = 1.7911\,\text{MPa}$	$c_2/c_1 = 0.9703$	$c_3/c_1 = 0.0245$	
Derived material parameters			
$\rho = 0.9729$ **(see Eq. (3a))**	$\chi^{ss} = 1.7117\ s^{-1}$ **(see Eq. (3b))**	$\mu(\omega_{\text{chem}} + \rho) \equiv \frac{E_0}{3} = 3.5210\,\text{MPa}$	

Note that the small strain instantaneous shear modulus ($\mu(\omega_{\text{chem}} + \rho)$) and critical stretch ratio (λ_c) from Table 1 are consistent with the estimates in SI (Section S5).

Our material parameters from the optimization scheme can predict reasonably well the loading history case which is not used in optimization process. The example being the

cyclic test with LR (0.0014/s) and UR (0.0014/s). We observe that our material parameters simulate this loading history well. More importantly, if we use less experimental data in our optimization scheme - for example, by choosing alternative stretch ratio cases instead of all the stretch ratios in tensile-relaxation tests or by choosing alternative loading rates cases in cyclic tests or in simple tension tests, the optimized material parameters will fit all the experimental data well including the ones which we skipped in optimization process, with less than 10% error between simulations and experiments.

5. Results

We compare our simulation results with simple tension, tensile-relaxation, and cyclic loading experimental data. These are shown in the following sections. It should be noted that simulations for all the different tests use the same material parameters from Table 1. Specifically, we solve Eqs. (1a) and (2) using the parameters in Table 1 to determine nominal stress and healing rates $\chi(t)$ respectively.

5.1. Nominal stress: Cyclic tests (small strains)

The uniaxial cyclic tests for loading (LR) and unloading rates (UR) of 0.014/s each in Fig. 1a and of 0.0014/s each in Fig. 1b for a small strain of 10% are shown in Fig. 1. This figure shows that our model slightly overestimates the experimental data for both cases.

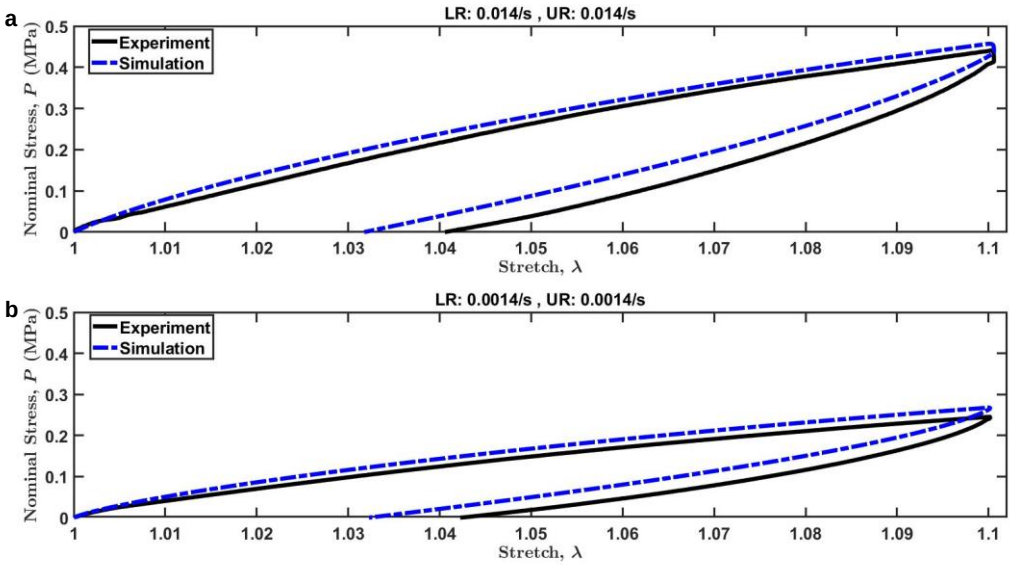

Fig. 1. Nominal stress P (MPa) vs nominal stretch λ for loading and unloading tests with two different strain rates are shown. (a) Loading rate (LR) and unloading rate (UR) of 0.014/s each. (b) LR and UR of 0.0014/s each. Solid black lines represent the experiment data and our simulation results using parameters in Table 1 are shown as dash-dotted blue lines.

5.1.1. Large strain

In Fig. 2 we compare experimental data with our model prediction for cyclic tests with different loading (LR) and unloading rates (UR) in the large strain regime. Fig. 2 shows our model captures the experimental data well for all cases.

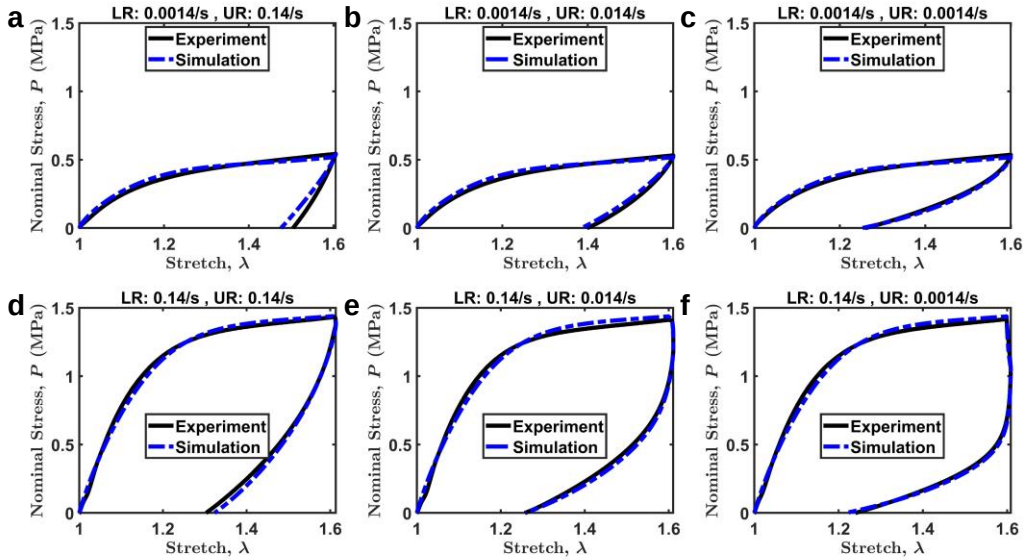

Fig. 2. Nominal stress P (MPa) vs nominal stretch λ for loading and unloading tests with different strain rates are shown here. (a), (b), and (c): The upper plots have a loading rate (LR) of 0.14/s and unloading rates (UR) of 0.14/s, 0.014/s, and 0.0014/s from left to right respectively. (d), (e), and (f): Similarly, the lower plots have a loading rate of 0.0014/s and unloading rates of 0.14/s, 0.014/s, and 0.0014/s from left to right respectively. Solid black lines represent the experiment data and our simulation results using parameters in Table 1 are shown as dash-dotted blue lines.

5.2. Tensile-Relaxation tests

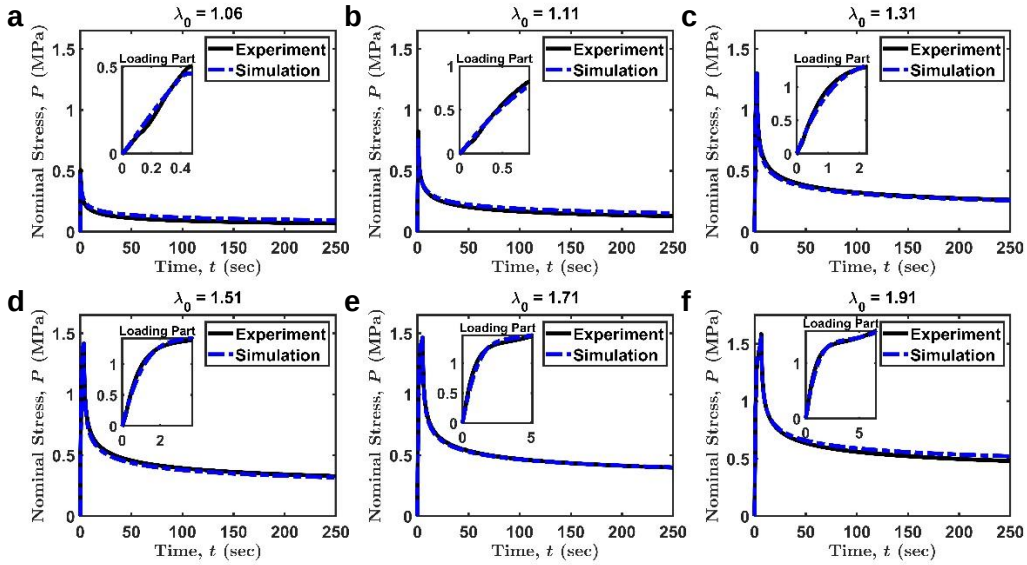

Fig. 3. Nominal stress P (MPa) vs time t (sec) for tensile-relaxation tests with different nominal stretch ratios are shown here. Solid black lines represent the experiment data and our simulation results using parameters in Table 1 are shown as

dash-dotted blue lines. Loading part of the tests are shown as insets. Relaxation tests are carried out at six stretch ratios (a) $\lambda_0 = 1.06$, (b) $\lambda_0 = 1.11$, (c) $\lambda_0 = 1.31$, (d) $\lambda_0 = 1.51$, (e) $\lambda_0 = 1.71$, and (f) $\lambda_0 = 1.91$.

We compare our model with 6 different relaxation tests carried out with different stretch ratios λ_0.

Again, our model is in good agreement with experimental data in both the loading and the relaxation phases for all cases.

5.3. Simple Tension

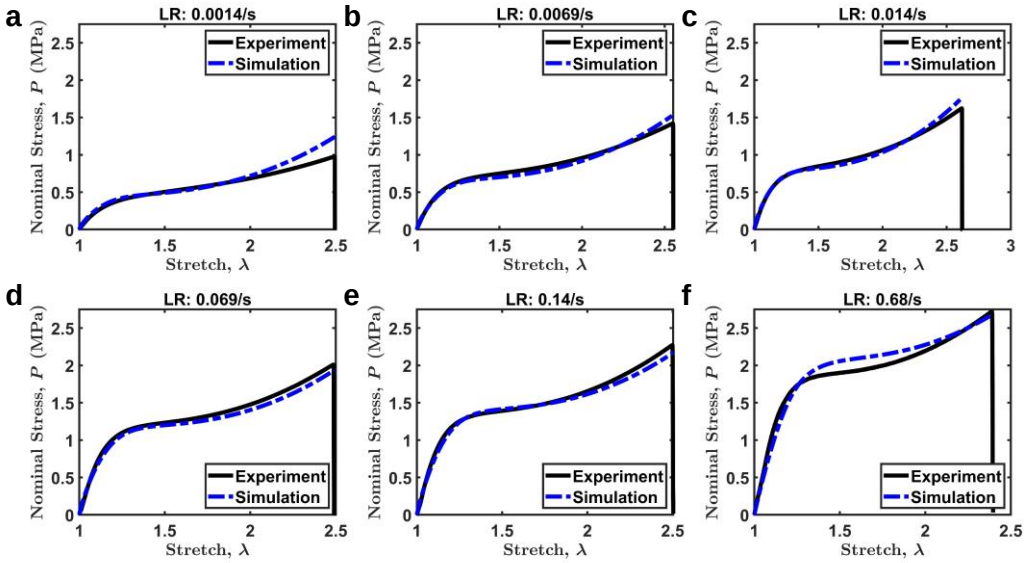

Fig. 4. Nominal stress P (MPa) vs nominal stretch λ for simple tension tests with six loading rates (LR) are presented here. (a) 0.0014/s, (b) 0.0069/s, (c) 0.014/s, (d) 0.069/s, (e) 0.14/s, and (f) 0.68/s. Solid black lines represent the experiment data and our simulation results using parameters in Table 1 are shown as dash-dotted blue lines. Simple tension tests with 6 different loading rates ranging over two decades are presented in Fig. 4. Our model predicts the experimental data for loading rates of 0.069/s and 0.14/s cases well. For the loading rate of 0.0014/s-0.014/s, we observe an overestimation of nominal stress at higher stretch ratios after 2, as the model tends to harden more than the experimental data for slower loading rates. Similarly, at a higher loading rate of 0.68/s, experiment is slightly overestimated by our model. On an average, the relative error between theory and experiment is less than 10% except for the lowest loading rate case of 0.0014/s at higher stretch ratios.

5.4. Load bearing characteristics of physical and chemical crosslinks, Healing rate

The stress carried by physical and chemical bonds for different loading histories are shown in Fig. 5. To present a general trend, we select one case each from simple tension, tensile-relaxation, and cyclic tests. In simple tension, we observe that at lower stretch ratios, most of the stress is carried by physical bonds. This is because $\omega_{\text{chem}} = 0.01$, so most of the load is carried by the physical crosslinks (recall $\rho \approx 0.97$ at the beginning of test, see Table 1). At higher stretch ratios (> 2.2), due to accelerated breaking, a significant fraction of physical bonds break, so the chemical network starts to carry more load. In the tensile-relaxation test, most of the load is carried by physical bonds during the loading phase as the stretch ratios are too low to activate accelerated bond breaking. During relaxation, the healed bonds do not carry any load (the integral term in Eq. (1a) is practically zero). As the initially connected physical bonds continue to break, the stress contribution from these bonds decreases continuously, and the load is carried entirely by the chemical crosslinks. During the cyclic test, as the maximum strains are around 60%, most of the load is carried by physical bonds as the fraction of chemical bonds in the network is only 1%.

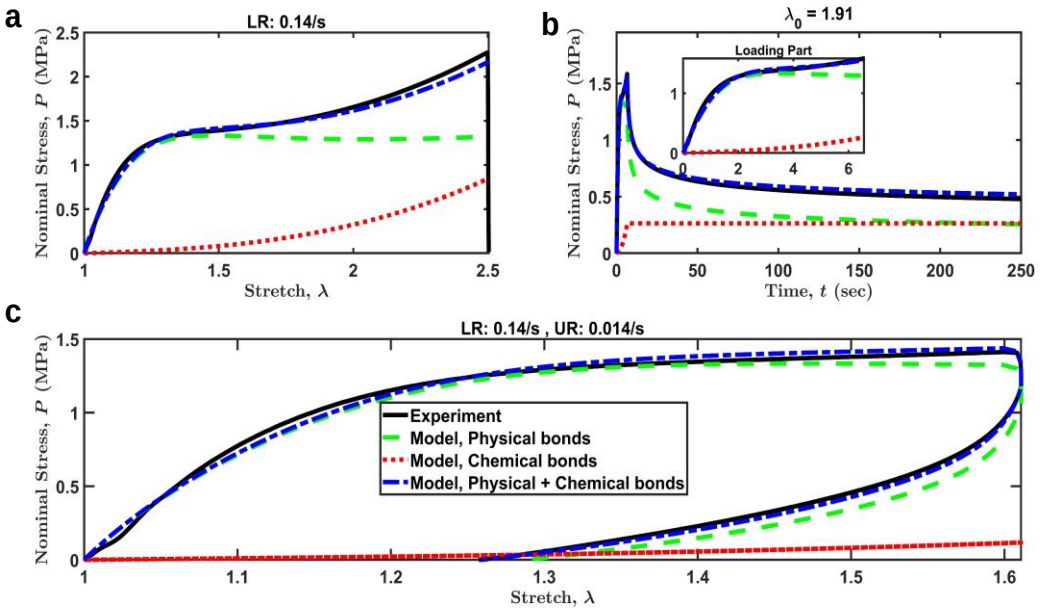

Fig. 5. For different loading histories, stress contributions from both physical and

chemical bonds are computed using our model. (a) simple tension, (b) tensile-relaxation, and (c) cyclic test. The tensile test is carried out using a loading rate (LR) of 0.14/s. The stretch ratio in the tensile-relaxation test is $\lambda_0 \approx 1.91$. The cyclic test has a loading rate (LR) of 0.14/s and an unloading rate (UR) of 0.014/s. Solid black lines represent the experiment data, the stress contribution from physical bonds is shown in green dotted lines, the stress contribution from chemical bonds is shown in red dotted lines, and total stress contribution from both physical and chemical bonds is represented by blue dash-dotted lines.

Next, we study the healing rate predicted by our model during these experiments.

Fig. 6 presents a few representative time dependent healing rates for simple tension, tensile-relaxation, and cyclic tests.

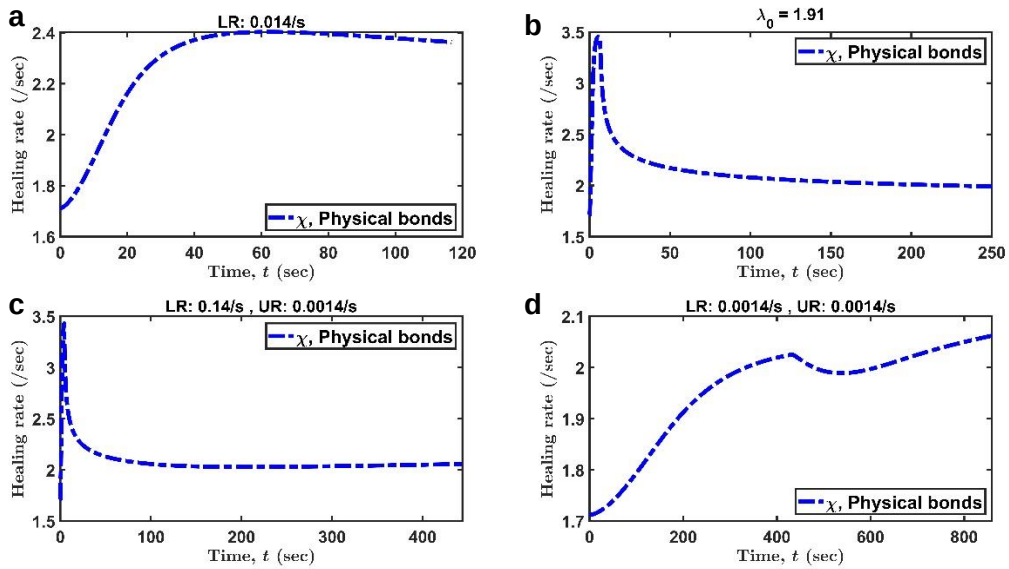

Fig. 6. Healing rate ($\chi(t)$) (in /s) for physical bonds (blue dash-dotted lines) vs time (s) for three types of mechanical testing are shown here. (a) The top left plot is a simple tension test for a constant loading rate (LR) where $\dot{\lambda} =$ 0.014/s. (b) The top right plot is a tensile-relaxation test with a stretch ratio of $\lambda_0 \approx 1.91$. (c) and (d) The two lower plots are cyclic tests with a loading-unloading rates (LR-UR) of 0.14/s-0.0014/s and 0.0014/s-0.0014/s respectively. The unloading starts at around a strain of 60%.

Fig. 6a shows that in a simple tension test, the healing rate first increases and then reaches a plateau. In the increasing region, the number of broken physical crosslinks increases, and since healing rate is proportional to the number of broken bonds, the healing rate increases too. At some point there is no further increase in the number of broken physical bonds, and the healing rate becomes approximately constant. Fig. 6b

shows that during the relaxation part of a tensile-relaxation test, the reattached physical bonds do not carry load, and they break continuously. At long times, the load is carried entirely by the chemical network. In a cyclic test (Fig. 6c, 6d), the healing rate of physical bonds increases during the loading phase. During unloading, either there is a drop in the healing rate or there is hardly any increase after the peak of the loading phase. In Fig. 6c, the loading rate is much faster than the unloading rate, so the behavior is similar to a relaxation test, i.e., the physical crosslinks that reattach during unloading carry very little load. This situation is different in Fig. 6d where the loading and unloading rates are similar, so the physical crosslinks that reattached after the peak load carry substantial load.

6. Discussion and Conclusion

A finite strain constitutive model with time rate and strain dependent bond kinetics is used to study the viscoelastic behavior of the chemical PA gel. Our model predictions agree well with experimental behavior of the gel for simple tension, tensile-relaxation, and cyclic (loading-unloading) tests.

We found that fitting is not sensitive to the choice of strain energy function. This is reasonable since the failure stretch of these chemical gels is around 2.5, so strain hardening effects are not expected to be significant. Data fitting is more sensitive to the choice of the accelerated breaking function f in Eq. (5). Here we note that the accelerated breaking function f given by Eq. (5) differs from our previous work[33] which is

$$f(I_1) = \exp\left\{\left(1+\frac{I_1-3}{I_c-3}\right)^m - 1\right\}, \quad I_c = \lambda_c^2 + \frac{2}{\lambda_c}. \tag{7}$$

In the SI (Section S7), we show that our experiments can be fitted almost as well with this accelerated breaking function. However, the critical stretch ratio λ_c required to produce a good fit is around 1.08, which is lower than what we observe in our experiments ($\lambda_c \in (1.2, 1.3)$). The substantial differences in mechanical behavior of the two systems (chemical + physical vs pure physical gel) suggested that the breaking

kinetics of bonds in the two systems can be different. Because of this, we use the power law breaking accelerated function given by Eq. (5).

In this paper, the behavior of the gel is studied only under uniaxial loading. We notice that in simple tension tests at very slow loading rates (~0.0014/sec), the stress is overestimated by our model. Our model requires more scrutiny in this regime. By subjecting the gel to multi-axial loading and more complex loading histories, we intend to address the limitations and improve our model in a future work.

Acknowledgements

This material is based upon work supported by the National Science Foundation under Grant No. CMMI-1903308. J.P.G. acknowledges support from the Japan Society for the Promotion of Science KAKENHI (grant no. JP17H06144). K.P.C. acknowledges support from the Japan Society for the Promotion of Science KAKENHI (grant no. JP19K23617). J.P.G. and K. P. C. acknowledge support from the Institute for Chemical Reaction Design and Discovery by World Premier International Research Initiative, MEXT, Japan.

Conflicts of Interest

We declare no conflicts of interest.

REFERENCES

[1] K.Y. Lee, D.J. Mooney, Hydrogels for Tissue Engineering, Chem. Rev. 101 (2001) 1869–1880. https://doi.org/10.1021/cr000108x.

[2] B.R. Freedman, D.J. Mooney, Biomaterials to Mimic and Heal Connective Tissues, Adv. Mater. 31 (2019) 1806695. https://doi.org/10.1002/adma.201806695.

[3] C.K. Kuo, P.X. Ma, Ionically crosslinked alginate hydrogels as sca!olds for tissue engineering: Part 1. Structure, gelation rate and mechanical properties, (2001) 11.

[4] H.J. Kwon, Tissue Engineering of Muscles and Cartilages Using Polyelectrolyte Hydrogels, Advances in Materials Science and Engineering. 2014 (2014) 1–7. https://doi.org/10.1155/2014/154071.

[5] H.J. Kwon, K. Yasuda, J.P. Gong, Y. Ohmiya, Polyelectrolyte hydrogels for replacement and regeneration of biological tissues, Macromol. Res. 22 (2014) 227–235. https://doi.org/10.1007/s13233-014-2045-6.

[6] Md.T.I. Mredha, Y.Z. Guo, T. Nonoyama, T. Nakajima, T. Kurokawa, J.P. Gong, A Facile Method to Fabricate Anisotropic Hydrogels with Perfectly Aligned Hierarchical

Fibrous Structures, Adv. Mater. 30 (2018) 1704937. https://doi.org/10.1002/adma.201704937.
[7] T.R. Hoare, D.S. Kohane, Hydrogels in drug delivery: Progress and challenges, Polymer. 49 (2008) 1993–2007. https://doi.org/10.1016/j.polymer.2008.01.027.
[8] Y. Qiu, K. Park, Environment-sensitive hydrogels for drug delivery, Advanced Drug Delivery Reviews. 64 (2012) 49–60. https://doi.org/10.1016/j.addr.2012.09.024.
[9] K. Park, W.S.W. Shalaby, H. Park, Biodegradable hydrogels for drug delivery, Technomic Pub, Lancaster, PA, 1993.
[10] J.P. Gong, Why are double network hydrogels so tough?, Soft Matter. 6 (2010) 2583. https://doi.org/10.1039/b924290b.
[11] J.P. Gong, Y. Katsuyama, T. Kurokawa, Y. Osada, Double-Network Hydrogels with Extremely High Mechanical Strength, Adv. Mater. 15 (2003) 1155–1158. https://doi.org/10.1002/adma.200304907.
[12] Y.-H. Na, T. Kurokawa, Y. Katsuyama, H. Tsukeshiba, J.P. Gong, Y. Osada, S. Okabe, T. Karino, M. Shibayama, Structural Characteristics of Double Network Gels with Extremely High Mechanical Strength, Macromolecules. 37 (2004) 5370–5374. https://doi.org/10.1021/ma049506i.
[13] A. Nakayama, A. Kakugo, J.P. Gong, Y. Osada, M. Takai, T. Erata, S. Kawano, High Mechanical Strength Double-Network Hydrogel with Bacterial Cellulose, Adv. Funct. Mater. 14 (2004) 1124–1128. https://doi.org/10.1002/adfm.200305197.
[14] J.P. Gong, Materials both Tough and Soft, Science. 344 (2014) 161–162. https://doi.org/10.1126/science.1252389.
[15] J.-Y. Sun, X. Zhao, W.R.K. Illeperuma, O. Chaudhuri, K.H. Oh, D.J. Mooney, J.J. Vlassak, Z. Suo, Highly stretchable and tough hydrogels, Nature. 489 (2012) 133–136. https://doi.org/10.1038/nature11409.
[16] T. Nakajima, H. Sato, Y. Zhao, S. Kawahara, T. Kurokawa, K. Sugahara, J.P. Gong, A Universal Molecular Stent Method to Toughen any Hydrogels Based on Double Network Concept, Adv. Funct. Mater. 22 (2012) 4426–4432. https://doi.org/10.1002/adfm.201200809.
[17] Y.N. Ye, M. Frauenlob, L. Wang, M. Tsuda, T.L. Sun, K. Cui, R. Takahashi, H.J. Zhang, T. Nakajima, T. Nonoyama, T. Kurokawa, S. Tanaka, J.P. Gong, Tough and Self-Recoverable Thin Hydrogel Membranes for Biological Applications, Adv. Funct. Mater. 28 (2018) 1801489. https://doi.org/10.1002/adfm.201801489.
[18] Y. Huang, D.R. King, T.L. Sun, T. Nonoyama, T. Kurokawa, T. Nakajima, J.P. Gong, Energy-Dissipative Matrices Enable Synergistic Toughening in Fiber Reinforced Soft Composites, Adv. Funct. Mater. 27 (2017) 1605350. https://doi.org/10.1002/adfm.201605350.
[19] H. Guo, C. Mussault, A. Brûlet, A. Marcellan, D. Hourdet, N. Sanson, Thermoresponsive Toughening in LCST-Type Hydrogels with Opposite Topology: From Structure to Fracture Properties, Macromolecules. 49 (2016) 4295–4306. https://doi.org/10.1021/acs.macromol.6b00798.
[20] T.-T. Mai, T. Matsuda, T. Nakajima, J.P. Gong, K. Urayama, Damage cross-effect and anisotropy in tough double network hydrogels revealed by biaxial stretching, Soft Matter. 15 (2019) 3719–3732. https://doi.org/10.1039/C9SM00409B.
[21] C. Bilici, S. Ide, O. Okay, Yielding Behavior of Tough Semicrystalline Hydrogels, Macromolecules. 50 (2017) 3647–3654. https://doi.org/10.1021/acs.macromol.7b00507.
[22] R. Tamate, K. Hashimoto, T. Horii, M. Hirasawa, X. Li, M. Shibayama, M. Watanabe, Self-Healing Micellar Ion Gels Based on Multiple Hydrogen Bonding, Adv. Mater. 30 (2018) 1802792. https://doi.org/10.1002/adma.201802792.

[23] X. Hu, M. Vatankhah-Varnoosfaderani, J. Zhou, Q. Li, S.S. Sheiko, Weak Hydrogen Bonding Enables Hard, Strong, Tough, and Elastic Hydrogels, Adv. Mater. 27 (2015) 6899–6905. https://doi.org/10.1002/adma.201503724.
[24] H.J. Zhang, T.L. Sun, A.K. Zhang, Y. Ikura, T. Nakajima, T. Nonoyama, T. Kurokawa, O. Ito, H. Ishitobi, J.P. Gong, Tough Physical Double-Network Hydrogels Based on Amphiphilic Triblock Copolymers, Adv. Mater. 28 (2016) 4884–4890. https://doi.org/10.1002/adma.201600466.
[25] T.L. Sun, T. Kurokawa, S. Kuroda, A. Bin Ihsan, T. Akasaki, K. Sato, M.A. Haque, T. Nakajima, J.P. Gong, Physical hydrogels composed of polyampholytes demonstrate high toughness and viscoelasticity, Nature Materials. 12 (2013) 932–937. https://doi.org/10.1038/nmat3713.
[26] F. Luo, T.L. Sun, T. Nakajima, T. Kurokawa, Y. Zhao, K. Sato, A.B. Ihsan, X. Li, H. Guo, J.P. Gong, Oppositely Charged Polyelectrolytes Form Tough, Self-Healing, and Rebuildable Hydrogels, Adv. Mater. 27 (2015) 2722–2727. https://doi.org/10.1002/adma.201500140.
[27] X. Zhang, Y. Liu, J. Wen, Z. Zhao, H. Chen, X. Liu, S. Liu, Host–guest interaction-mediated fabrication of a hybrid microsphere-structured supramolecular hydrogel showing high mechanical strength, Soft Matter. 16 (2020) 3416–3424. https://doi.org/10.1039/D0SM00271B.
[28] M. Nakahata, Y. Takashima, A. Harada, Highly Flexible, Tough, and Self-Healing Supramolecular Polymeric Materials Using Host-Guest Interaction, Macromol. Rapid Commun. 37 (2016) 86–92. https://doi.org/10.1002/marc.201500473.
[29] S. Burattini, H.M. Colquhoun, J.D. Fox, D. Friedmann, B.W. Greenland, P.J.F. Harris, W. Hayes, M.E. Mackay, S.J. Rowan, A self-repairing, supramolecular polymer system: healability as a consequence of donor–acceptor π–π stacking interactions, Chem. Commun. (2009) 6717. https://doi.org/10.1039/b910648k.
[30] M.A. Haque, T. Kurokawa, G. Kamita, J.P. Gong, Lamellar Bilayers as Reversible Sacrificial Bonds To Toughen Hydrogel: Hysteresis, Self-Recovery, Fatigue Resistance, and Crack Blunting, Macromolecules. 44 (2011) 8916–8924. https://doi.org/10.1021/ma201653t.
[31] D.C. Tuncaboylu, M. Sari, W. Oppermann, O. Okay, Tough and Self-Healing Hydrogels Formed via Hydrophobic Interactions, Macromolecules. 44 (2011) 4997–5005. https://doi.org/10.1021/ma200579v.
[32] R. Long, K. Mayumi, C. Creton, T. Narita, C.-Y. Hui, Time Dependent Behavior of a Dual Cross-Link Self-Healing Gel: Theory and Experiments, Macromolecules. 47 (2014) 7243–7250. https://doi.org/10.1021/ma501290h.
[33] S.P. Venkata, K. Cui, J. Guo, A.T. Zehnder, J.P. Gong, C.-Y. Hui, Constitutive modeling of bond breaking and healing kinetics of physical Polyampholyte (PA) gel, Extreme Mechanics Letters. 43 (2021) 101184. https://doi.org/10.1016/j.eml.2021.101184.
[34] K. Cui, T.L. Sun, T. Kurokawa, T. Nakajima, T. Nonoyama, L. Chen, J.P. Gong, Stretching-induced ion complexation in physical polyampholyte hydrogels, Soft Matter. 12 (2016) 8833–8840. https://doi.org/10.1039/C6SM01833E.
[35] K. Cui, T.L. Sun, X. Liang, K. Nakajima, Y.N. Ye, L. Chen, T. Kurokawa, J.P. Gong, Multiscale Energy Dissipation Mechanism in Tough and Self-Healing Hydrogels, Physical Review Letters. 121 (2018) 185501. https://doi.org/10.1103/PhysRevLett.121.185501.
[36] X. Li, K. Cui, T.L. Sun, L. Meng, C. Yu, L. Li, C. Creton, T. Kurokawa, J.P. Gong, Mesoscale bicontinuous networks in self-healing hydrogels delay fatigue fracture,

Proceedings of the National Academy of Sciences. 117 (2020) 7606–7612. https://doi.org/10.1073/pnas.2000189117.
[37] T.L. Sun, F. Luo, W. Hong, K. Cui, Y. Huang, H.J. Zhang, D.R. King, T. Kurokawa, T. Nakajima, J.P. Gong, Bulk Energy Dissipation Mechanism for the Fracture of Tough and Self-Healing Hydrogels, Macromolecules. 50 (2017) 2923–2931. https://doi.org/10.1021/acs.macromol.7b00162.
[38] K. Cui, Y.N. Ye, T.L. Sun, L. Chen, X. Li, T. Kurokawa, T. Nakajima, T. Nonoyama, J.P. Gong, Effect of Structure Heterogeneity on Mechanical Performance of Physical Polyampholytes Hydrogels, Macromolecules. 52 (2019) 7369–7378. https://doi.org/10.1021/acs.macromol.9b01676.
[39] K. Cui, Y.N. Ye, T.L. Sun, C. Yu, X. Li, T. Kurokawa, J.P. Gong, Phase Separation Behavior in Tough and Self-Healing Polyampholyte Hydrogels, Macromolecules. 53 (2020) 5116–5126. https://doi.org/10.1021/acs.macromol.0c00577.
[40] K. Cui, Y.N. Ye, C. Yu, X. Li, T. Kurokawa, J.P. Gong, Stress Relaxation and Underlying Structure Evolution in Tough and Self-Healing Hydrogels, ACS Macro Lett. (2020) 1582–1589. https://doi.org/10.1021/acsmacrolett.0c00600.
[41] R. Long, K. Mayumi, C. Creton, T. Narita, C.-Y. Hui, Rheology of a dual crosslink self-healing gel: Theory and measurement using parallel-plate torsional rheometry, Journal of Rheology. 59 (2015) 643–665. https://doi.org/10.1122/1.4915275.
[42] J. Guo, R. Long, K. Mayumi, C.-Y. Hui, Mechanics of a Dual Cross-Link Gel with Dynamic Bonds: Steady State Kinetics and Large Deformation Effects, Macromolecules. 49 (2016) 3497–3507. https://doi.org/10.1021/acs.macromol.6b00421.

SUPPORTING INFORMATION

Constitutive modeling of strain-dependent bond breaking and healing kinetics of chemical Polyampholyte (PA) gel

Sairam Pamulaparthi Venkata[a,4#], Kunpeng Cui[b,4#], Jingyi Guo[a], Alan T. Zehnder[a], Jian Ping Gong[b,c,d], & Chung-Yuen Hui[a,c*]

[a] Field of Theoretical and Applied Mechanics, Department of Mechanical and Aerospace Engineering, Cornell University, Ithaca, New York, 14853, United States

[b] Institute for Chemical Reaction Design and Discovery (WPI-ICReDD), Hokkaido University, Sapporo 001-0021, Japan

[c] Soft Matter GI-CoRE, Hokkaido University, Sapporo 001-0021, Japan

[d] Faculty of Advanced Life Science, Hokkaido University, Sapporo 001-0021, Japan

[*] **Corresponding Author**, E-mail: ch45@cornell.edu (C.-Y.H.)

#These two authors contributed equally to this paper.

1. Discussion on healing rate and survivability function

Physically, the healing rate must increase with the number of broken bonds. The simplest assumption is that healing rate is directly proportional to the number of broken bonds divided by a characteristic healing time. This is a reasonable assumption since healing is achieved by ionic bonding to the number of available sites, so the reaction rate should be proportional to the number of broken bonds.

Eq. (1b) (main file) is based on the following physical reasoning. The rate of *decrease* of connected bonds N should increase with the number of connected bonds, that is,

$$-dN/dt \propto b(N), \qquad \text{(S1)}$$

where b is a monotonically increasing function of N. The function b can be inferred from a load relaxation test, since in our theory the healed bonds during a perfect

[4] These authors contributed equally to this work. Numerical simulations are done by Sairam Pamulaparthi Venkata. Experimental data is provided by Kunpeng Cui.

relaxation test do not carry load. In a relaxation test, the amount of load relaxation is directly proportional to the number of broken bonds, this allows us to determine $N(t)$ and we found $b(N) \propto N^{\alpha_B}$. In our previous *PVA* gel system[1,2], experiments showed that the bond breaking kinetics is *insensitive* to the applied stretch, this means that the rate of change of the survivability function can be written as

$$-\frac{d\phi_B}{dt} = \frac{1}{t_B}\phi_B^{\alpha_B}. \qquad \text{(S2)}$$

However, for the PA gel system, we found that the bond breaking kinetics is sensitive to the stretch. Therefore, we modify Eq. (S2) to reflect the effect of stretching on bond breaking. Using the affine approximation, we assume that the force acting on a chain is a function of first invariant of right Cauchy-Green tensor $I_1 = \mathbf{F}^T\mathbf{F}$, where $\mathbf{F}$ is the deformation tensor. As a result, the function b in Eq. (S1) also depends on I_1. We assume that b is separable, so for a chain formed at a time τ and survived until a time $t > \tau$, the rate of change of survivability function is

$$-\frac{d\phi_B}{dt} = \frac{1}{t_B}\phi^{\alpha_B} f\left[H(\tau,t)\right], \qquad H(\tau,t) = \text{trace}\left[\left(F^{\tau\to t}\right)^T F^{\tau\to t}\right]. \qquad \text{(S3)}$$

There is some similarity between our idea and Erying's theory[3](e.g. separability) which proposed that the bond dissociation rate has the form

$$-dN/dt \propto N\, exp\left(\frac{L_a\bar{F}}{k_BT}\right), \qquad \text{(S4)}$$

where L_a is the activation length for bond dissociation and $\bar{F}$ is the tensile force acting on a single polymer chain.

2. *Steady state healing rate*

From the second term in the R.H.S of Eq. (2) (main file), we notice that the fraction of connected physical bonds at any time t is given by

$$\int_{-\infty}^{t} \phi_B(\tau, t, H^{\tau\to t})\chi(\tau)d\tau. \qquad \text{(S5a)}$$

By definition, the fraction of connected physical bonds *before the start of loading* ($t = 0$) is denoted by ρ. Here is it important to note that $H^{\tau\to 0} = 3$ since no loading

occurs for time less than 0, that is, the deformation gradient is the identity tensor for time $t<0$. In addition, for $t<0$, the healing rate $\chi(t)$ is a constant given by its steady state value χ^{ss}, since the sample has rested for sufficiently long times so that the system is in dynamic equilibrium. Using Eq. (S5a), we get

$$\rho = \int_{-\infty}^{0} \phi_B(\tau, t=0, H^{\tau\to 0})\chi(\tau)d\tau$$

$$= \chi^{ss}\int_{-\infty}^{0}\left[1+\frac{\alpha_B-1}{t_B}\int_{\tau}^{0} f\left(H^{\tau\to 0}=3\right)ds\right]^{\frac{1}{1-\alpha_B}} d\tau, \qquad . \qquad \text{(S5b)}$$

$$= \chi^{ss}\int_{-\infty}^{0}\left[1+\frac{\alpha_B-1}{t_B}(-\tau)\right]^{\frac{1}{1-\alpha_B}} d\tau = \frac{\chi^{ss}t_B}{2-\alpha_B}, \quad \forall\, 1<\alpha_B<2.$$

In the last step, we have used the fact that $f\left(H^{\tau\to 0}=3\right)=1$.

By setting $t=0$ in the Eq. (2) (main file) and Eq. (1b) (main file) with $f=1$ for $t\le 0$, we determine the steady state healing rate of physical bonds to be

$$\chi^{ss}t_H + 0 = \omega_{\text{phys}} - \chi^{ss}\frac{t_B}{2-\alpha_B}\left[\underbrace{\phi_B(0,0)}_{1}\right]^{2-\alpha_B} \Rightarrow \chi^{ss} = \frac{\omega_{\text{phys}}}{t_H + \frac{t_B}{2-\alpha_B}}. \qquad \text{(S5c)}$$

3. *Total strain energy*

We assume that the polymer chains instantaneously relax as the bond breaks and carry zero stress. Also, the chains reattach in a relaxed state and carry no strain energy. By following a similar procedure as in our physical PA gel work[4] along with the addition of strain energy due to chemical bonds, we get the total strain energy $W(t)$ to be

$$\underset{\text{Total strain energy}}{W(t)} = \underbrace{\omega_{\text{chem}}W_0\left(I_1(t)\right)}_{\substack{\text{Strain energy due to}\\ \text{chemical cross-links}}} + \underbrace{\int_{-\infty}^{t}\phi_B(\tau,t)\chi(\tau)W_0\left[H(\tau,t)\right]d\tau}_{\substack{\text{Strain energy due to}\\ \text{physical cross-links}}}, \qquad \text{(S6)}$$

$$I_1(t) = \text{trace}\left[\left(\mathbf{F}^{0\to t}\right)^T\left(\mathbf{F}^{0\to t}\right)\right].$$

4. *Derivation of nominal stress from strain energy: Coleman-Noll Procedure*

Following a similar procedure as in our previous works on PVA gel[1,2,5] and on physical PA gel[4], we briefly describe our procedure here. From Eq. (S6), the total strain energy density $W(t)$ of the chemical PA gel system is given by

$$W(t) = \omega_{\text{chem}} W_0[I_1(t)] + \int_{-\infty}^{t} \chi(\tau)\phi_B(\tau,t,H(\tau,t))W_0\left[H(\tau,t)\right]d\tau, \qquad \text{(S7)}$$

Using Eq. (S7) and $W_0\left[H(t,t)\right]=0$, as $H(t,t)=3$, we can calculate the change of strain energy density with respect to time as

$$\begin{aligned}\dot{W}(t) &\equiv \frac{dW(t)}{dt}, \\ &= \omega_{\text{chem}} \frac{d}{dt}\left(W_0\left[I_1(t)\right]\right) + \int_{-\infty}^{t} \chi(\tau)\phi_B(\tau,t,H(\tau,t)) \left.\frac{dW_0(I_1)}{dI_1}\right|_{I_1=H(\tau,t)} \frac{\partial H(\tau,t)}{\partial t} d\tau \\ &+ \int_{-\infty}^{t} \chi(\tau) \frac{\partial}{\partial t}\left(\phi_B(\tau,t,H(\tau,t))\right) W_0\left[H(\tau,t)\right]d\tau.\end{aligned} \qquad \text{(S8)}$$

As in our physical PA gel work[4], the time derivative term of $H(\tau,t)$ in Eq. (S8) can be written as

$$\frac{\partial H(\tau,t)}{\partial t} = \frac{\partial}{\partial t}\left(\text{trace}\left[\left(\mathbf{F}^{\tau\to t}\right)^T \mathbf{F}^{\tau\to t}\right]\right) = 2F_{ik}^{\ \tau\to t}\left(F_{jk}^{\ 0\to\tau}\right)^{-1} \cdot \dot{F}_{ij}^{\ 0\to t}. \qquad \text{(S9)}$$

Also, we observe that the time derivative of survivability function does not contain time rate of change of deformation, $\dot{F}_{ij}^{\ 0\to t}$. Terms associated with $\dot{\mathbf{F}}$ in Eq. (S8) are equated with $\left[P_{ij} + p\left(F_{ji}^{\ 0\to t}\right)^{-1}\right]\dot{F}_{ij}^{\ 0\to t}$ in the energy balance equation to get

$$\begin{aligned}\omega_{\text{chem}} \left.\frac{dW_0(I_1)}{dI_1}\right|_{I_1=I_1(t)} \frac{dI_1(t)}{dt} + \int_{-\infty}^{t} \chi(\tau)\phi_B(\tau,t,H(\tau,t)) \left.\frac{dW_0(I_1)}{dI_1}\right|_{I_1=H(\tau,t)} \frac{\partial H(\tau,t)}{\partial t} d\tau \\ = \left[P_{ij} + p\left(F_{ji}^{\ 0\to t}\right)^{-1}\right]\dot{F}_{ij}^{\ 0\to t}.\end{aligned} \qquad \text{(S10)}$$

where $\mathbf{P}$ is the first Piola-Kirchhoff stress tensor with p being the Lagrange multiplier enforcing incompressibility. Using Eqs. (S8)-(S10) we get

$$\left[P_{ij}+p\left(F_{ji}^{\,0\to t}\right)^{-1}\right]\dot{F}_{ij}^{\,0\to t}=\omega_{\text{chem}}\left.\frac{dW_0(I_1)}{dI_1}\right|_{I_1=I_1(t)}2F_{ij}^{0\to t}\dot{F}_{ij}^{\,0\to t}+$$
$$\int_{-\infty}^{t}\chi(\tau)\phi_B(\tau,t,H(\tau,t))\left.\frac{dW_0(I_1)}{dI_1}\right|_{I_1=H(\tau,t)}2F_{ik}^{\,\tau\to t}\left(F_{jk}^{\,0\to\tau}\right)^{-1}\cdot\dot{F}_{ij}^{\,0\to t}d\tau.$$

(S11a)

and

$$P_{ij}=-p\left(F_{ji}^{0\to t}\right)^{-1}+\omega_{\text{chem}}\left.\frac{dW_0(I_1)}{dI_1}\right|_{I_1=I_1(t)}2F_{ij}^{0\to t}+\int_{-\infty}^{0}\chi^{ss}\phi_B(\tau,t,H(\tau,t))2\left.\frac{dW_0(I_1)}{dI_1}\right|_{I_1(t)}F_{ij}^{\,0\to t}d\tau$$
$$+\int_{0}^{t}\chi(\tau)\phi_B(\tau,t,H(\tau,t))2\left.\frac{dW_0(I_1)}{dI_1}\right|_{I_1=H(\tau,t)}F_{ik}^{\,\tau\to t}\left(F_{jk}^{\,0\to\tau}\right)^{-1}d\tau.$$

(S11b)

The nominal stress in Eq. (S7b) can re-written in tensor notation as

$$\mathbf{P}(t)=-p\left(\mathbf{F}^{0\to t}\right)^{-T}+\omega_{\text{chem}}\left.2\frac{dW_0}{dI_1}\right|_{I_1(t)}\mathbf{F}^{0\to t}+\left\{\chi^{ss}\frac{t_B}{2-\alpha_B}\left[\phi_B\left(0,t,I_1(t)\right)\right]^{2-\alpha_B}\right\}\left.2\frac{dW_0}{dI_1}\right|_{I_1(t)}\mathbf{F}^{0\to t}$$
$$+\int_{0}^{t}\phi_B(\tau,t,H(\tau,t))\chi(\tau)\left.2\frac{dW_0}{dI_1}\right|_{I_1=H(\tau,t)}\mathbf{F}^{\tau\to t}\left(\mathbf{F}^{0\to\tau}\right)^{-T}d\tau.$$

(S12)

4.1. Nominal stress in Uniaxial Tension test

Let the nominal stretch at any given time t be $\lambda(t)$. Now the deformation gradient tensor becomes

$$\boldsymbol{F}^{0\to t}=\begin{bmatrix}\lambda(t) & 0 & 0\\ 0 & 1/\sqrt{\lambda(t)} & 0\\ 0 & 0 & 1/\sqrt{\lambda(t)}\end{bmatrix},\quad \text{with } \det\mathbf{F}=1. \tag{S13}$$

Substituting Eq. (S13) in Eq. (S12) and using $P_{22}=0$ to determine p, the nominal stress under uniaxial tension loading is

$$
\begin{aligned}
P_{11}(t) \equiv P(t) &= \left[\omega_{\text{chem}} + \chi^{ss} \int_{-\infty}^{0} \phi\left(\tau, t, H^{\tau\to t}\right) d\tau \right] 2 \left. \frac{dW_0}{dI_1} \right|_{I_1(t)} \left(\lambda(t) - \lambda(t)^{-2} \right) \\
&+ \int_0^t \left[\chi(\tau) \phi\left(\tau, t, H^{\tau\to t}\right) 2 \left. \frac{dW_0}{dI_1} \right|_{H^{\tau\to t}} \left[\frac{\lambda(t)}{\lambda^2(\tau)} - \frac{\lambda(\tau)}{\lambda^2(t)} \right] \right] d\tau, \\
&= \left[\omega_{\text{chem}} + \chi^{ss} \frac{t_B}{2-\alpha_B} \left[\phi\left(\tau = 0, t, H^{0\to t}\right) \right]^{2-\alpha_B} \right] 2 \left. \frac{dW_0}{dI_1} \right|_{I_1(t)} \left(\lambda(t) - \lambda(t)^{-2} \right) \\
&+ \int_0^t \left[\chi(\tau) \phi\left(\tau, t, H^{\tau\to t}\right) 2 \left. \frac{dW_0}{dI_1} \right|_{H^{\tau\to t}} \left[\frac{\lambda(t)}{\lambda^2(\tau)} - \frac{\lambda(\tau)}{\lambda^2(t)} \right] \right] d\tau.
\end{aligned}
\tag{S14}
$$

4.2. Nominal stress in Tensile-Relaxation test

In an actual experiment, it takes a finite loading time t_1 before we achieve the desired nominal stretch ratio λ_0. Once the desired stretch ratio is reached it is held constant to start the relaxation test.

The nominal stress in the loading direction is given by

$$
P(t) = \begin{cases}
\left[\omega_{\text{chem}} + \chi^{ss} \frac{t_B}{2-\alpha_B} \left[\phi\left(\tau = 0, t, H^{0\to t}\right) \right]^{2-\alpha_B} \right] 2 \left. \frac{dW_0}{dI_1} \right|_{I_1(t)} \left(\lambda(t) - \lambda(t)^{-2} \right) & \\
+ \int_0^t \left[\chi(\tau) \phi\left(\tau, t, H^{\tau\to t}\right) 2 \left. \frac{dW_0}{dI_1} \right|_{I_1 = H^{\tau\to t}} \left[\frac{\lambda(t)}{\lambda^2(\tau)} - \frac{\lambda(\tau)}{\lambda^2(t)} \right] \right], & \text{if } t \le t_1 \\
\left[\omega_{\text{chem}} + \chi^{ss} \frac{t_B}{2-\alpha_B} \left[\phi\left(\tau = 0, t, H^{0\to t}\right) \right]^{2-\alpha_B} \right] 2 \left. \frac{dW_0}{dI_1} \right|_{I_1(t)} \left(\lambda_0 - \lambda_0^{-2} \right) & \\
+ \int_0^{t_1} \left[\chi(\tau) \phi\left(\tau, t, H^{\tau\to t}\right) 2 \left. \frac{dW_0}{dI_1} \right|_{I_1 = H^{\tau\to t}} \left[\frac{\lambda_0}{\lambda^2(\tau)} - \frac{\lambda(\tau)}{\lambda_0^2} \right] \right]. & \text{if } t > t_1
\end{cases}
$$

. (S15)

5. Material parameter estimates from experiments

5.1.Estimate for small strain instantaneous shear modulus

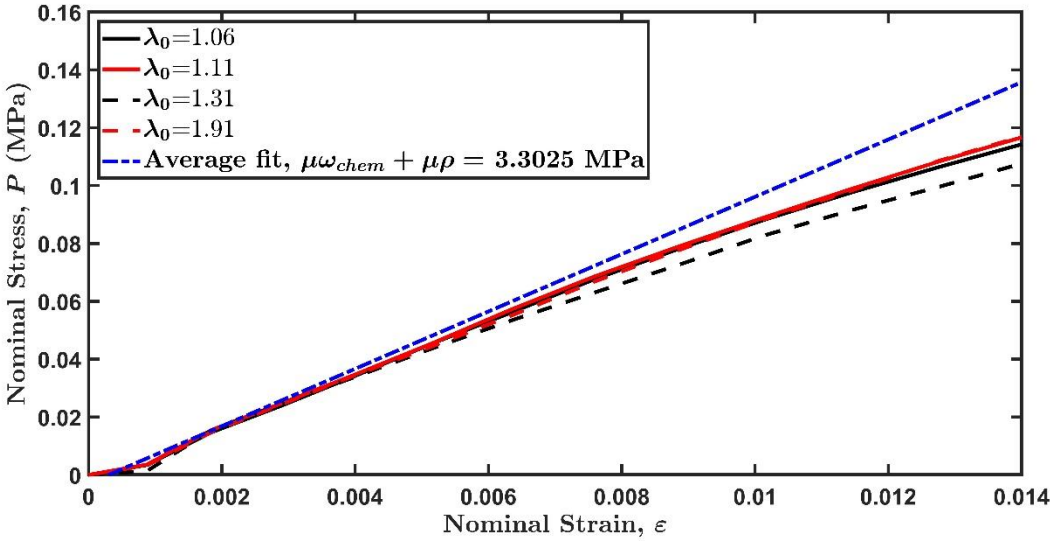

Fig. S1. Fitting the initial slope from the loading portion of four tensile-relaxation tests carried out at four stretch ratios λ_0 (solid lines). The experimental nominal stress – nominal strain plots shown here are from the same data set. We observe that all the four relaxation tests fall on the same line at small strains (less than 0.5%).

The nominal stress in a uniaxial tension test is given by Eq. (S14). As the loading begins, at small times and small strains, there are very few newly formed bonds and the fraction of physical bonds connected in the material are almost same as their steady state fraction ρ. This results in integral term in the Eq. (S14) to be small in comparison with the first term. As strains are small at short times, we can neglect the strain hardening $\left(2\dfrac{dW_0}{dI_1}\bigg|_{I_1(t)} \approx \mu \right)$ and strain dependent breaking terms to get

$$\begin{aligned} P_{11}\left(t\to 0^+\right) &\approx \mu\left(\omega_{\text{chem}} + \chi^{ss}\frac{t_B}{2-\alpha_B}\right)\left(\lambda\left(t\to 0^+\right) - \lambda\left(t\to 0^+\right)^{-2}\right), \\ &\approx 3\mu\left(\omega_{\text{chem}} + \chi^{ss}\frac{t_B}{2-\alpha_B}\right)\varepsilon = 3\mu\left(\omega_{\text{chem}} + \rho\right)\varepsilon = E_0\varepsilon \end{aligned}, \qquad \text{(S16)}$$

where E_0 is the instantaneous Young's modulus which represents the initial slope of the nominal stress – nominal strain curve. This allows us to use the initial slope from the loading portion of tensile-relaxation test to determine $\mu\left(\omega_{\text{chem}} + \rho\right)$ as shown in

Fig. S1. We notice the small strain instantaneous shear modulus to be $\mu(\omega_{\text{chem}}+\rho)\approx 3.30$ MPa (1/3 of the slope of the dotted blue line) from Fig. S1.

5.2.Estimate for critical stretch ratio λ_c

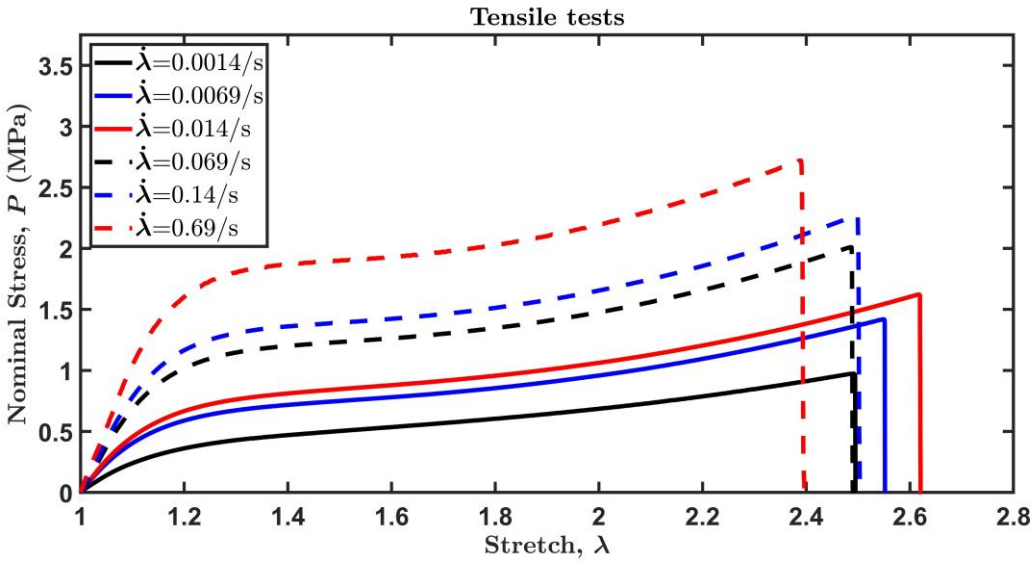

Fig. S2. Uniaxial tension test data for chemical PA-gel for different stretch rates.

Uniaxial tension test data in Fig. S2 shows that the slope of nominal stress versus nominal strain plots decrease rapidly around a critical strain of $\lambda_c \in (1.2, 1.3)$ for different loading rates. This critical strain was associated with "yielding" in the double network gel[6]. Also, the "yield" stress increases with increasing strain rate, but the yield strain remains almost the same. This observation is consistent with our assumption that the breaking kinetics in Eq. (1b) (main file) is controlled by the stretch/strain experienced by the bond.

6. Data sets used for optimization process

As in our physical PA gel work[4], we follow a similar procedure here. The data used for optimization process from simple tension, tensile-relaxation, and cyclic tests is shown in Fig. S3. Here, solid black lines represent the experimental data and blue dotted lines represent the optimization points. The objective function is to minimize the least squares error in nominal stress predicted by our model (see Eq. (S17)) at these optimization points. In Fig. S3, for brevity, LR and UR are used to represent

loading and unloading rates respectively. To capture the change in curvature of nominal stress with nominal strain accurately, more weightage is given to the curved regions by selecting relatively more optimization points around these regions. We use a *lsqcurvefit* inbuilt function with *trust-region-reflective* algorithm in *MATLAB 2018a* version for the optimization process.

$$\sum_i \left(\mathcal{F}(\boldsymbol{\eta}, xdata_i) - ydata_i\right)^2, \quad lb \le \boldsymbol{\eta} \le ub, \qquad \text{(S17)}$$

where $\boldsymbol{\eta}$ denotes a vector of nine material parameters in Table 1 (main file) and $\mathcal{F}$ refers to the nominal stress predicted by our model under different loading histories (simple tension, tensile-relaxation, and cyclic tests). Here, *xdata* is a column vector of selected nominal stretch values in simple tension and cyclic tests, and a column vector of selected time points in tensile-relaxation tests. Whereas *ydata* is the experimental nominal stress values at these corresponding *xdata* points. The *lb* and *ub* denote lower and upper bonds on $\boldsymbol{\eta}$ respectively.

For the optimization process to be computationally efficient and less time consuming, we replace the history dependent reattachment rate $\left(\chi(t)\right)$ with the steady state value $\left(\chi^{ss}\right)$. This assumption helps us avoid solving the integral equation (Eq. (2), main file). Now, as a part of optimization process, we obtain multiple local optimum sets with less than 10 percent relative error between model prediction and experiments at any optimization point. So, we use estimates from Section S5 to select an optimal parameter set from these multiple optimums.

Now, with this chosen parameter set and by solving the integral equation, we recalculate $\mathcal{F}(\boldsymbol{\eta}, xdata_i)$ to check if $\left|\mathcal{F}(\boldsymbol{\eta}, xdata_i) - ydata_i\right| \le 0.1\left|ydata_i\right| \ \forall\ i$ and slightly fine tune the parameter set to get the best possible fits.

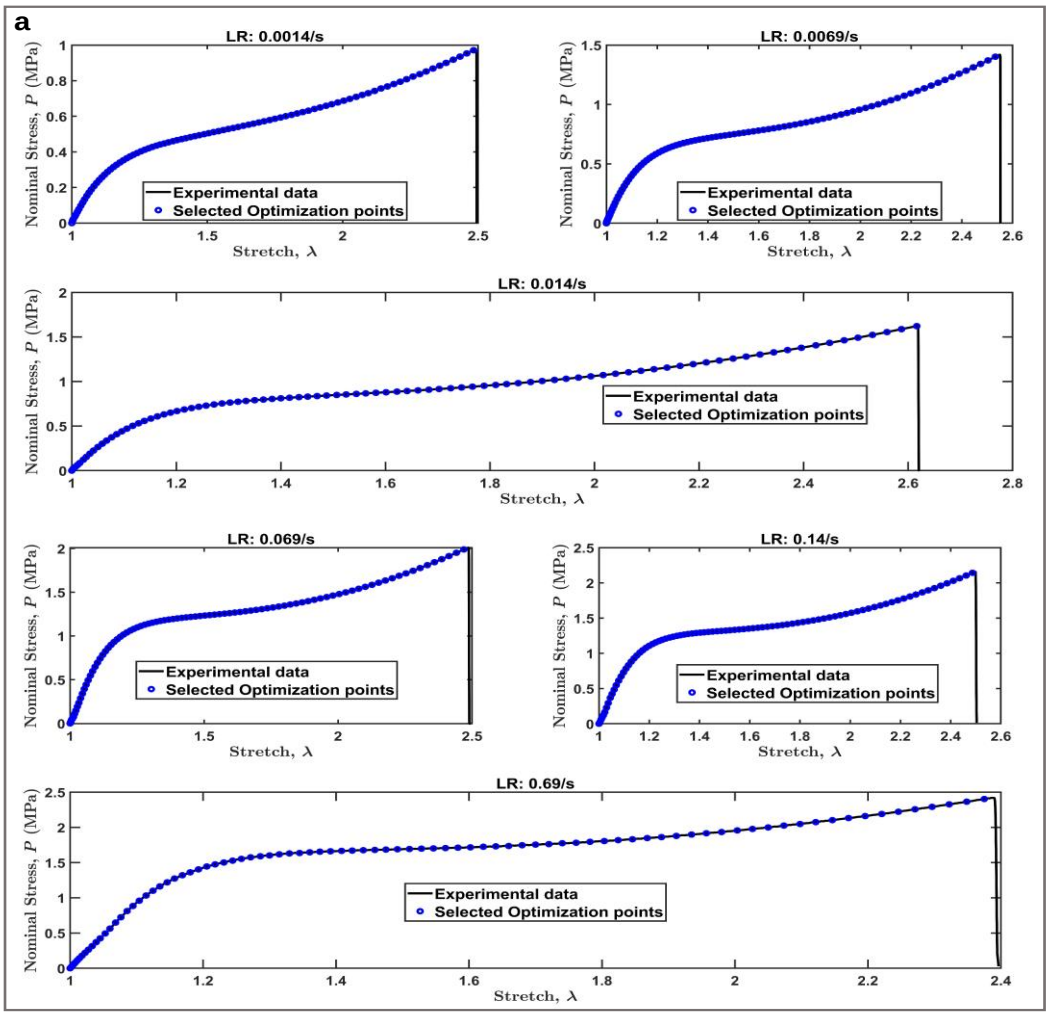
a
LR: 0.0014/s
LR: 0.0069/s
LR: 0.014/s
LR: 0.069/s
LR: 0.14/s
LR: 0.69/s
Nominal Stress, P (MPa)
Stretch, λ
Experimental data
Selected Optimization points

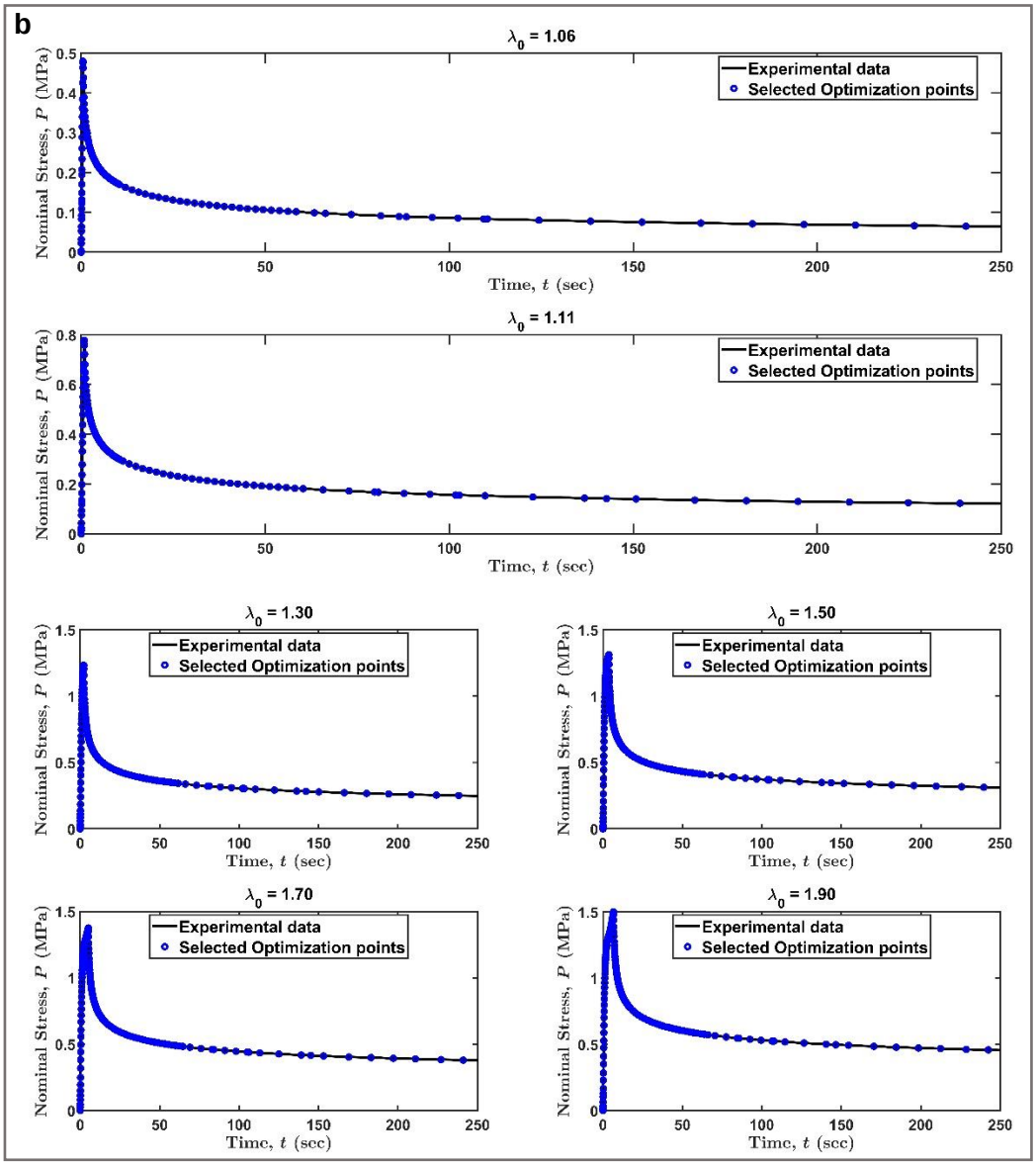
b
λ_0 = 1.06
Experimental data
Selected Optimization points
Nominal Stress, P (MPa)
Time, t (sec)
λ_0 = 1.11
λ_0 = 1.30
λ_0 = 1.50
λ_0 = 1.70
λ_0 = 1.90

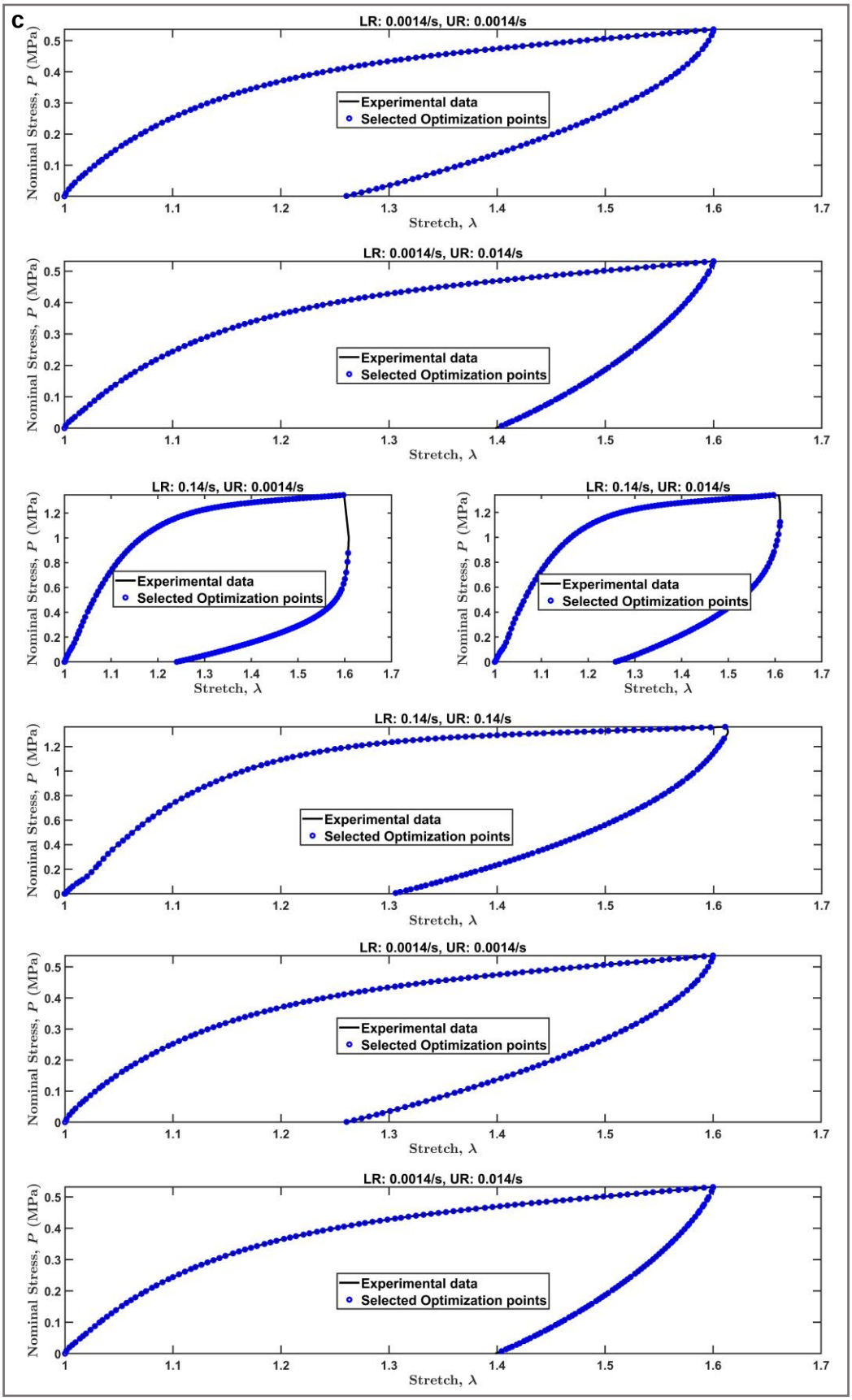
c
LR: 0.0014/s, UR: 0.0014/s
LR: 0.0014/s, UR: 0.014/s
LR: 0.14/s, UR: 0.0014/s
LR: 0.14/s, UR: 0.014/s
LR: 0.14/s, UR: 0.14/s
LR: 0.0014/s, UR: 0.0014/s
LR: 0.0014/s, UR: 0.014/s
Experimental data
Selected Optimization points
Nominal Stress, P (MPa)
Stretch, λ

Fig. S3. We present all the representative data sets used for optimization process here (a) simple tension, (b) tensile-relaxation tests, and (c) loading-unloading tests which are used for least squares optimization process are presented here. All the 9 independent material parameters in Table 1 (main file) are optimized to get the minimum least squares error in nominal stress at the selected optimization points (shown as blue dotted circles) from all the curves shown here. Here, LR represents loading rate and UR represents unloading rate.

7. *Exponential of power law form of breaking function and results*

As mentioned in the main file (Section 6), here we use an accelerating breaking function of form $f(I_1)=\exp\left\{\left(1+\frac{I_1-3}{I_c-3}\right)^m-1\right\}$, $I_c=\lambda_c^2+\frac{2}{\lambda_c}$ as in our previous work[4] and observe almost as good fits as in the results presented in the main file (Section 5). The material parameters for the model with f of exponential of power law form are mentioned in the Table S1.

Table S1: The material parameters required for constitutive model are listed below.

Strain dependent parameters			
$\alpha_B=1.8023$	$t_B=0.1169\,\text{sec}$	$t_H=0.01\,\text{sec}$	$\omega_{\text{phys}}=0.99$
Strain dependent accelerated breaking function parameters, f			
$m=0.5452$		$\lambda_c=1.0854$	
Undamaged network strain energy density function, Yeoh's model, W_0			
$c_1\equiv\mu/2=1.8500\,\text{MPa}$	$c_2/c_1=0.2968$	$c_3/c_1=0.1566$	
Derived material parameters			
$\rho=0.9735$ **(see Eq. (3a), main file)**	$\chi^{SS}=1.6466\ s^{-1}$ **(see Eq. (3b), main file)**	$\mu(\omega_{\text{chem}}+\rho)\equiv\frac{E_0}{3}=3.6390\,\text{MPa}$	

Using the material parameters from Table S1, the following numerical results are computed.

7.1. Cyclic tests

7.1.1. Small strain

The uniaxial cyclic tests for two different loading and unloading rates are presented in the Fig. S4. In comparison to the Fig. 1 (main file), the model with f of power law

form fits the loading part slightly better for both the loading-unloading histories in small strain regime (see Fig. S4).

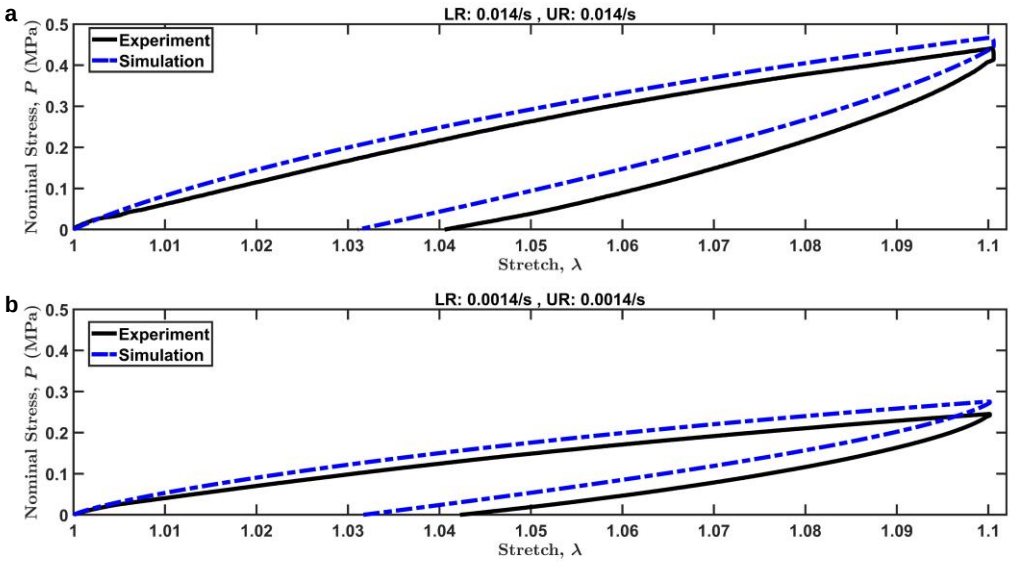

Fig. S4. Nominal stress P (MPa) vs nominal stretch λ for loading and unloading tests with two different strain rates are shown here. (a) The upper plot has a loading rate (LR) and unloading rate (UR) of 0.014/s each. (b) The lower plot has a loading rate (LR) and unloading rate (UR) of 0.0014/s each. Solid black lines represent the experiment data and our simulation results using parameters in Table S1 are shown as dash-dotted blue lines.

7.1.2. Large strain

We observe the nominal stress fits for cyclic tests under large strain using f with exponential of power law form (see Fig. S5) or power law form (see Fig. 2, main file) are both in good agreement with experiments.

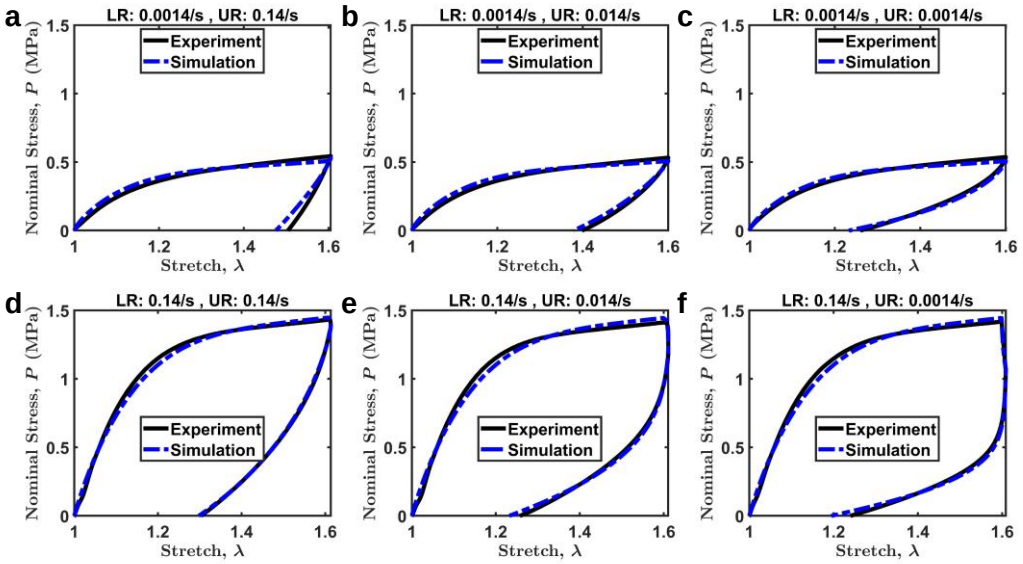

Fig. S5. Nominal stress P (MPa) vs nominal stretch λ for loading and unloading tests with different strain rates are shown here. (a), (b), and (c): The upper plots have a loading rate (LR) of 0.14/s and unloading rates (UR) of 0.14/s, 0.014/s, and 0.0014/s from left to right respectively. (d), (e), and (f): Similarly, the lower plots have a loading rate of 0.0014/s and unloading rates of 0.14/s, 0.014/s, and 0.0014/s from left to right respectively. Solid black lines represent the experiment data and our simulation results using parameters in Table S1 are shown as dash-dotted blue lines.

7.2. Tensile-Relaxation tests

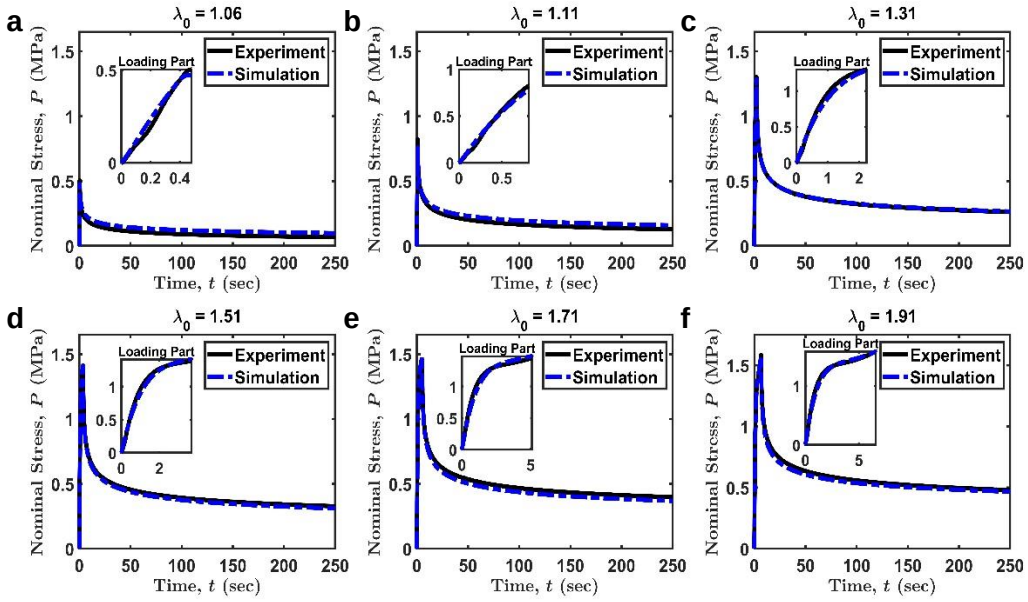

Fig. S6. Nominal stress P (MPa) vs time t (sec) for tensile-relaxation tests with different nominal stretch ratios are shown here. Solid black lines represent the

experiment data and our simulation results using parameters in Table S1 are shown as dash-dotted blue lines. Loading part of the tests are shown as insets. Relaxation tests are carried out at six stretch ratios (a) $\lambda_0 = 1.06$, (b) $\lambda_0 = 1.11$, (c) $\lambda_0 = 1.31$, (d) $\lambda_0 = 1.51$, (e) $\lambda_0 = 1.71$, and (f) $\lambda_0 = 1.91$.

From Fig. S6 and Fig. 3 (main file), we observe that predictions from both the models are in good agreement with the tensile-relaxation tests.

7.3. Simple Tension

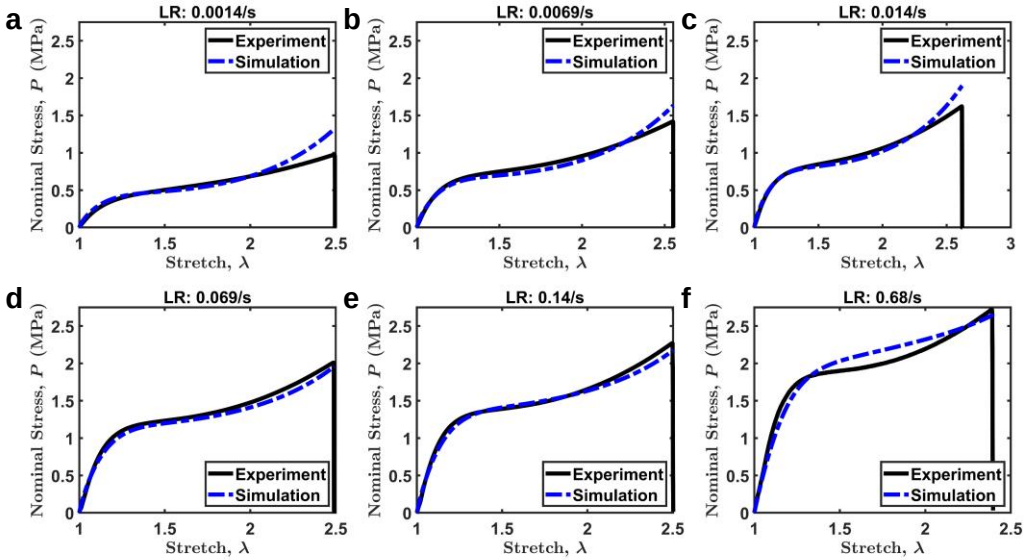

Fig. S7. Nominal stress P (MPa) vs nominal stretch λ for simple tension tests with six loading rates (LR) are presented here. (a) 0.0014/s, (b) 0.0069/s, (c) 0.014/s, (d) 0.069/s, (e) 0.14/s, and (f) 0.68/s. Solid black lines represent the experiment data and our simulation results using parameters in Table S1 are shown as dash-dotted blue lines.

By comparing Fig. S7 with Fig. 4 (main file), we observe that the model with acceleration breaking function f of power law form fits the tensile tests slightly better for loading rates 0.0014/s-0.014/s. But the general behavior captured by both the models is almost similar.

7.4. Load bearing characteristics of physical and chemical bonds

From Fig. S8 and Fig. 5 (main file), we notice that for both the models, the stress carried by both physical and chemical bonds for different loading histories are almost similar. This is because the behavior of accelerating breaking function f from both the models is almost the same (see, Fig. S9). So, the rate at which the physical bonds break is also similar, as characteristic breaking time t_B and rate of decay of survivability function α_B are close enough in both these models (see Table S1 and Table 1, main file). This leads to similar loading bearing characteristics in both these models.

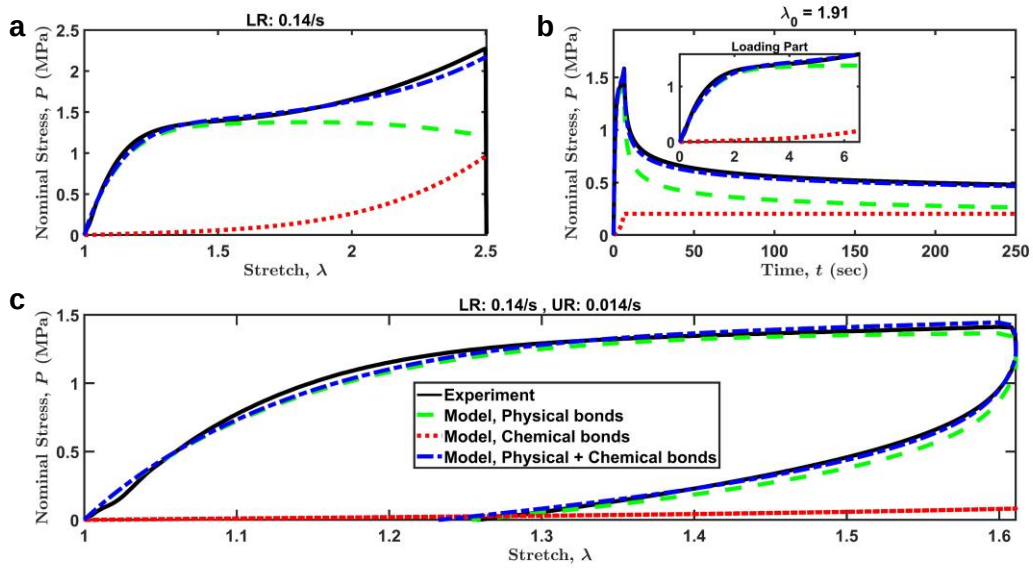

Fig. S8. For different loading histories, stress contributions from both physical and chemical bonds are computed using our model. (a) simple tension, (b) tensile-relaxation, and (c) cyclic test. The tensile test is carried out using a loading rate (LR) of 0.14/s. The stretch ratio in the tensile-relaxation test is $\lambda_0 \approx 1.91$. The cyclic test has a loading rate (LR) of 0.14/s and an unloading rate (UR) of 0.014/s. Solid black lines represent the experiment data, the stress contribution from physical bonds is shown in green dotted lines, the stress contribution from chemical bonds is shown in red dotted lines, and total stress contribution from both physical and chemical bonds is represented by blue dash-dotted lines.

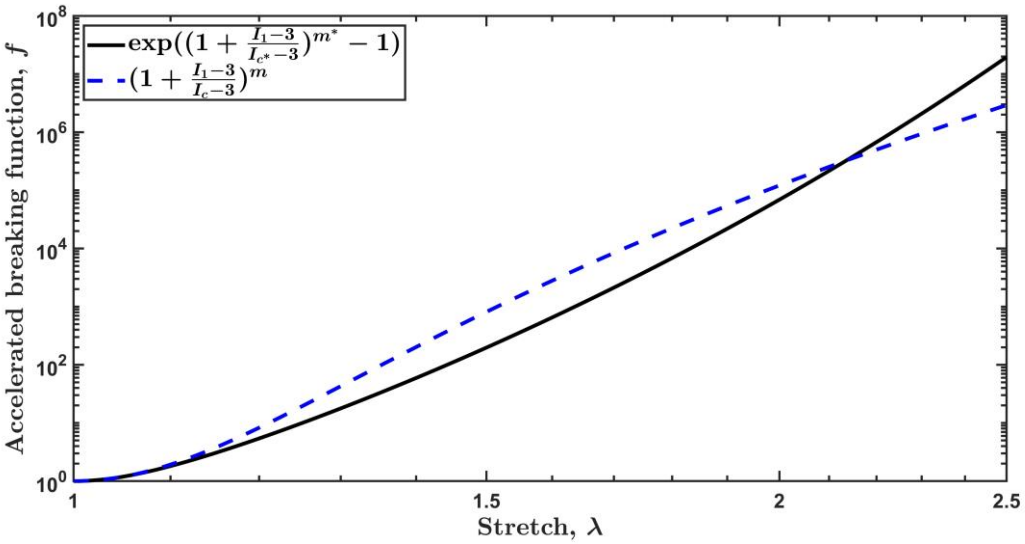

Fig. S9. Behavior of accelerating breaking function f for two different models. The values of material parameters I_{c^*} and m^* are same as I_c and m in Table S1. The values of material parameters I_c and m in power law form model are same as the ones in the Table 1 (main file).

Next, we observe the behavior of time dependent healing rate.

Fig. S10 plots show that the behavior of healing rate of physical bonds for this model is almost similar to the ones presented in the Fig. 6 (main file). We observe healing rates for the accelerating breaking function of power law form model (See Fig. 6, main file) to be slightly higher when compared to the exponential of power law form model (See Fig. S10) under different loading histories. On a general note, healing rate increases during the loading part and decreases continuously during the relaxation part.

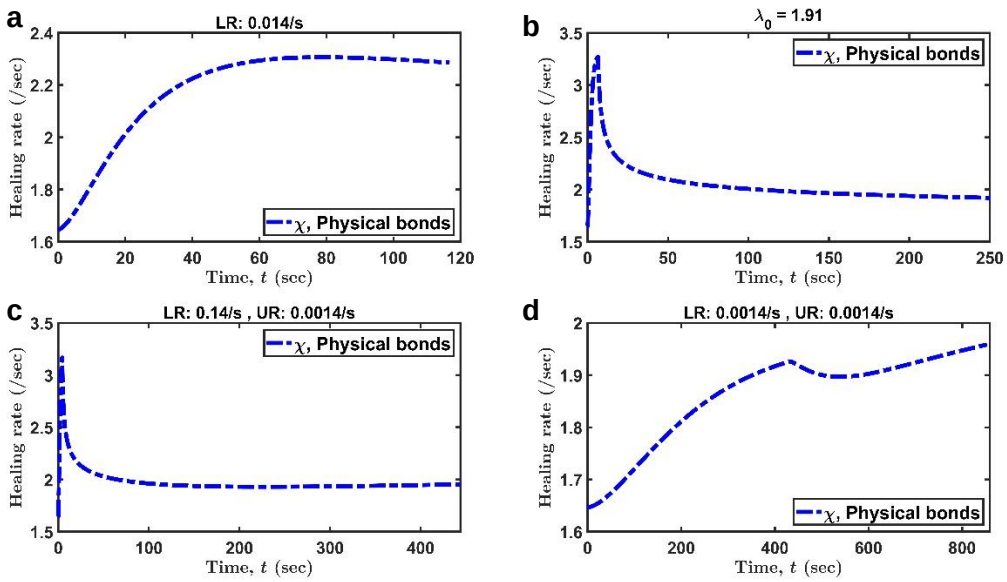

Fig. S10. Healing rate ($\chi(t)$) (in /s) for physical bonds (blue dash-dotted lines) vs time (s) for three types of mechanical testing are shown here. (a) The top left plot is a simple tension test for a loading rate (LR) of 0.014/s. (b) The top right plot is a tensile-relaxation test with a desired nominal stretch ratio of $\lambda_0 \approx 1.91$. (c) and (d) The two lower plots are cyclic tests with a loading-unloading rates (LR-UR) of 0.14/s-0.0014/s and 0.0014/s-0.0014/s.

References

[1] R. Long, K. Mayumi, C. Creton, T. Narita, C.-Y. Hui, Time Dependent Behavior of a Dual Cross-Link Self-Healing Gel: Theory and Experiments, Macromolecules. 47 (2014) 7243–7250. https://doi.org/10.1021/ma501290h.

[2] J. Guo, R. Long, K. Mayumi, C.-Y. Hui, Mechanics of a Dual Cross-Link Gel with Dynamic Bonds: Steady State Kinetics and Large Deformation Effects, Macromolecules. 49 (2016) 3497–3507. https://doi.org/10.1021/acs.macromol.6b00421.

[3] A. Tobolsky, H. Eyring, Mechanical Properties of Polymeric Materials, J. Chem. Phys. 11 (1943) 125–134. https://doi.org/10.1063/1.1723812.

[4] S.P. Venkata, K. Cui, J. Guo, A.T. Zehnder, J.P. Gong, C.-Y. Hui, Constitutive modeling of bond breaking and healing kinetics of physical Polyampholyte (PA) gel, Extreme Mech. Lett. 43 (2021) 101184. https://doi.org/10.1016/j.eml.2021.101184.

[5] R. Long, K. Mayumi, C. Creton, T. Narita, C.-Y. Hui, Rheology of a dual crosslink self-healing gel: Theory and measurement using parallel-plate torsional rheometry, J. Rheol. 59 (2015) 643–665. https://doi.org/10.1122/1.4915275.

[6] T. Matsuda, T. Nakajima, Y. Fukuda, W. Hong, T. Sakai, T. Kurokawa, U. Chung, J.P. Gong, Yielding Criteria of Double Network Hydrogels, Macromolecules. 49 (2016) 1865–1872. https://doi.org/10.1021/acs.macromol.5b02592.